bioRxiv preprint doi: https://doi.org/10.1101/2020.05.28.119164. this version posted June 10, 2020. The copyright holder for this preprint (which was not certified by peer review) is the author/funder. All rights reserved. No reuse allowed without permission.

Insulin-like growth factor 2 (IGF2) protects against Huntington´s disease through the extracellular disposal of protein aggregates.

Paula García-Huerta[1,2,3*], Paulina Troncoso-Escudero[1,2,3,8*], Di Wu[4], Arun Thiruvalluvan[4], Marisol Cisternas[1,2,8], Daniel R. Henríquez[2,5], Lars Plate[6], Pedro Chana-Cuevas[7], Cristian Saquel[2,8], Peter Thielen[9], Kenneth A. Longo[10], Brad J. Geddes[10], Gerardo L. Lederkremer[11,12], Neeraj Sharma[11,12], Marina Shenkman[11,12], Swati Naphade[13], Lisa M. Ellerby[13], Pablo Sardi[14], Carlos Spichiger[15], Hans G. Richter[16], Felipe A. Court[2,8,13], R. Luke Wiseman[6], Christian Gonzalez-Billault[2,5,13], Steven Berginк[4], Rene L. Vidal[1,2,8#] and Claudio Hetz[1,2,3,9,13#].

[1] *Biomedical Neuroscience Institute, Faculty of Medicine, University of Chile, Santiago, Chile.*
[2] *Center for Geroscience, Brain Health and Metabolism, Santiago, Chile.*
[3] *Program of Cellular and Molecular Biology, Institute of Biomedical Sciences, University of Chile, Santiago, Chile.*
[4] *Department of Biomedical Sciences of Cells & Systems, University Medical Center Groningen, University of Groningen, Groningen, The Netherlands.*
[5] *Department of Cell Biology, Faculty of Sciences, University of Chile, Santiago, Chile.*
[6] *Department of Molecular Medicine, The Scripps Research Institute, La Jolla, CA, USA*
[7] *Faculty of Medical Sciences, University of Santiago de Chile, Santiago, Chile.*
[8] *Center for Integrative Biology, Faculty of Sciences, University Mayor, Chile.*
[9] *Department of Immunology and Infectious diseases, Harvard School of Public Health, Boston, MA, 02115, USA.*
[10] *Proteostasis Therapeutics, Cambridge, MA, USA.*
[11] *Sagol School of Neuroscience, Tel Aviv University, Tel Aviv, Israel*
[12] *George Wise Faculty of Life Sciences, School of Molecular Cell Biology and Biotechnology, Tel Aviv University, Tel Aviv, Israel*
[13] *Buck Institute for Research on Aging, Novato, CA, 94945, USA.*
[14] *Department of Molecular Biology, Genzyme Corporation, 49 New York Avenue, Framingham, MA, USA.*
[15] *Institute of Biochemistry and Microbiology, Faculty of Sciences, University Austral of Chile, Valdivia, Chile.*
[16] *Institute of Anatomy, Histology and Pathology, Faculty of Medicine, University Austral of Chile, Valdivia, Chile.*

*Equal contribution

#Corresponding authors: Claudio Hetz, Institute of Biomedical Sciences, Sector B, second floor, Faculty of Medicine, University of Chile, Independencia 1027, Santiago, Chile. P.O.Box 70086. Phone: +56-229786506. Email: chetz@med.uchile.cl or chetz@buckinstitute.org. www.hetzlab.cl and Rene Vidal, Center for Integrative Biology, Universidad Mayor, Santiago, Chile. Phone: +56225189241. Email: rene.vidal@umayor.cl

One sentence summary: IGF2 reduces the load of intracellular protein aggregates through the extracellular disposal of the mutant protein.

bioRxiv preprint doi: https://doi.org/10.1101/2020.05.28.119164. this version posted June 10, 2020. The copyright holder for this preprint (which was not certified by peer review) is the author/funder. All rights reserved. No reuse allowed without permission.

Abstract

Impaired neuronal proteostasis is a salient feature of many neurodegenerative diseases, highlighting alterations in the function of the endoplasmic reticulum (ER). We previously reported that targeting the transcription factor XBP1, a key mediator of the ER stress response, delays disease progression and reduces protein aggregation in various models of neurodegeneration. To identify disease-modifier genes that may explain the neuroprotective effects of XBP1 deficiency, we performed gene expression profiling of brain cortex and striatum of these animals and uncovered insulin-like growth factor 2 (*Igf2*) as the major upregulated gene. Here we studied the impact of IGF2 signaling on protein aggregation in models of Huntington´s disease (HD) as proof-of-concept. Cell culture studies revealed that IGF2 treatment decreases the load of intracellular aggregates of mutant huntingtin and a polyglutamine peptide. These results were validated using induced pluripotent stem cells (iPSC)-derived medium spiny neurons from HD patients. The reduction in the levels of mutant huntingtin was associated with a decrease in the half-life of the intracellular protein. The decrease in the levels of abnormal protein aggregation triggered by IGF2 were independent of the activity of autophagy and the proteasome pathways, the two main routes for mutant huntingtin clearance. Conversely, IGF2 signaling enhanced the secretion of soluble mutant huntingtin species through exosomes and microvesicles involving changes in actin dynamics. Administration of IGF2 into the brain of HD mice using gene therapy led to a significant decrease in the levels of mutant huntingtin in three different animal models. Moreover, analysis of human post-mortem brain tissue, and blood samples from HD patients showed a reduction of IGF2 level. This study identifies IGF2 as a relevant factor deregulated in HD, operating as a disease modifier that buffers the accumulation of abnormal protein aggregates.

bioRxiv preprint doi: https://doi.org/10.1101/2020.05.28.119164. this version posted June 10, 2020. The copyright holder for this preprint (which was not certified by peer review) is the author/funder. All rights reserved. No reuse allowed without permission.

Introduction

Protein misfolding and aggregation are considered one of the initial events resulting in neurodegeneration in a variety of brain diseases including amyotrophic lateral sclerosis (ALS), Parkinson's, Alzheimer's, fronto-temporal dementia and Huntington´s disease (HD), which are collectively classified as protein misfolding disorders (PMDs) *(1, 2)*. The proteostasis network is fundamental to maintain the stability of the proteome and prevent abnormal protein aggregation *(3)*. Chaperones resident in the cytosol and the endoplasmic reticulum (ER) ensure precise folding of newly synthesized native proteins. Quality control mechanisms identify misfolded proteins and facilitate their removal via the proteasome, lysosome and autophagy pathways *(4)*. Importantly, the buffering capacity of the proteostasis network is reduced during aging, which may increase the risk to accumulate protein aggregates and undergo neurodegeneration *(4, 5)*. One of the main nodes of the proteostasis network altered in neurodegenerative diseases involves the ER, the main site for protein folding and quality control in the cell *(6-8)*. ER stress instigates a rapid and coordinated signaling pathway known as the unfolded protein response (UPR) to enforce adaptive programs and restore proteostasis *(9)*. Conversantly, irremediable ER stress results in cell death by apoptosis *(10)*.

The UPR is initiated by the activation of specialized stress transducers highlighting inositol-requiring transmembrane kinase/endonuclease (IRE1α) as the most conserved signaling branch *(11)*. IRE1α is an ER-located kinase and endoribonuclease that, upon activation, controls the processing of the mRNA encoding X-box-binding protein 1 (XBP1), resulting in the expression of a stable and active transcription factor known as XBP1s *(12)*. XBP1s upregulates genes related to protein folding, quality control, ER translocation, ERAD, among other processes *(13-15)*. In *C. elegans* organisms, the expression of XBP1 in neurons controls organism aging *(16)*, which may involve a crosstalk with classical signaling pathways regulating normal aging including the insulin-like growth factor (IGF)-1 and FOXO (DAF16) pathways *(17)*. We have previously studied the functional contribution of XBP1 to various neurodegenerative conditions. Despite initial expectations that targeting this central UPR mediator will exacerbate disease progression, we observed that genetic disruption of the IRE1α/XBP1 pathway in the brain led to neuroprotection in models of ALS *(18)*, Parkinson´s disease *(19)*, Alzheimer´s disease *(20, 21)* and HD *(22)*, associated with reduced accumulation of abnormal protein aggregates. These findings illustrate the broader significance of XBP1

bioRxiv preprint doi: https://doi.org/10.1101/2020.05.28.119164. this version posted June 10, 2020. The copyright holder for this preprint (which was not certified by peer review) is the author/funder. All rights reserved. No reuse allowed without permission.

and the UPR to the progression of neurodegenerative diseases, highlighting the need to identify the mechanisms of action mediating neuroprotection.

To uncover novel regulatory elements that may underlie the beneficial effects of ablating XBP1 expression in the brain, here we performed a gene expression profile study in cortex and striatum of a XBP1 conditional knockout mice ($XBP1_{cKO}$) and identified *Igf2* as the major upregulated gene. We then investigated the significance of IGF2 to abnormal protein aggregation using HD models as proof-of concept. HD is an autosomal disease, which belongs to a group of tandem repeat diseases caused by a CAG codon expansion known as polyglutamine disorders. HD is caused by mutations in the huntingtin (Htt) gene, involving the generation of an abnormal tract of over 40 glutamine residues (polyQ) at the N-terminal region *(23)*. HD patients develop a combination of motor, cognitive and psychological symptoms, associated with progressive neurodegeneration of the striatum and cerebral cortex *(24)*. Mutant Htt (mHtt) often forms insoluble inclusions that alter cellular homeostasis including the function of the ER *(25, 26)*. Here, we provide evidence indicating that IGF2 signaling decreases the accumulation of intracellular mHtt and polyglutamine peptide aggregates in various cell culture models of HD. Unexpectedly, the decrease of mutant huntingtin and polyglutamine peptide aggregates was independent of the activity of the proteasome or autophagy pathways. Instead, IGF2 treatment enhanced the non-conventional disposal of soluble polyglutamine peptide species into the extracellular space through the secretion via microvesicles and exosomes. To validate our results *in vivo*, we developed a therapeutic approach to deliver IGF2 into the brain using recombinant viruses, which resulted in significant reduction of mHtt levels in three different preclinical models of HD. Furthermore, we observed a dramatic reduction in IGF2 levels in brain and blood samples derived from HD patients, in addition to medium spiny neurons generated from HD iPSCs. We propose that IGF2 signaling operates as a disease modifier, where its deregulation enhances the abnormal accumulation of mHTT in HD. Overall, this study uncovered a previously unanticipated role of IGF2 in handling protein aggregates in HD.

bioRxiv preprint doi: https://doi.org/10.1101/2020.05.28.119164. this version posted June 10, 2020. The copyright holder for this preprint (which was not certified by peer review) is the author/funder. All rights reserved. No reuse allowed without permission.

Results

Igf2 is upregulated in the brain of XBP1 deficient mice

To define the regulatory network involved in the neuroprotective effects triggered by XBP1 deficiency in the brain, we generated XBP1$_{cKO}$ mice using the Nestin-Cre system *(27)*. Animals of 12 to 14 months old were euthanized and brain tissue was dissected to obtain both cortex and striatum to perform a global gene expression profile analysis using a total of 29 animals. Surprisingly, global analysis indicated that the extent of gene expression changes was modest. A comparison between the two brain tissues indicated poor overlap in gene expression changes between brain cortex and striatum where only the expression of *Igf2* was modified in both brain areas, showing higher expression in XBP1$_{cKO}$ mice (Fig. 1A).

Although the top regulated genes in XBP1$_{cKO}$ mice displayed a consistent fold change of at least 1.5-fold, few genes including *Igf2* showed a robust statistical significantly (q-value = 0) (Supplementary Table S1). Ingenuity pathway analysis (IPA) suggested a relation between *Igf2* with key biological pathways related to neuronal dysfunction associated with Htt and the amyloid precursor protein (Fig. 1B). A second IPA analysis found Htt as candidate of "upstream regulators" with several target genes deregulated (*Igf2, Gfap, Mmp14, Mpeg1* and *Serpine3*) and lowest p-value (data no shown).

We then validated the changes in the expression levels of *Igf2* in the brain of XBP1$_{cKO}$ mice using real-time PCR and detected a significant increase when compared to wild-type littermates (Fig. 1C). To determine whether the upregulation of *Igf2* occurs in the context of neurodegenerative diseases when XBP1 expression is ablated, we analyzed brain tissue derived from a HD model (YAC128 transgenic mice) that was crossed with our XBP1$_{cKO}$ mice *(22)*. We measured mRNA levels in the striatum of XBP1$_{cKO}$-YAC128 mice and confirmed the increase in the levels of *Igf2* compared to control animals (Supplementary Fig. S1A). As control, we also monitored *Igf1* levels and did not detect any significant differences between XBP1$_{cKO}$-YAC128 and control mice (Supplementary Fig. S1B), indicating that *Xbp1* deficiency in the nervous system results in the selective upregulation of *Igf2* expression.

bioRxiv preprint doi: https://doi.org/10.1101/2020.05.28.119164. this version posted June 10, 2020. The copyright holder for this preprint (which was not certified by peer review) is the author/funder. All rights reserved. No reuse allowed without permission.

IGF2 reduces polyQ and mHtt aggregation

Although IGF2 is the less studied member of the insulin-like peptide family, which includes IGF1 and insulin, recent studies have uncovered the importance of IGF2 in brain physiology and neurodegeneration. For example, IGF2 overexpression restored memory function and decreased the accumulation of amyloid β in models of AD *(28, 29)*. In ALS, IGF2 is differentially expressed in resistant motoneurons and its overexpression extends the survival of mutant SOD1 mice *(30)*. However, the mechanisms involved in these protective activities needs to be further defined. Since the accumulation of misfolded protein in neurons is a common feature of all of these diseases, we decided to explore the possible function of IGF2 as a disease modifier agent in PMDs.

We first performed cell culture studies to determine the consequences of IGF2 expression over abnormal protein aggregation. Neuro2a cells were transfected with expression vectors for polyQ$_{79}$-EGFP together with IGF2 or empty vector (Mock) followed by the analysis of intracellular inclusions. Quantification of the number of cells containing GFP puncta by fluorescence microscopy revealed a strong reduction in the number of polyQ$_{79}$-EGFP inclusions, when co-transfected with IGF2 vector (Fig. 2A). Then, we monitored the aggregation of polyQ$_{79}$-EGFP using biochemical approaches. Again, IGF2 or IGF2-HA expression led to a near complete reduction in the accumulation of both high molecular weight and detergent insoluble and monomeric species of polyQ$_{79}$-EGFP using standard detection by western blot (Fig. 2B and Supplementary Fig. 2A, respectively), whereas polyQ$_{79}$-EGFP mRNA levels were equal in both conditions (Supplementary Fig. 2B). Similar results were obtained when protein extracts were analyzed by filter trap, an assay that detects protein aggregates by size using a 200 nm cellulose acetate filter (Fig. 2C and Supplementary Fig. S2C). Because similar results were obtained with both IGF2 and IGF2-HA constructs, the following experiments were performed using the tagged version.

To evaluate if the effects on aggregation were specific for IGF2, we measured aggregation levels of polyQ$_{79}$-EGFP in cells co-transfected with an IGF1 expression vector. Side-by-side comparison indicated that only IGF2 reduced the levels of polyQ$_{79}$-EGFP aggregates (Fig. 2D). Since XBP1 deficiency also affects the accumulation of protein aggregates associated with other diseases, we performed additional experiments to determine the effects of IGF2 over ALS-linked mutant SOD1^{G85R}. Remarkably, the co-expression of mutant SOD1 with IGF2-HA also modified its aggregation as assessed by

bioRxiv preprint doi: https://doi.org/10.1101/2020.05.28.119164. this version posted June 10, 2020. The copyright holder for this preprint (which was not certified by peer review) is the author/funder. All rights reserved. No reuse allowed without permission.

western blot, in addition to reduce the levels of its monomeric form, similar to the effects observed with polyQ$_{79}$-EGFP aggregation (Fig. 2E), suggesting broader implications to neurodegeneration.

To define if IGF2 exerts its function from the extracellular compartment, we treated cells expressing polyQ$_{79}$-EGFP with conditioned media enriched in IGF2. In these experiments we also included a construct that expresses a fragment of mutant huntingtin spanning exon 1 with 85 CAG repeats (GFP-mHttQ$_{85}$). We transiently expressed polyQ$_{79}$-EGFP or GFP-mHttQ$_{85}$ in Neuro2a cells pre-treated with IGF2-enriched media generated from Neuro2a cells transfected with IGF2 or empty vector for 24 h. A clear reduction in the extent of protein aggregation was observed in cells exposed to IGF2-enriched media using three different assays (Fig. 3A-C). These results suggest that IGF2 may exert its function in a paracrine manner, probably activating signaling pathways through the binding to a membrane receptor. Interestingly, treatment of cells with insulin did not reduce polyQ$_{79}$-EGFP aggregation levels in our cellular model (Fig. 3D), similar to the results obtained with IGF1 overexpression.

We then evaluated if IGF2 could reduce the content of pre-formed aggregates. Thus, we expressed polyQ$_{79}$-EGFP or GFP-mHttQ$_{85}$ for 24 h and then treated Neuro2a cells with IGF2-enriched or control media. In agreement with our previous results, exposure of cells to IGF2-conditioned media attenuated the load of misfolded polyQ$_{79}$-EGFP or GFP-mHttQ$_{85}$ species (Fig. 3E, F), suggesting that IGF2 may trigger the degradation or disaggregation of abnormal protein aggregates.

IGF2 reduces the aggregation of expanded polyglutamine proteins

To further validate our results, we evaluated the effects of IGF2 expression on a cellular model that expresses full-length mHtt. To this aim, HEK293 cells were transfected with expression vectors for a myc-tagged version of full-length mHtt with a repetition of 103 glutamines (FL HttQ$_{103}$-myc) together with IGF2 or empty vector (Mock). Again, we observed that the expression of IGF2 caused a significant reduction in the levels of both monomeric and detergent insoluble species of the FL HttQ$_{103}$-myc using western blot analysis (Fig. 4A). These results were also confirmed when cell lysates were analyzed by dot blot (Fig. 4B). Overall, IGF2 expression leads to decrease levels of monomeric and aggregated forms of full-length mHtt.

Next, to increase the relevance of the current study, we moved forward and determined the possible effects of IGF2 in a human model of HD that do not rely on

bioRxiv preprint doi: https://doi.org/10.1101/2020.05.28.119164. this version posted June 10, 2020. The copyright holder for this preprint (which was not certified by peer review) is the author/funder. All rights reserved. No reuse allowed without permission.

overexpression using induced pluripotent stem cells (iPSCs) derived from patients *(31, 32)*. Thus, we generated human medium spiny neurons (MSNs) using iPSC-derived from HD patients and control subjects (Fig. 4C, D). To express IGF2, we packed its cDNA into an adeno-associated viral vector (AAV) using serotype 2, which has a high tropism for neurons. MSN cultures were transduced with AAV-IGF2 or AAV-Mock for 17 days followed by western blot analysis to determine the levels of mHtt. Remarkably, expression of IGF2 resulted in a decrease in the total levels of mHtt in HD-derived MSNs (Fig. 4E, right panel). Importantly, treatment of MSN cultures from control subjects did not modify the levels of wild-type Htt (Fig. 4E, left panel). Taken together, these results indicate that IGF2 expression reduces the content of mHtt in various models of HD.

The expansion of polyglutamine tracks is the underlying cause of different diseases, including six spinocerebellar ataxias (SCA), where SCA3 is the most common form of the disease, and the second form of polyglutamine disease after HD *(33)*. SCA3 involves the expansion in the polyglutamine track in Ataxin-3, resulting in its abnormal protein aggregation. To validate the possible effects of IGF2 expression on the levels of other disease-related genes, we generated neuronal cultures using iPSC obtained from SCA3 patients (Fig. 4F-H) and exposed them to IGF2-enrriched conditioned cell culture media. In this experimental setting, exposure of cells to glutamate results in the abnormal aggregation of mutant Ataxin-3, reflected in the accumulation of the mutant protein in the detergent insoluble fraction *(34)* (Fig. 4I). Exposure of cells to IGF2-enriched media led to reduced levels of mutant Ataxin-3 aggregates (Fig. 4J). Thus, IGF2 has broader effects in reducing the abnormal aggregation of polyglutamine-containing proteins.

IGF2 reduces the half-life of intracellular soluble mHtt

The reduction in the steady-state levels of mHtt aggregates induced by the exposure of cells to IGF2 may be explained by an attenuation in the synthesis rate or an increase its degradation rate. We performed pulse-label experiments in HEK293T cells co-transfected with a mHttQ$_{43}$-GFP construct together with IGF2 or empty vector (Mock). To evaluate translation rate, a pulse with S$_{35}$ labeled methionine and cysteine was performed for increasing intervals on a total period of 60 minutes. These experiments indicated that the biosynthesis of mHtt was identical in cells expressing or not IGF2 (Fig. 5A). In addition, general protein synthesis was not affected by IGF2 expression (Supplementary Fig. S3A). Then, we monitored the decay in the levels of mHttQ$_{43}$-GFP in cell extracts using pulse-chase to define its half-life. Remarkably, expression of IGF2

bioRxiv preprint doi: https://doi.org/10.1101/2020.05.28.119164. this version posted June 10, 2020. The copyright holder for this preprint (which was not certified by peer review) is the author/funder. All rights reserved. No reuse allowed without permission.

dramatically reduced the half-life of mHttQ$_{43}$-GFP in the cell extract (Fig. 5B), without affecting the global stability of the proteome (Supplementary Fig. S3B). In these experiments, we did not observe the presence of high-molecular weight species of mHttQ$_{43}$, suggesting that IGF2 was affecting the stability of the soluble or monomeric forms. Taken together, our data suggests that IGF2 signaling reduces the content of total mHtt associated with a shortening of the half-life of the protein inside the cell.

The autophagy and proteasome pathways are not involved in the reduction of polyQ aggregates induced by IGF2

Two major protein degradation routes are well established mediators of mHtt clearance, the proteasome and macroautophagy pathways *(35, 36)*. We monitored mHtt levels after inhibiting lysosomal function with chloroquine or the proteasome with bortezomib. To this end, HEK293T cells were co-transfected with mHttQ$_{43}$-GFP and IGF2 expression vectors followed by a radioactive pulse 24 h later to perform a chase experiment in the presence of the inhibitors. Surprisingly, neither chloroquine nor bortezomib treatments reverted the effects of IGF2 on mHtt levels (Fig. 5C). As controls for the activity of the inhibitors, we monitored the levels of LC3 and p62 (markers of autophagy-mediated degradation) and the pattern of total ubiquitination (Supplementary Fig. S3c).

Since the pulse chase methodology demonstrated that IGF2 decreases mHtt intracellular content, we performed further experiments to determine if autophagy or the proteasome mediate the reduction in the load of polyQ aggregates. Although a slight increase in the number of intracellular inclusions was observed at the basal condition after treating cells with the proteasome inhibitors lactacystin or MG132, no changes were observed in the number of polyQ$_{79}$-EGFP inclusions in IGF2 expressing cells in presence of the inhibitors when compared to vehicle (Fig. 5D and Supplementary Fig. S4A). We confirmed these observations in Neuro2a cells by measuring polyQ$_{79}$-EGFP aggregation by western blot and filter trap analysis (Fig. 5E and Supplementary Fig. S4B; see positive controls of total ubiquitination in Supplementary Fig. S4C). Again, the basal increase of polyQ aggregates after inhibiting the proteasome was lost in IGF2 treated cells. These results suggest that (i) IGF2 signaling may change the proportion between aggregate/soluble forms of polyQ inside the cell, or (ii) it may redirect polyQ aggregates toward a different pathway to mediate its clearance.

bioRxiv preprint doi: https://doi.org/10.1101/2020.05.28.119164. this version posted June 10, 2020. The copyright holder for this preprint (which was not certified by peer review) is the author/funder. All rights reserved. No reuse allowed without permission.

Based on our previous studies linking XBP1 deficiency with the upregulation of autophagy in neurons *(22)*, we evaluated autophagy activation in cells overexpressing IGF2. Neuro2a cells were transfected with IGF2 in the presence or absence of polyQ$_{79}$-EGFP expression vector. Then, autophagy was monitored after inhibiting lysosomal activity with chloroquine, followed by the analysis of LC3 and p62 levels *(37)*. We observed that IGF2 did not stimulate autophagy in Neuro2a cells, but slightly reduced LC3-II accumulation (Fig. 5F). A similar trend was observed when we measured p62 levels in cells expressing polyQ$_{79}$-EGFP (Supplementary Fig. S4D). Likewise, treatment of cells with chloroquine did not recover protein aggregation of cells exposed to IGF2 as measured with three independent methods (Fig. 5G-I). As control, in these experiments we monitored the accumulation of LC3-II and p62 in cells exposed to chloroquine (Supplementary Fig. S4E). Similarly, inhibition of lysosomal activity with chloroquine did not recover the normal levels of polyQ$_{79}$-EGFP aggregation in HEK293T cells stimulated with IGF2 (Supplementary Fig. S4F, G, see positive controls in Supplementary Fig. S4H), confirming our previous results. Finally, we obtained similar results using the autophagy inhibitors bafilomycin A$_1$ and 3-methyladenine (Supplementary Fig. S4I, J, respectively). Overall, these results suggest that the reduction in the load of polyQ$_{79}$-EGFP aggregates induced by IGF2 treatment is independent of the proteasome and autophagy/lysosomal pathways. Our data suggests that IGF2 may reduce the levels of soluble and monomeric forms of mHtt or polyQ, reducing their aggregation levels by shifting the intracellular equilibrium toward a non-aggregated form. Alternatively, IGF2 signaling may reroute the clearance of protein aggregates toward an alternative pathway that is independent of the activity of the proteasome and macroautophagy/lysosomes.

IGF2 signaling triggers polyQ secretion through extracellular vesicles

Since IGF2 administration bypassed the basal clearance of polyQ aggregates by the main degradation pathways, we explored the possibility that polyQ peptides are redirected to another compartment. mHtt has been found in the cerebrospinal fluid *(38)*, as well as in neuronal allografts transplanted into the brain of HD patients *(39)* and can be secreted and transmitted from cell to cell. Recent studies in cell culture models validated this concept suggesting that mHtt can be exported to the extracellular space by non-conventional mechanisms *(40)*. To determine the impact of IGF2 treatment in mHtt secretion, we monitored its presence in the cell culture media. Remarkably, enhanced secretion of polyQ$_{79}$-EGFP was observed in cells expressing IGF2 when cell culture

bioRxiv preprint doi: https://doi.org/10.1101/2020.05.28.119164. this version posted June 10, 2020. The copyright holder for this preprint (which was not certified by peer review) is the author/funder. All rights reserved. No reuse allowed without permission.

media was analyzed using dot blot (Fig. 6A, left panel). This phenomenon was also observed in cells overexpressing FL HttQ$_{103}$-myc when IGF2 was expressed (Supplementary Fig. S4K). Similarly, analysis of SOD1^{G85R} levels in the cell culture media indicated that IGF2 induces its secretion (Fig. 6A, middle panel), whereas no changes where observed in a cytosolic marker such as tubulin (Fig. 6A, right panel), suggesting no cell lysis or cytosol leaking. In agreement with this, analysis of cell viability using propidium iodide staining and FACS analysis in cells expressing polyQ$_{79}$-EGFP in the presence or absence of IGF2 indicated no toxicity under our experimental conditions (Supplementary Fig. S4L). We then determined whether polyQ$_{79}$-EGFP aggregates were also secreted upon IGF2 treatment. Although the signal was low, we detected the presence of large polyQ$_{79}$-EGFP aggregates outside the cell at basal levels using filter trap, a phenomenon that was incremented 2-fold in cells expressing IGF2 (Fig. 6B). However, we cannot discard that these aggregated form of polyQ$_{79}$-EGFP were generated in the cell culture media after secretion or during the concentration process of the supernatants.

Given that IGF2 is a soluble factor, we evaluated which receptors mediated the enhancement of polyQ secretion. Thus, we used siRNAs to interfere insulin and IGF1 receptors (InsR and IGF1R), in addition to a blocking antibody to target the IGF2 receptor (IGF2R). Remarkably, antagonizing IGF2R decreased almost in half the levels of polyQ$_{79}$-EGFP secretion, whereas the knockdown of InsR or IGF1R did not have any effect (Fig. 6C). Taken together, these results indicate that IGF2 signaling reduces the load of polyQ$_{79}$-EGFP in the cell through the engagement of IGF2R, resulting in the extracellular disposal of polyQ proteins.

While the precise mechanisms of mHtt secretion are not completely understood, several possibilities have been suggested, including synaptic vesicle release *(41)*, vesicular transport *(42)*, exosomes/extracellular vesicles release *(43, 44)*, exophers *(45)* and secretory lysosomes *(40)*. Since the initial link connecting IGF2 with mHtt was through the UPR, we evaluated if the polyQ peptide is secreted by the conventional secretory pathway. Blocking ER to Golgi trafficking with brefeldin A was unable to ablate polyQ$_{79}$-EGFP secretion in IGF2 stimulated cells (Fig. 6D, E). We then explored the presence of polyQ$_{79}$-EGFP in extracellular vesicles. First, we used Nanoparticle Tracking Analysis system to determine the size distribution and concentration of vesicles in the cell culture media of cells expressing IGF2. We found enhanced release of vesicles in IGF2-expressing cells, showing an average diameter between 30-150 nm, whereas a minor portion (<1%) had a larger diameter (Fig. 6F). Interestingly, we observed that the

bioRxiv preprint doi: https://doi.org/10.1101/2020.05.28.119164. this version posted June 10, 2020. The copyright holder for this preprint (which was not certified by peer review) is the author/funder. All rights reserved. No reuse allowed without permission.

population of vesicles increased under IGF2 expression picked around 100 nm, suggesting an enhancement of exosome release *(46)*. Thus, we purified extracellular vesicles followed by western blot analysis and observed higher content of polyQ$_{79}$-EGFP in vesicles obtained from IGF2-expressing cells (Fig. 6G).

We then isolated microvesicles and exosomes-enriched fractions through sequential centrifugation. Remarkably, increased levels of polyQ$_{79}$-EGFP were detected in both fractions in cells expressing IGF2 using western blot analysis (Fig. 6H, see controls of purification in Supplementary Fig. S4M, N). Importantly, mostly monomeric and soluble forms of polyQ$_{79}$-EGFP were secreted through microvesicles and exosomes, and no detergent insoluble aggregates were observed in this analysis. Thus, IGF2 signaling enhances the secretion of polyQ$_{79}$-EGFP through exosomes and microvesicles, reducing the levels of polyQ$_{79}$-EGFP inside the cell.

Cytoskeleton remodeling contributes to polyQ secretion induced by IGF2

To define possible downstream effectors mediating the effects of IGF2 signaling in abnormal protein aggregation, we employed an unbiased approach to screen for global changes in protein expression. To characterize proteome remodeling upon stimulation with IGF2, we applied quantitative proteomics using Tandem Mass Tag-Multi-Dimensional Protein Identification Technology (MuDPIT) *(47)*. Using this approach, we identified a total of 199 proteins that changed their expression levels with a p value < 0.05 and a minimum log2 > 0.1-fold change (Fig. 7A and Supplementary Table S2). IGF2 expression did not result in major proteomic changes. However, functional enrichment analysis revealed that IGF2 expression triggered fluctuations in proteins related to macromolecular complex disassembly, protein transport and cytoskeleton reorganization (Fig. 7B). A cluster of proteins modified by IGF2 were related to actin cytoskeleton dynamics and regulation, including several actin binding proteins, Rho GTPases, vimentin, dynactin, dyneins, among other factors (Supplementary Table S3).

Since actin cytoskeleton is key to modulate protein secretion and vesicular trafficking *(48)*, we decided to explore if IGF2 had any impact in the regulation of actin cytoskeleton dynamics using Lifeact, a fluorescent peptide designed to visualize polymerized actin in living cells *(49)*. Neuro2a cells were plated on coverslips and recorded using time-lapse confocal microscopy. Unexpectedly, IGF2 treatment generated very fast changes in actin dynamics and cell morphology within minutes, reflected in

bioRxiv preprint doi: https://doi.org/10.1101/2020.05.28.119164. this version posted June 10, 2020. The copyright holder for this preprint (which was not certified by peer review) is the author/funder. All rights reserved. No reuse allowed without permission.

increased development of filopodia and the appearance of actin clusters in the cytosol of the cell (Fig. 7C, see Supplementary videos 1 and 2). These results were confirmed in murine embryonic fibroblasts by visualizing the actin cytoskeleton in fixed cells stained with phalloidin-rhodamine (Fig. 7D).

Actin cytoskeleton dynamics are dependent on the activity of small GTPases from the Rho family *(50)*. Among the small GTPases of the Rho family, Cdc42, Rac, and Rho are recognized as the most important regulators of actin assembly, controlling the formation of filopodia, lamellipodia and stress fibers *(51)*. Considering the central role of Rac1 in cytoskeleton dynamics, we evaluated Rac activity upon IGF2 stimulation. Neuro2a cells were treated for 5 minutes with IGF2-enriched media and Rac1 activity was measured using pull-down assays using p21-activated kinase that binds specifically to the Rac1-GTP but not to the inactive form of Rac1 (Rac1-GDP) *(52)*, followed by western blot analysis. These results demonstrate that the amount of active Rac1 coupled to GTP was increased very quickly after IGF2 treatment (Fig. 7E).

We tested the functional contribution of actin dynamics to the release of polyQ$_{79}$-EGFP peptide into the extracellular space. Neuro2a cells were transiently transfected with both a dominant negative (Rac1$_{17N}$) and a constitutive active (Rac1$_{V12}$) forms of Rac1. Remarkably, Rac1$_{17N}$ was able to block IGF2-enhanced secretion of polyQ$_{79}$-EGFP (Fig. 7F). In contrast, Rac1$_{V12}$ expression facilitated polyQ$_{79}$-EGFP secretion at basal levels, whereas no differences were observed in IGF2-stimulated cells suggesting that the pathway was already saturated (Fig. 7F). In agreement with these findings, inhibition of Rac1-GTPase activity with NSC23766 significantly decreased the secretion of polyQ$_{79}$-EGFP (Fig. 7G). These effects paralleled with an increase in the levels of intracellular polyQ$_{79}$-EGFP aggregation in cells treated with IGF2 in the presence of NSC23766 (Fig. 7H). Taken together, these results suggest that IGF2 signaling triggers rapid changes in cytoskeleton dynamics that result in the routing of polyQ$_{79}$-EGFP peptide into the extracellular space.

IGF2 reduces mHtt aggregation in vivo

Based on the significant reduction of mHtt aggregation observed in cells overexpressing IGF2, we moved forward to develop a therapeutic strategy to deliver IGF2 into the brain of HD mice using the stereotaxic injection of AAVs to then assess the impact on mHtt levels. We previously developed an animal model of HD to monitor mHtt aggregation based on the local delivery into the striatum of a large fragment of mHtt of

bioRxiv preprint doi: https://doi.org/10.1101/2020.05.28.119164. this version posted June 10, 2020. The copyright holder for this preprint (which was not certified by peer review) is the author/funder. All rights reserved. No reuse allowed without permission.

588 amino acids containing 95 glutamine repetitions fused to monomeric RFP (Htt588Q$_{95}$-RFP) *(53)*. To validate the effects of IGF2 in the aggregation of this mHtt construct, we first performed co-expression experiments in Neuro2a cells followed by fluorescent microscopy and western blot analysis. IGF2 expression decreased mHtt aggregation in both experimental settings (Supplementary Fig. S5A).

To determine the possible impact of IGF2 in mHtt aggregation levels *in vivo*, we performed unilateral stereotaxic injections of a mixture of AAVs to deliver Htt588Q$_{95}$-RFP together with IGF2 or empty vector (Mock) into the striatum (Figure 8A, left panel). Two weeks after AAV delivery, mice were euthanized, and the striatum was dissected for biochemical analysis. We confirmed the overexpression of IGF2 in the striatum using PCR (Supplementary Fig. S5B). Local expression of IGF2 in adult mice resulted on a marked decrease of mHtt aggregation of near 90% when evaluated by western blot analysis (Fig. 8A, middle and right panel). Consistent with our cell culture experiments, monomeric forms of mHtt were also reduced in the brain of HD mice injected with AAV-IGF2 (Fig. 8A, middle and right panel). To assess the impact of overexpressing IGF2 on neuronal survival, we measured DARPP-32 levels as a marker of medium spiny neuron viability *(22)*. Interestingly, significantly higher levels of DARPP-32 were detected in AAV-IGF2-treated animals when compared to control virus (Fig. 8a, middle and right panel).

Considering our positive results obtained using the viral HD model, we then evaluated our gene therapy strategy to deliver IGF2 in the YAC128 transgenic model on a heterozygous condition. This mouse model expresses full-length mHtt with 128 tandem glutamines using an artificial chromosome that contains al endogenous regulatory elements *(54)*. First, we performed bilateral stereotaxic injections of AAV-IGF2 or empty vector into the striatum of 3-month old YAC128 mice followed by biochemical analysis of brain extracts four weeks later (Fig. 8B, left panel). This strategy led to a significant reduction of full-length mHtt expression in the striatum, reaching near 80% decrease on average (Fig. 8B, middle and right panel). Because stereotaxic injections only transduce a restricted area of the striatum restricting the analysis on motor function, we employed a second route of AAV delivery to generate a global spreading of the viral particles through the brain to assess the impact of IGF2 on mHtt levels and motor control. The delivery of AAVs into the ventricle of new-born pups has been reported to result on an efficient spreading of the virus throughout the nervous system *(55)*. We injected AAV-IGF2 or control vector in postnatal day 1 or 2 (P1-P2) YAC128 mice and dissected the

bioRxiv preprint doi: https://doi.org/10.1101/2020.05.28.119164. this version posted June 10, 2020. The copyright holder for this preprint (which was not certified by peer review) is the author/funder. All rights reserved. No reuse allowed without permission.

striatum 3 months after (Figure 8C, left panel). Western blot analysis demonstrated that IGF2 expression significantly reduces the total levels of mHtt in the brain of YAC128 animals (Fig. 8C, middle and right panel; see controls for IGF2 expression in Supplementary Fig. S5C). Finally, we determined the functional consequences of administrating our IGF2-based gene therapy on the clinical progression of experimental HD. YAC128 mice develop a variety of functional deficits, including motor learning deficits on rotarod beginning at 2 months *(56)* and motor impairment starting at 4 months of age *(57, 58)*. We monitored the motor performance of postnatal-treated YAC128 mice with control or AAV-IGF2 using the rotarod assay. We reported that this model shows a sustained impairment of motor control when assessed using the rotarod assay, with constant values for several weeks *(22)*. Remarkably, delivery of IGF2 into the nervous system improved the average motor performance over time of HD transgenic mice (Fig. 8D).

To complement our *in vivo* validation, we took advantage of a third model, the R6/2 mice, a transgenic HD model that expresses exon 1 of human huntingtin containing ~150 CAG repeats *(59)*, which allows the visualization of intracellular mHtt inclusions. Thus, we evaluated the effects of IGF2 administration in the brain of R6/2 mice by performing bilateral stereotaxic injections of AAV-IGF2 or AAV-Mock into the striatum of 4 weeks old R6/2 mice, followed by tissue immunofluorescence analysis of the brains four weeks later (Figure 8E, upper panel). A strong reduction in the content of mHtt-positive inclusions was observed upon AAV-IGF2 administration (Figure 8E, lower panel). Quantification of these experiments indicated a significant reduction of near 60% in the brain of R6/2 mice treated with AAV-IGF2 (Fig. 8F). Taken together, these results indicate that the artificial enforcement of IGF2 expression in the brain reduces abnormal protein aggregation in different HD models.

IGF2 levels are reduced in the striatum and blood samples of HD patients

Due to the dramatic effects of IGF2 on intracellular mHtt levels, we moved forward to explore the possible alterations on IGF2 expression in HD patient samples. We monitored the levels of IGF2 in human caudate-putamen derived from HD patients and age-matched control subjects obtained from the Harvard Brain Bank (Supplementary Table S4).

bioRxiv preprint doi: https://doi.org/10.1101/2020.05.28.119164. this version posted June 10, 2020. The copyright holder for this preprint (which was not certified by peer review) is the author/funder. All rights reserved. No reuse allowed without permission.

Western blot analysis of protein extracts revealed a near 66% reduction on average of IGF2 levels in the brain of HD patients when compared to the control group (Fig. 9A).

Considering the unexpected decrease of IGF2 levels in HD postmortem brain tissue, we evaluated the presence of IGF2 in peripheral blood mononuclear cells (PBMCs) from HD patients. We obtained blood samples from a cohort of 24 patients recruited in the Enroll-HD international platform (Supplementary Table S5). Although control PBMCs presented a clear expression of IGF2, HD-derived cells showed reduced IGF2 levels, observing an almost 80% decrease on its protein levels using western blot analysis (Fig. 9B). These results were confirmed when mRNA levels of IGF2 were measured in the same samples, observing a near 90% decreased in its levels (Fig. 9C). Since IGF2 is a soluble secreted factor and its plasma levels have been suggested as a possible biomarker of cancer *(60, 61)*, we decided to measure the quantity of IGF2 in plasma from HD patients using ELISA. This analysis revealed a slight but significant decrease in the amount of circulating IGF2 present in the plasma samples derived from HD patients when compared to control subjects (Fig. 9D), which may be related to the different contribution of tissues and cell types to plasmatic IGF2 levels. Taken together, these results suggest that IGF2 levels are drastically reduced in the brain and blood cells of HD patients.

bioRxiv preprint doi: https://doi.org/10.1101/2020.05.28.119164. this version posted June 10, 2020. The copyright holder for this preprint (which was not certified by peer review) is the author/funder. All rights reserved. No reuse allowed without permission.

Discussion

Proteostasis impairment is observed in a variety of neurodegenerative diseases and is a central hallmark of aging *(62)*. Our previous studies uncovered an unexpected connection between the UPR and autophagy, two central nodes of the proteostasis network, where a dynamic balance between both pathways sustains cellular function *(18, 22)*. However, it remained to be defined if other mechanisms may underlie the beneficial targeting of the UPR in neurons. To identify novel disease modifiers, we performed a gene expression profile analysis of striatal and cortical areas of XBP1 ablated animals and uncovered the upregulation of *Igf2* as the major hit. This prompted us to investigate the consequences of manipulating IGF2 in the context of PMDs using HD as a proof-of-concept. Based in our findings, and other studies, we speculate that growth factor signaling may play an important role in boosting relevant pro-survival effectors that fine tune the proteostasis network *(63)*.

IGF1 and IGF2 are mitogenic polypeptides with structural homology to insulin. IGF2 binds with higher affinity to IGF2R, but can also associate with lower affinity to IGF1R and the insulin receptor *(64, 65)*. IGF2 regulates cell proliferation, growth, differentiation and survival *(66)*. In general, the biological effects of IGF2 have been historically mapped to the IGF1R, and to a lower extent to the insulin receptor, impacting cell survival and proliferation *(67)*. Unlike insulin and IGF1 receptors, IGF2R does not have intrinsic tyrosine kinase activity and has higher affinity for IGF2 than IGF1, and does not bind insulin *(68)*. IGF2R controls extracellular IGF2 levels as it promotes its endocytosis towards lysosomal-mediated degradation *(68)*. However, IGF2R can initiate specific responses affecting various cellular processes, possibly involving the activation of heteromeric G proteins and downstream calcium signaling, in addition to the activation of PKC and MAP kinases (reviewed in *(68)*). Intracellular IGF2R also controls the uptake and trafficking of lysosomal enzymes from the trans-Golgi network to the lysosomes *(68)*. While fetal IGF2 is abundant, its levels are decreased after birth and are also further reduced during aging *(29)*. In humans, altered dosage of the *IGF2* gene can result in developmental problems and its deregulation has been widely correlated with cancer *(69)*. In adults, *IGF2* is almost exclusively expressed in the brain, especially in the choroid plexus, the brain vasculature and meninges *(70)*. Initial assessment of the significance of *IGF2* expression to animal physiology was provided by the observation that full knockout

bioRxiv preprint doi: https://doi.org/10.1101/2020.05.28.119164. this version posted June 10, 2020. The copyright holder for this preprint (which was not certified by peer review) is the author/funder. All rights reserved. No reuse allowed without permission.

animals develop growth defects *(71)*, whereas it overexpression generates embryonic lethality *(72, 73)*.

Recent findings highlight the physiological function of IGF2 in cognition, neuronal differentiation and survival. Several studies have demonstrated the relevance of IGF2 to memory consolidation *(74-76)*, in addition to memory extinction *(77)*, cognitive and social learning *(78, 79)* and brain stem cells proliferation in adults related to learning, memory and anxiety *(80)*. At the molecular level, IGF2 regulates the formation of dendritic spines *(29)* and synapses *(76)*, in addition to control adult neurogenesis in the hippocampus *(81)*. At the dentate gyrus, the autocrine action of IGF2 may explain the proliferative effects on neural stem cells *(81)*. Importantly, the effects of IGF2 in learning, memory and neurogenesis have been mapped to the stimulation of IGF2R. Thus, it might be feasible that IGF2 contributes to neuroprotection in HD through additional mechanisms, improving synaptic plasticity, connectivity, neuronal survival and neuronal function. We are currently addressing this hypothesis by assessing the possible impact of IGF2 in the clinical progression of HD using gain- and loss-of-function. Our current study proposes that IGF2 has a relevant role in controlling cellular proteostasis by fine-tuning the load of misfolded proteins through a novel mechanism involving the extracellular disposal of these misfolded proteins through extracellular vesicles (Figure 9E). We speculate that the reduction in the levels of soluble non-aggregated forms of mHtt and polyQ may shift the equilibrium in the amyloid cascade, reducing the proportion of abnormal protein aggregates inside the cell.

Our results suggest that the upregulation of IGF2 in animals with perturbed UPR may serve as a backup mechanism to sustain neuronal function when the adaptive capacity of the proteostasis network is severely compromised. We are currently investigating the mechanisms explaining the upregulation of IGF2 in XBP1 deficient brains. IGF2 expression is controlled by four different promoters and the presence of several mRNA binding proteins *(82)*, in addition to the regulation by genomic imprinting according to a parental origin *(71, 83, 84)*. IGF2 is also modulated in various pathological context including brain injury *(85)*, schizophrenia *(86)*, Alzheimer´s disease *(29, 87)*, in addition to normal aging *(29, 88)*. Recent studies also indicated that the administration of IGF2 through gene therapy or the infusion of recombinant proteins into the brain ameliorates AD pathogenesis, reducing synaptic dysfunction *(28, 29)*. Similarly, treatment of SOD1 transgenic mice with AAVs encoding for IGF2 delayed disease progression, improving motor neuron survival *(30)*. These findings are consistent with

bioRxiv preprint doi: https://doi.org/10.1101/2020.05.28.119164. this version posted June 10, 2020. The copyright holder for this preprint (which was not certified by peer review) is the author/funder. All rights reserved. No reuse allowed without permission.

the pro-survival role of IGF2 in motor neurons *(89)*, in addition to its ability to induce axonal sprouting *(90, 91)*. All these reports highlight the neuroprotective potential of IGF2 in various diseases affecting the nervous system.

Although several mechanisms have been proposed to be involved in the secretion of mHtt *(41-44)*, a recent report suggested that secretory lysosomes are the major route for mHtt release into the extracellular space *(40)*. Our results suggest that IGF2 signaling leads to a re-routing of mHtt, mostly the soluble forms, toward the secretion in extracellular vesicles. As a limitation of our study, we cannot exclude the possibility that IGF2 administration will enhance the propagation of abnormal mHtt conformations because our experimental settings were not designed to study disease spreading throughout the brain. Based on our results, we propose that soluble species of mHtt are secreted upon stimulation with IGF2, a form of the protein that is expected to lack the capacity to seed aggregation and propagate the protein misfolding process. It is most likely that the reduced aggregation observed in our experiments is due to a restricted availability of the soluble mHtt substrate, shifting the balance toward the accumulation of non-pathogenic mHtt species and reducing the overall intracellular levels of the protein. In addition, microglia has been shown to express IGF2R and IGF1R *(92)*, opening the possibility that IGF2 may impact other cell types affected in HD. In fact, based on the data available in AD models *(28, 29)*, we speculate that IGF2 administration may also enhance the extracellular clearance of mHtt by glial cells or by the action of extracellular proteases. Besides, recent studies suggested that mHtt is cleared faster in astrocytes than in neurons *(93)*.

Our findings in human HD-derived tissue suggest that the downregulation of IGF2 during the progression of the disease may enhance or accelerate the accumulation of abnormal mHtt species. In contrast, increased plasmatic levels of IGF1 in HD patients predict a worst prognosis, involving a faster and stronger cognitive decline *(94, 95)*. These effects were not observed when insulin levels were monitored in longitudinal studies *(95)*. Moreover, analysis of YAC128 mice also revealed an increase in IGF1 expression in the brain and blood of symptomatic animals *(96, 97)*. Since IGF2 levels were dramatically downregulated in human brain tissue derived from HD patients, we speculate that the delivery of IGF2 into the brain using gene therapy may serve as a strategy to restore its normal levels in the brain of HD patients.

Overall, our study places IGF2 as an interesting disease modifier agent and as an interesting candidate molecule for the treatment of HD. Since IGF2 is a soluble factor,

bioRxiv preprint doi: https://doi.org/10.1101/2020.05.28.119164. this version posted June 10, 2020. The copyright holder for this preprint (which was not certified by peer review) is the author/funder. All rights reserved. No reuse allowed without permission.

the development of gene transfer strategies to augment IGF2 levels in the brain may emerge as an attractive approach for future therapeutic development. Based on the available literature and our current study we speculate that IGF2 administration to HD patients may have important beneficial consequences beyond proteostasis control and mHtt aggregation, including multiple points of action such as improvement of neuronal connectivity and synaptic plasticity, in addition to enhance axonal regeneration, neuronal survival, neurogenesis/tissue repair and improvement in motor control.

bioRxiv preprint doi: https://doi.org/10.1101/2020.05.28.119164. this version posted June 10, 2020. The copyright holder for this preprint (which was not certified by peer review) is the author/funder. All rights reserved. No reuse allowed without permission.

Materials and methods

Animal care

XBP1$_{flox/flox}$ mice were crossed with mice expressing Cre recombinase under the control of the Nestin promoter to achieve the conditional deletion of XBP1 in the nervous system (XBP1$_{cKO}$) *(27)*. We employed as HD models the R6/2 transgenic mice, expressing exon 1 of the human huntingtin gene carrying approximately 150 CAG repeat expansions *(98)*, and the full-length human Htt transgenic mice with 128 CAG repetitions termed YAC128 *(54)*, both obtained from The Jackson Laboratory. To generate experimental animals, XBP1$_{cKO}$ mice were crossed with the YAC128 model on FVB background and every generation breed to pure background XBP1$_{cKO}$ mice for four to six generations to obtain experimental animals. For proper comparison, all biochemical and behavioral analysis were performed on groups of littermates of the same breeding generation. Unless indicated, YAC128 and littermate control animals were used and maintained on a pure C57BL/6J background. Mice were maintained in a quiet, ventilated, and temperature-controlled room (23ºC), with a standard 12 h light cycle, and monitored daily. Mice were housed in polystyrene solid bottom plastic cages fitted with a filtertop. Mice were fed with LabDiet pellets and drinking water ad libitum. For euthanasia, mice received CO_2 narcosis. Animal care and experimental protocols were performed according to procedures approved by the "Guide for the Care and Use of Laboratory Animals" (Commission on Life Sciences. National Research Council. National Academy Press 1996), the Institutional Review Board's Animal Care and Use Committee of the Harvard School of Public Health, the Bioethical Committee of the Faculty of Medicine, University of Chile (CBA 0670 FMUCH) and the Bioethical Committee of the Center for Integrative Biology, University Mayor (07-2017). We used XBP1$_{cKO}$ (N = 17) and litter matte control (N = 12) animals to gene expression analysis. For gene therapy analysis, we used 4-6 YAC128 mice per experimental group and 8 R6/2 mice per experimental group.

Microarray

XBP1$_{cko}$ animals were euthanized at 12-14 months of age and perfused with heparinized saline buffer. Brains were removed and placed in RNAlater. Brain cortex and striatum were dissected and mouse whole-genome profiling was performed using the Illumina BeadChip® platform (Illumina; San Diego, CA). According to the manufacturer, probes on the Illumina MouseWG-6 v2.0 Expression BeadChip were derived from the

bioRxiv preprint doi: https://doi.org/10.1101/2020.05.28.119164. this version posted June 10, 2020. The copyright holder for this preprint (which was not certified by peer review) is the author/funder. All rights reserved. No reuse allowed without permission.

National Center for Biotechnology Information Reference Sequence (NCBI RefSeq) database (Build 36, release 22), supplemented with probes derived from the Mouse Exonic Evidence Based Oligonucleotide (MEEBO) set, as well as exemplar protein-coding sequences described in the RIKEN FANTOM2 database. The MouseWG-6 v2.0 BeadChip contains the full set of the MouseRef-8 Expression BeadChip probes with an additional 11,603 probes from the above databases. Raw data was quantile normalized and differentially expressed genes identified using the ArrayAnalysis software *(99)*. Genes that were significantly up or down regulated were identified using Significance Analysis of Microarrays (SAM) *(100)*. SAM assigns a score to each gene based on a change in gene expression relative to the standard deviation of repeated measurements. For genes with scores greater than an adjustable threshold, SAM uses permutations of the repeated measurements to estimate the percentage of genes identified by chance the false discovery rate (FDR). Analysis parameters were set to 800 permutations, and genes with q-value =0% were used for genomics analysis.

To identify functional connections between deregulated transcripts, both network and pathway analyses of the genes filtered by microarray were performed using Ingenuity Pathways Analysis (IPA; QIAGEN Inc., https://www.qiagenbioinformatics.com/products/ingenuitypathway-analysis). The significance of networks was calculated by integrated Ingenuity algorithms. IPA computes a score for each gene network according to the fit of that network to the user-defined set of "focus genes." The score is derived from a P value and indicates the likelihood of the focus genes in a network being found together due to random chance. Relevant pathways with p-values less than 0.05 were considered. In addition, IPA compares the direction of change for the differentially expressed genes with expectations based on the literature (cured in the Ingenuity Knowledge Base) to predict an integrated direction of change for each function, using the z-score algorithm. For heatmap representation of deregulated transcripts the software HeatmapGenerator was used *(101)*.

RNA isolation, RT-PCR and real-time PCR

Total RNA was prepared from tissues or cells placed in cold PBS using Trizol following the manufacturer's instructions (Life Technologies). The cDNA was synthesized with SuperScript III reverse transcriptase (Life Technologies) using random primers p(dN)6 (Roche). Quantitative PCR reactions were performed using standard protocols using EvaGreen™ in the Stratagene Mx3000P system (Agilent Technologies). The relative

bioRxiv preprint doi: https://doi.org/10.1101/2020.05.28.119164. this version posted June 10, 2020. The copyright holder for this preprint (which was not certified by peer review) is the author/funder. All rights reserved. No reuse allowed without permission.

amounts of mRNAs were calculated from the values of comparative threshold cycle by using Actin as a control. PCR or RT-PCR were performed using the following primers: For mouse: *Igf2* 5'- GTCGCATGCTTGCCAAAGAG-3' and 5'- GGTGGTAACACGATCAGGGG-3', mouse *Actin* 5'- TACCACCATGTACCCAGGCA-3' and 5'- CTCAGGAGGAG AATGATCTTGAT-3', *Igf1* 5'- AAAGCAGCCCCGCTCTATCC-3' and 5'- CTTCTGAGTCTTGGGCATGT A-3', *Acot1* 5'- TGCAAAGCCCTCTGGTAGAC-3' and 5'- CTCGCTCTTCCAGTTGTGGT-3', *insulin receptor 5'*- TCAAGACCAGA CCGAAGATT-3' and 5'- TCTCGAAGATAACCAGGGCATAG-3', *Igf1r* 5'- CATGTGCTGGCAGTATAACCC-3' and 5'- TCG GGA GGC TTG TTC TCC T-3'. For human *IGF2* 5'- GTGCTGTTTCCGCAGCTG-3' and 5'- AGGGGTCGACACGTCCCTC-3', *Actin* 5'- GCGAGAAGATGACCCAGATC-3' and 5'- CCAGTGGTACGGCCAGAGG-3', HA 5'- TAGACGTAATCTGGAACATCG-3'.

Reagents, plasmids and transfection

Lactacystin, MG-132, chloroquine, 3-methyladenine, bafilomycin A_1, brefeldin A and recombinant insulin were purchased from Sigma. NSC23766 was purchased from Santa Cruz. GW4869 was purchased from Cayman Chemicals. Phalloidin was purchased from Molecular Probes, Invitrogen. Blocking antibody for IGF2R was purchased from Santa Cruz (sc-25462). Cell media and antibiotics were obtained from Invitrogen (MD, USA). Fetal calf serum was obtained from Hyclone and Sigma. All transfections for plasmids were performed using the Effectene reagent (Qiagen). DNA was purified with Qiagen kits. $PolyQ_{79}$-EGFP is a 79 polyglutamine tract in-frame fused to EGFP in the N-terminal; GFP-$mHttQ_{85}$ contains the first 171 amino acids of the first exon of the huntingtin gene with a tract of 85 glutamines fused to GFP in the N-terminal, was kindly provided by Dr. Paulson Henry (University of Michigan). Myc-tagged full-length huntingtin with a 103 polyglutamine region (FL Htt103Q-myc) is in pcDNA3, and was kindly provided by the Coriell Institute. pAAV-$mHttQ_{85}$-mRFP contains the first 588 amino acids of the huntingtin gene with a tract of 85 glutamines, fused to mRFP (Zuleta *et al.*, 2012). IGF2 cDNA was obtained from pSPORT6 kindly provided by Dr. Oliver Bracko and subcloned with or without the HA epitope into a pAAV vector. $SOD1_{G85R}$-EGFP was described before *(102)*. siRNA pool for IGFR1 and InsR were purchased from Origene and transfections were made with Lipofectamine® RNAiMAX transfection Reagent from Invitrogene.

bioRxiv preprint doi: https://doi.org/10.1101/2020.05.28.119164. this version posted June 10, 2020. The copyright holder for this preprint (which was not certified by peer review) is the author/funder. All rights reserved. No reuse allowed without permission.

Microscopy, western blot and filter trap analysis

Neuro2a and HEK293T cells were obtained from ATCC and maintained in Dulbecco's modified Eagles medium supplemented with 5% fetal bovine serum and Penicillin/Streptomycin (Gibco). 3 x 10_5 cells were seeded in 6-well plate and maintained by indicated times in DMEM cell culture media supplemented with 5% bovine fetal serum and non-essential amino acids. Treatment with autophagy, proteasome or exocytosis inhibitors was generally performed for 16 h unless indicated.

We visualized the formation of intracellular polyQ$_{79}$-EGFP, GFP-mHttQ$_{85}$ and Htt588Q$_{95}$-RFP inclusions in live cells after transient transfection using epifluorescent microscopy. We quantified the intracellular inclusion using automatized macros done in Image J software. Protein aggregation was evaluated by western blot in total cell extracts prepared in 1% Triton X-100 in PBS containing proteases and phosphatases inhibitors (Roche). Sample quantification was performed with the Pierce BCA Protein Assay Kit (Thermo Scientific).

For western blot analysis, cells were collected and homogenized in RIPA buffer (20 mM Tris pH 8.0, 150 mM NaCl, 0.1% SDS, 0.5% Triton X-100) containing protease and phosphatase inhibitors (Roche). After sonication, protein concentration was determined in all experiments by micro-BCA assay (Pierce), and 25-100 µg of total protein was loaded onto 8 to 15 % SDS-PAGE minigels (Bio-Rad Laboratories, Hercules, CA) prior transfer onto PVDF membranes. Membranes were blocked using PBS, 0.1% Tween-20 (PBST) containing 5% milk for 60 min at room temperature and then probed overnight with primary antibodies in PBS, 0.02% Tween-20 (PBST) containing 5% skimmed milk. The following primary antibodies and dilutions were used: anti-GFP 1:1000 (Santa Cruz, Cat. nº SC-9996), anti-SOD1 (Cell signaling, Cat. nº 2770), anti-polyQ 1:1000 (Sigma, Cat. nº P1874), anti-HSP90 1:2000 (Santa Cruz, Cat. nº SC-13119), anti-GAPDH 1:2000 (Santa Cruz, Cat. nº SC-365062), anti-HA 1:500 (Santa Cruz, Cat. nºSC-805), anti-IGF2 1:1000 (Abcam, Cat. nº Ab9574), anti-LC3 1:1000 (Cell Signaling, Cat. nº 2775S), anti-p62 1:1000 (Abcam, Cat. nº Ab56416), anti-polyUbiquitin 1:5000 (Santa Cruz, Cat. nº SC-8017), anti-DARPP32 1:1000 (Millipore, Cat. nº ab10518), anti-tubulin 1:2000 (Oncogene, Cat. nº CP06), Rac1 clone 23A8 1:1000 (Millipore, Cat. nº 05-389), for cofilin and p-cofilin we used homemade antibody at a 1:1000 dilution (Dr. James Bamburg). Bound antibodies were detected with peroxidase-coupled secondary antibodies incubated for 2 h at room temperature and the ECL system.

bioRxiv preprint doi: https://doi.org/10.1101/2020.05.28.119164. this version posted June 10, 2020. The copyright holder for this preprint (which was not certified by peer review) is the author/funder. All rights reserved. No reuse allowed without permission.

For western blot analysis using FL Htt103Q-myc, cells were grown in 100 mm dishes and cell lysis was done in 100 µl of 1% SDS in PBS for 5 min at 95˚C. Samples were then diluted 1:5 with 2% Triton X100, pelleted in a microcentrifuge for 30 min at 4˚C and 50 µl of the supernatant was loaded on SDS–PAGE. After transfer to a nitrocellulose membrane, blocking was done in 5% low-fat milk and 0.1% Tween-20 in PBS for 1 hr. Incubation with the primary antibody was overnight at 4˚C. The following primary antibodies and dilutions were used: anti-calnexin 1:1000 (Sigma-Aldrich, Cat. nº C4731), anti-Htt 1:1000 (Cell Signaling, cat nº2773S) and anti-myc (custom produced from 9E10 hybridoma). After three washes in 0.1% Tween-20 in PBS, incubation with the appropriate secondary antibody was for 1 hr at room temperature. After washing, ECL was performed and the membrane was exposed and quantified in a Bio-Rad ChemiDocXRS Imaging System (Bio-Rad, Hercules, CA).

For western blot analysis using HD MSNs protein extracts, MSNs were harvested in M-PER Mammalian Protein Extraction Reagent (Pierce) with cOmplete Mini EDTA-free protease inhibitor (1 tablet/10 mL) (Roche). Whole-cell lysates were sonicated with a 5 second pulse followed by a 5 second rest (X 5 times) at 40% amplitude. Samples were centrifuged at 14,000 rpm at 4°C for 20 min, and supernatant was collected and stored at −20°C. Protein concentrations were estimated using the BCA assay (Pierce). Cell lysates were denatured under reducing conditions by boiling 10–20 µg total protein with 1 µL of 1M DTT and 4X LDS sample buffer (Invitrogen) at 95°C for 10 min. SDS-PAGE was performed using NuPage 4-12% Bis-Tris gels (Invitrogen) or 3-8% tris-acetate gels. Gels were run in 1X MOPS or 1X tris-acetate SDS running buffer containing 500 µL of antioxidant (Life technologies) for 90 min, and transferred to 0.45 µm nitrocellulose membrane using 1X NuPage transfer buffer at 20 V for 14 h. Membranes were blocked with 5% non-fat milk in TBS with 0.1% Tween 20 (TBS-T) for 1 hr at room temperature (RT) and incubated with primary antibody reconstituted in 5% non-fat milk overnight at 4°C. The following primary antibodies and dilutions were used: anti-Htt 1:500 (Millipore, MAB2166) and anti-vinculin 1:500 (Sigma-Aldrich, Cat. nºV9131). Secondary antibodies were incubated for 2 h at RT. Blots were washed in TBS-T for 10 min (3X), and developed using Pierce ECL (Thermo Scientific). Vinculin served as loading control. Densitometry analysis was performed using ImageQuant TL v2005.

For western blots using SCA3 iPSCs-derived neurons, neuronal cells were washed in HBSS and scraped, cells were immediately frozen in liquid N2 followed by lysis in RIPA buffer (50 mM Tris, 150 mM NaCl, 0.2% Triton X-100) containing 25 mM EDTA.

bioRxiv preprint doi: https://doi.org/10.1101/2020.05.28.119164. this version posted June 10, 2020. The copyright holder for this preprint (which was not certified by peer review) is the author/funder. All rights reserved. No reuse allowed without permission.

For fractionation, lysates containing 1–2 µg/µl total protein dissolved in 50 mM Tris, 150 mM NaCl, 0.2% Triton X-100, 25 mM EDTA (RIPA buffer) were centrifuged at 22,000g for 30 min at 4ºC. The pellet fractions were separated from supernatants (Triton X-100-soluble fraction) and homogenized by sonication in RIPA buffer containing 2% SDS (SDS fraction). β-mercaptoethanol (5%) was added in all the samples and subsequently incubated at 99˚C for 5 min. Gels were loaded with 10-20 µg of the Triton X-100 fraction and 40 µl of the SDS fraction. Proteins were resolved by SDS-PAGE, transferred to nitrocellulose membrane and then processed for western blotting. Membranes were subsequently incubated with HRP-conjugated secondary antibodies (Amersham) at 1:7000 dilution. Visualization was performed with enhanced chemiluminescence. Samples were probed with primary antibodies: Ataxin-3 (Aviva Systems Biology; Cat#ARP50507_P050), βIII-tubulin (Abcam; Cat#ab7751), GAPDH (Fitzgerald; Cat#10R-G109A).

For filter trap assays, protein extracts were diluted into a final concentration of SDS 1% and were subjected to vacuum filtration through a 96-well dot blot apparatus (Bio-Rad Laboratories, Hercules, USA) containing a cellulose acetate membrane with pores with a 0.2 µm diameter (Whatman, GE Healthcare) as described in (Torres et al., 2015). Membranes were then blocked using PBS, 0.1% Tween-20 (PBST) containing 5% milk and incubated with primary antibody at 4°C overnight. Image quantification was done with the Image Lab software from BioRad.

Pulse-chase experiments

HEK293T cells were seeded in 6 well plates and transiently transfected using polyethylenimine (PEI) with pcDNA-GFP-HttQ$_{43}$ and mRFP/IGF2 constructs (in a ratio of 1:9). We used these constructs instead of the polyQ$_{79}$-EGFP peptide because this experiment was standardized using GFP-HttQ$_{43}$. For pulse labeling of cells (^{35}S incorporation), after 24 h of transfection cells were washed twice with pre-warmed pulse labeling medium (methionine and cysteine free DMEM (Gibco) containing 10% dialyzed FBS (Thermo Scientific), Glutamax (Life technologies) and Penicillin/ Streptomycin (Gibco) and kept for 45 min in pre-warmed pulse labeling medium to deplete the intracellular pool of cysteine and methionine. 0.1 mCi/mL ^{35}S (EasyTag™ EXPRESS35S Protein Labeling Mix) were added in pre-warmed pulse labeling medium and pulsed for different time periods. Before harvesting the cells, the radioactive solution was removed and cells were washed twice with 1 mL PBS containing 15 µM

bioRxiv preprint doi: https://doi.org/10.1101/2020.05.28.119164. this version posted June 10, 2020. The copyright holder for this preprint (which was not certified by peer review) is the author/funder. All rights reserved. No reuse allowed without permission.

cycloheximide. Cells were scraped in 250 µL immunoprecipitation lysis buffer (150 mM NaCl, 50 mM Tris-HCl pH 7.5, 0.5% NP-40, 0.5 mM $MgCl_2$, 3% glycerol, 0.9 mM DTT) and protease inhibitor cocktail (complete Sigma-Aldrich) and lysed by repetitive passage (8 times) through a syringe with 26-gauge needle (0.45 mm). Samples were centrifuged (20.000 x g) and the supernatant was collected. 50 µL cell lysate was kept for input. 800 µL TNE buffer (50 mM Tris-HCl pH 8.0, 150 mM NaCl, 1 mM EDTA) was added to rest of the sample, and the GFP-$HttQ_{43}$ was immunoprecipitated using GFP-trap (Chormotek, gtma-100). GFP-trap beads were added to each sample and incubated overnight at 4ºC. Beads were collected on a magnetic rack and washed twice in immunoprecipitation wash buffer (0.2% NP40, 0.2% SDS, protease inhibitors), and twice in high salt buffer (TNE with 500 mM NaCl). Beads were boiled in sample buffer (4% SDS, 10% 2-mercaptoethanol, 20% glycerol, 0.004% bromophenol blue and 0.125 M tris HCl) and analyzed using SDS page and western blotting or autoradiography. To determine half-life, 0.1 mCi ^{35}S was added to each well and incubated for 90 min. After washing chase medium (DMEM containing 10% FCS, Glutamax, P/S, 1 mg/mL methionine and 1 mg/mL cysteine (Gibco)) was added to cells and incubated for different time points. Sample preparations and immunoprecipitation of GFP-$HttQ_{43}$ was performed as described for the pulse labeling experiments.

mHtt secretion and dot blot detection

$PolyQ_{79}$-EGFP secretion was analyzed as described before *(40)*. In brief, to collect secreted proteins, Neuro2a cells were transiently transfected for a total period of 32 h, incubated in Optimem for the last 24 hrs. Cell culture media was collected and centrifuged for 5 min at 5000 r.p.m to eliminate cell debris, and then applied to a 96-well dot blot apparatus (Bio-Rad Laboratories, Hercules, USA) on a PVDF membrane. Membranes were then blocked and proteins were detected following the western blot protocol.

For the detection of FL Htt103Q-myc using dot blot, HEK293 cells were grown on 60 mm plates in 3 mL medium and transfected with plasmids for the expression of FL Htt103Q-myc together with IGF2 or empty vector. Cells and medium were collected 24 h post transfection. After washing with PBS cells were lysed in 200 µl of 1% SDS in PBS with protease inhibitor cocktail. After boiling for 5 min, sample duplicates (50 µl for cell lysates and 100 µl for medium) were loaded on a nitrocellulose membrane (pre-wet with PBS) in a dot blotting apparatus. After 2 washes with PBS the membrane was transferred

bioRxiv preprint doi: https://doi.org/10.1101/2020.05.28.119164. this version posted June 10, 2020. The copyright holder for this preprint (which was not certified by peer review) is the author/funder. All rights reserved. No reuse allowed without permission.

into 5% milk blocking solution. Proteins were detected following the western blot protocol.

Vesicle isolation and nanoparticle tracking analysis

Extracellular vesicles were isolated from cell culture media. Briefly, Neuro2a cells were cultured for 24 h in Optimem. Collected medium was then depleted of cells and cellular debris at 2,000 x g for 10 min at 4ºC. Extracellular vesicles were isolated by centrifugation of the collected supernatant at 110,000 x g for 70 min at 4°C. The resultant pellet was resuspended in PBS 1X with proteases and phosphatases inhibitors cocktail. Vesicles were analyzed for size and concentration using nanoparticle tracking analysis (NanoSight, NS300/ZetaSizer instrument). Microvesicles and exosomes were isolated from cell culture media using Neuro2a. First, cell culture media was depleted of cells and cellular debris at 2,000 x g for 10 min at 4ºC. Then, microvesicles were pelleted by centrifugation of the collected supernatant at 11,000 x g for 34 min at 4°C. Finally, exosomes were isolated from the collected supernatant from microvesicles purification by centrifugation at 110,000 x g for 70 min at 4ºC. The resultant pellet was then washed in PBS and centrifuged again for 70 min at 110,000 x g at 4 °C. The resultant pellet was resuspended in PBS 1X with proteases and phosphatases inhibitors cocktail.

Quantitative proteomics

Neuro2a cells in 6-well plates were transiently transfected with IGF2 or empty expression vectors for 24 h. Lysates were prepared in RIPA buffer containing proteases and phosphatases inhibitors cocktail (Roche). After extracts sonication, protein concentration was determined with BCA (Thermo Fisher). For each sample, 20 µg of lysate was washed by chloroform/methanol precipitation. Samples for mass spectrometry analysis were prepared as described (Plate *et al.*, 2016). Air-dried pellets were resuspended in 1% RapiGest SF (Waters) and brought up in 100 mM HEPES (pH 8.0). Proteins were reduced with 5 mM Tris(2-carboxyethyl) phosphine hydrochloride (Thermo Fisher) for 30 min and alkylated with 10 mM iodoacetamide (Sigma Aldrich) for 30 min at ambient temperature and protected from light. Proteins were digested for 18 h at 37°C with 0.5 µg trypsin (Promega). After digestion, the peptides from each sample were reacted for 1 h with the appropriate TMT-NHS isobaric reagent (Thermo Fisher) in 40% (v/v) anhydrous acetonitrile and quenched with 0.4% ammonium bicarbonate for 1 hr. Samples with different TMT labels were pooled and acidified with 5% formic acid. Acetonitrile was

bioRxiv preprint doi: https://doi.org/10.1101/2020.05.28.119164. this version posted June 10, 2020. The copyright holder for this preprint (which was not certified by peer review) is the author/funder. All rights reserved. No reuse allowed without permission.

evaporated on a SpeedVac and debris was removed by centrifugation for 30 min at 18,000 x *g*. MuDPIT microcolumns were prepared as described *(103)*. LCMS/MS analysis was performed using a Q Exactive mass spectrometer equipped with an EASY nLC 1000 (Thermo Fisher). MuDPIT experiments were performed by 5 min sequential injections of 0, 10, 20, 30, …, 100% buffer C (500 mM ammonium acetate in buffer A) and a final step of 90% buffer C / 10% buffer B (20% water, 80% acetonitrile, 0.1% formic acid, v/v/v) and each step followed by a gradient from buffer A (95% water, 5% acetonitrile, 0.1% formic acid) to buffer B. Electrospray was performed directly from the analytical column by applying a voltage of 2.5 kV with an inlet capillary temperature of 275°C. Data-dependent acquisition of MS/MS spectra was performed with the following settings: eluted peptides were scanned from 400 to 1800 m/z with a resolution of 30,000 and the mass spectrometer in a data dependent acquisition mode. The top ten peaks for each full scan were fragmented by HCD using a normalized collision energy of 30%, a 100 ms activation time, a resolution of 7,500, and scanned from 100 to 1,800 m/z. Dynamic exclusion parameters were 1 repeat count, 30 ms repeat duration, 500 exclusion list size, 120 s exclusion duration, and exclusion width between 0.51 and 1.51. Peptide identification and protein quantification was performed using the Integrated Proteomics Pipeline Suite (IP2, Integrated Proteomics Applications, Inc., San Diego, CA) as described previously *(47)*.

Rac1 pull-down assay and actin dynamics

Neuro2a cells were cultured for 2 days in 100-mm-diameter plastic plates (10^7 cells/plate) and then stimulated with IGF2 conditioned medium for 5 min at 37°C and 5% CO_2. For Rac1 activation assays the expression and purification of the CRIB domain (amino acids 67–150) of p21-activated kinase (Pak1) were performed as follows: BL21 (DE3) *E. coli* strains carrying pGEX-GST-CRIB were grown overnight at 37°C in Luria broth media containing ampicillin. Cultures were diluted 1:100 and grown in fresh medium at 37°C to an OD_{600} of 0.7. Next, IPTG was added to a final concentration of 1 mM, the cultures were grown for an additional 2 h and then samples were collected and sonicated in lysis buffer A (50 mM Tris-HCl, pH 8.0; 1% Triton X-100; 1 mM EDTA; 150 mM NaCl; 25 mM NaF; 0.5 mM PMSF and protease inhibitor complex (Roche)). Cleared lysates were affinity purified with glutathione-Sepharose beads (Amersham). Loaded beads were washed ten times with lysis buffer B (lysis buffer A with 300 mM NaCl) at 4°C. GST fusion protein was quantified and visualized in SDS-polyacrylamide gels stained with

bioRxiv preprint doi: https://doi.org/10.1101/2020.05.28.119164. this version posted June 10, 2020. The copyright holder for this preprint (which was not certified by peer review) is the author/funder. All rights reserved. No reuse allowed without permission.

Coomassie brilliant blue. Purified loaded beads were incubated for 70 min at 4°C with 1 mg of either Neuro2a lysates using fishing buffer (50 mM Tris-HCl, pH 7.5; 10% glycerol; 1% Triton X-100; 200 mM NaCl; 10 mM $MgCl_2$; 25 mM NaF and protease inhibitor complex). The beads were washed three times with washing buffer (50 mM Tris-HCl, pH 7.5; 30 mM $MgCl_2$; 40 mM NaCl) and then re-suspended in SDS-PAGE sample buffer. Bound Rac1-GTP was subjected to western blot analysis.

To measure actin dynamics, Neuro2a cells were seeded onto fibronectin-coated 25-mm coverslips, transfected with EGFP-Lifeact using Lipofectamine® 2000 Transfection Reagent and imaged in HBSS medium supplemented with HEPES using a confocal microscope (Zeiss LSM 710) with a 63×/1.4 NA oil-immersion objective at 37°C. Images were acquired every 30 s for 5 min, and the number of cells showing actin clusters were quantified. For phalloidin staining we used Phalloidin tetramethylrodamyne (Sigma) following the manufacturer's instructions.

Adeno-associated viral vector injections

All AAV (serotype 2) vectors were produced by triple transfection of HEK293T cells using a rep/cap plasmid and pHelper (Stratagene, La Jolla CA, USA), and purified by column affinity chromatography as previously described *(104)*. For stereotactic injections, mice were anesthetized using a 100 mg/kg Ketamine, 10 mg/kg Xylazine mixture (Vetcom), and affixed to a mouse stereotaxic frame (David Kopf Instruments). Wild-type C57BL/6J male mice (3 months-old) were co-injected in the right striatum with 4 µl of virus AAV-Htt588Q_{95}-mRFP and AAV-IGF2 or AAV-Mock in a relation 3:2 as we described before *(53)*. The injection of AAVs suspension was performed at two points of the striatal region using a 5 µl Hamilton syringe (Hamilton) using the following coordinates: +0.7 mm anterior, +1.7 mm lateral and -3 to 3.2 mm depth, with a 1 µl/min infusion rate. After 2 weeks, mice were euthanized for biochemistry analysis. YAC128 mice (3 months-old) were injected bilaterally in a single point in the striatum with 2 µl of AAV-IGF2 or AAV-Mock. Stereotaxic coordinates with respect to the bregma used were: +0.7 mm anterior, +1.7 mm lateral and -3.1 mm depth, with a 1 µl/min infusion rate. After 1 month mice were euthanized for biochemistry analysis. Four weeks-old R6/2 mice were injected bilaterally in a single point in the striatum with 1.5 µl of AAV-IGF2 or AAV-Mock. Stereotaxis coordinates with respect to the bregma used were: +0.8 mm anterior, +1.8 mm lateral and 3.1 mm depth, with a 1 µl/min infusion rate. Four weeks after the injection, mice were euthanized for histochemical analysis.

bioRxiv preprint doi: https://doi.org/10.1101/2020.05.28.119164. this version posted June 10, 2020. The copyright holder for this preprint (which was not certified by peer review) is the author/funder. All rights reserved. No reuse allowed without permission.

Rotarod test

Disease progression was monitored once every two weeks, using the rotarod assay as previously reported (Graham *et al.*, 2006). In brief, a training period was performed consisting of a first day of conditioning in the rotarod, following by three trials per day (with 2 h in between trials) over the course of 4 consecutive days. The data collected were considered an accurate reflection of the animal's coordination. For each testing, mice were acclimated to the room for ~15 min. The rotarod protocol consisted in (i) maximum speed, 40 r.p.m; (ii) time to reach maximum r.p.m, 120 s; (iii) time to 'no fall', 600 s; (iv) starting speed, 4 r.p.m; (v) trials per day, 3.

Tissue preparation and analysis

For biochemistry of the striatum, mice were euthanized by CO_2 narcosis, and brains were rapidly removed, rinsed with ice-cold 0.1 M phosphate buffer saline pH 7.4 (PBS), and placed on a cold surface to dissect different brain areas. Tissue samples were homogenized in 100 µl of ice-cold PBS (pH 7.4), supplemented with proteases and phosphateses inhibitor cocktail (Roche). The homogenate was divided for further mRNA and protein extraction following standard purification and quantification protocols. Protein extraction was performed in RIPA buffer (20 mM Tris pH 8.0, 150 mM NaCl, 0.1% SDS, 0.5% deoxycholate, and 0.5% Triton X-100) containing proteases and phosphatases inhibitor cocktail (Roche).

For tissue immunofluorescence analysis, mice were anesthetized and subjected to transcardial perfusion with ice-cold PBS (pH 7.4). Brains were removed and one hemisphere was fixed in 4% PFA for 24 h and then stored in a 30% sucrose solution. The other hemisphere was kept at -80 ºC. Fixed hemispheres were cut using a cryostat (Leica CM1520) and 20 µm-thick coronal slices were obtained from the striatum. Free-floating slices were preserved in PBS-Sodium azide 0.02% at 4ºC.

Tissue immunofluorescence analysis

Brain slices were washed three times with PBS (pH 7.4) and then blocked at room temperature for 1 hr with blocking solution (BSA 0.5% and Triton 0.2% in PBS pH 7.4). Brain slices were incubated with EM48 1:1000 (Millipore, MAB5374) and HA 1:500 (Cell Signaling, cat nº C29F4) antibodies in blocking solution for 24 h at 4ºC. Afterwards, slices were washed three times with PBS (pH 7.4) and then incubated for 2 h at room temperature with Alexa 488 goat anti mouse 1:1000 (Jackson ImmunoResearch, cat nº

bioRxiv preprint doi: https://doi.org/10.1101/2020.05.28.119164. this version posted June 10, 2020. The copyright holder for this preprint (which was not certified by peer review) is the author/funder. All rights reserved. No reuse allowed without permission.

115-545-166), Alexa 594 goat anti rabbit 1.1000 (Jackson ImmunoResearch, cat nº 111-545-144) and DAPI 1:10,000 (Merck, cat nº D9542). Finally, slices were washed three times with PBS (pH 7.4) and mounted in slides cover with gelatin using Fluoromount-G (Electron Microscopy Sciences, cat nº 17984-25).

Microscopy and quantification of brain slices

High-resolution images (330.49 x 330.49 μm) from brain slices were obtained using an inverted Leica DMi8 light microscope using a 40X objective. For the quantification of mutant huntingtin inclusions and DAPI-positive cells, 20-30 z-stacks were acquired in three different regions of the striatum of a single slice for each experiment (six-nine slices per animal analyzed). Images were deconvolved using the microscope software and mutant huntingtin inclusions and DAPI-positive cells were quantified using automatized macros from the Image J software.

Human samples

A total of 26 brain samples from the NIH NeuroBioBank were included in the study. Samples were obtained from 13 patients with clinical diagnosis of HD (grade 3 and 4 according to the neuronal loss observed) and 13 age-matched controls. Patients with HD met criteria proposed by the neuropathologist responsible in the Harvard Brain Tissue Resource Center *(105-107)*. Samples of human adult peripheral blood (18 ml) were collected using BD vacutainer heparin tubes and processed in ≤4 hours after extraction. Plasma and PBMC were obtained by Ficoll gradient. Sampling was done according to the ethics committee form by the advisory board of the director of the local health service and the San Jose Hospital, University of Chile. Patients were recruited in the Enroll-HD project at the Movement disorder center (CETRAM) in Santiago, Chile (https://www.enroll-hd.org). Enroll-HD is a worldwide observational study for Huntington's disease families. It will monitor how the disease appears and changes over time in different people and is open to people who either have HD or are at-risk. This platform collects standardized data, in the same way and using the same methods around the world. This project develops a comprehensive database of patients followed by a team of neurologists. Total, circulating IGF2 levels were measured in plasma from 49 individuals, using an ELISA IGF2 kit (CrystalChem, Cat. nº 80575).

bioRxiv preprint doi: https://doi.org/10.1101/2020.05.28.119164. this version posted June 10, 2020. The copyright holder for this preprint (which was not certified by peer review) is the author/funder. All rights reserved. No reuse allowed without permission.

NSC culture and MSN differentiation

6-well plates were coated with 100 µg/ml poly-D-lysine (Sigma-Aldrich) followed by Matrigel (1:60) coating. HD and corrected C116 iPSC-derived neural stem cells (NSCs) were plated and cultured in Neural Proliferation Medium (NPM) (Neurobasal medium, 1X B-27 supplement (Life Technologies), 2mM L-Glutamine, 100U/ml penicillin, 100 µg/ml streptomycin, 10 ng/ml Leukemia inhibitory factor (LIF) (Peprotech, 300-05), 25 ng/ml basic Fibroblast Growth Factor (bFGF) (Peprotech, 100-18B), and 25 ng/ml Activin A (Peprotech, AF-120-14E) in humidified incubator under 37°C, 5% CO_2. For differentiation into medium spiny neurons (MSNs), NSCs (when at ~90% confluence) were treated with Synaptojuice A medium for 7 days followed by Synaptojuice B medium for 10 days at 37°C, 5% CO_2 *(108)*. 25 ng/ml Activin A was added to both Synaptojuice A and Synaptojuice B media. Half media change was performed every 2 days. NSCs were treated with AAV2-IGF2 or AAV2-PGK-empty (1 x 1011 VG per well) on day 1 of Synaptojuice A treatment. Untransduced MSNs were used as controls.

Generation of iPSCs of SCA-3 patients with episomal vectors

Generation of iPSCs derived from patients with spinocerebellar ataxia class 3 was described previously *(109)*. Human dermal fibroblasts (HDFs) were cultured in Dulbecco's modified Eagle media (DMEM, Gibco) containing 10% fetal bovine serum (FBS), 1 mM non-essential amino acids (NEAAs), 1X GlutaMAX, and 100 units/ml of penicillin with 100 µg/ml streptomycin. The episomal iPSC reprogramming plasmids, pCXLE-hOCT3/4, pCXLE-hSK and pCXLE-hMLN were purchased from Addgene. The plasmids used in our experiments were mixed in a ratio of 1:1:1 for efficient reprogramming. 3 µg of expression plasmid mixtures were electroporated into $5x10_5$ HDFs with Amaxa® Nucleofector Kit according to the manufacturer's instructions. After nucleofection, cells were plated in DMEM containing 10% FCS and 1% penicillin/streptomycin until it reaches 70-80% confluence. The culture medium was replaced the next day by human embryonic stem cell medium (HESM) containing knock-out (KO) DMEM, 20% KO serum replacement (SR), 1 mM NEAAs, 1X GlutaMAX, 0.1 mM β-mercaptoethanol, 1% penicillin/streptomycin and 10ng/ml bFGF (Invitrogen). Between 26-32 days after plating, colonies developed and colonies with a phenotype similar to human ESCs were selected for further cultivation and evaluation. Selected iPSC colonies were mechanically passaged on matrigel (BD, hES qualified matrigel) coated

bioRxiv preprint doi: https://doi.org/10.1101/2020.05.28.119164. this version posted June 10, 2020. The copyright holder for this preprint (which was not certified by peer review) is the author/funder. All rights reserved. No reuse allowed without permission.

plates containing mTeSR™1 (defined, feeder-free maintenance medium for human ESCs and iPSCs).

Generation of iPSC-derived neurons

IPSCs were dissociated manually and plated on a non-coated dish in human embryonic stem cell medium (HESM). After 4 days, embryoid bodies (EBs) were formed and transferred to neural differentiation medium containing DMEM/ F12, 1 mM NEAAs, 1× GlutaMAX, 1% penicillin/streptomycin, and 1X N1 supplement (100X) for another 4 days. EBs were plated on matrigel-coated plates for neural rosette formation for 8-10 days with 0.01 mM retinoic acid. Neural rosettes were handpicked and cultured in neural stem cell medium containing DMEM/F12, 1 mM NEAAs, 1X GlutaMAX, 1% penicillin/streptomycin, 1X N1 supplement (100X), 20 ng/mL FGF2 (peprotech), 20 ng/mL EGF (peprotech), and 2 µl/ml B27 supplement (Invitrogen). Terminal neural differentiation was induced by dissociating the neural stem cells (NSCs) using accutase (Sigma) for 20 min at 37ºC and plating them on a matrigel-coated plate for attachment. The next day, the medium of these cell cultures were changed to neuronal differentiation medium containing DMEM/F12, 1 mM NEAAs, 1X GlutaMAX, 1% penicillin/streptomycin, 1X N1 supplement (100X), 20 ng/mL BDNF (Peprotech), 20 ng/mL GDNF (Peprotech), 1 mM dibutyryl-cAMP (Sigma) and 2µl/ml B27 supplement (Invitrogen) for 80-90 days.

Excitatory stimulation of neurons

SCA3 neurons cultured in 6 well plates were washed three times with 2 mL HBSS (balanced salt solution) containing 25 mM Tris, 120 mM NaCl, 15 mM glucose, 5.4 mM KCl, 1.8 mM $CaCl_2$, 0.8 mM $MgCl_2$, pH 7.4. After treatment with L-glutamate 0.1 mM (Sigma no. G8415) in HBSS for 30 min, cells were washed again three times and left them to recover for 30 min in differentiation media followed by a second 30 min L-glutamate treatment in HBSS, and subsequently cultured in differentiation media or condition media (with or without IGF for 24 and 48 h until analyzed). For analysis of fragmentation and aggregation of Ataxin 3 by western blotting, extracts were analyzed either immediately after lysis or after fractionation.

Immunocytochemistry

IPSCs-derived neurons from SCA-3 patients were fixated with 4% paraformaldehyde for 20 min. Cells were blocked in 5% normal goat serum and 2% fetal calf serum; subsequently, samples were probed with primary antibodies: TRA-1-81 (Santa Cruz; sc-

bioRxiv preprint doi: https://doi.org/10.1101/2020.05.28.119164. this version posted June 10, 2020. The copyright holder for this preprint (which was not certified by peer review) is the author/funder. All rights reserved. No reuse allowed without permission.

21706), TRA-2-54 (made by group Peter Andrews lab, The University of Sheffield), OCT-4 (Santa Cruz; sc-5279), SOX-2 (Cell Signaling; #4900S), βIII-tubulin (Abcam; ab7751). Alexa 488 and Cy3-conjugated secondary antibodies were used in combination with Hoechst nuclear staining (1:1000). Images were obtained using a Leica TCS SP8 confocal microscope (Leica Microsystems).

Statistical analysis

Results were statistically compared using the Student's *t* test was performed for unpaired or paired groups. A p value of < 0.05 was considered significant (*: $p < 0.05$; **: $p < 0.01$; ***: $p < 0.001$; ****: $p<0.0001$)

Supplementary Materials

Supplementary Fig. 1. XBP1 deficiency does not alter *Igf1* mRNA levels.

Supplementary Fig. 2 IGF2 expression reduces polyQ79 monomer and aggregation.

Supplementary Fig. 3. IGF2 does not inhibit global protein synthesis or degradation.

Supplementary Fig. 4. Neither proteasome nor autophagy are involved in the reduction of polyQ levels after IGF2 expression.

Supplementary Fig. 5. Controls for secretion experiments.

Supplementary Fig. 6. Gene therapy to deliver IGF2 into the brain.

Supplementary Table 1. Top regulated genes in brain cortex and striatum of $XBP1_{cKO}$ mice.

Supplementary Table 2. List of proteins modified by IGF2 expression.

Supplementary Table 3. Set of proteins modified by IGF2 expression related to actin cytoskeleton dynamics.

Supplementary Table 4. Human post-mortem brain samples.

Supplementary Table 5. Blood samples from HD patients and healthy controls.

Video S1. Neuro2a treated with mock medium.

Video S2. Neuro2a treated with IGF2-enriched medium.

bioRxiv preprint doi: https://doi.org/10.1101/2020.05.28.119164. this version posted June 10, 2020. The copyright holder for this preprint (which was not certified by peer review) is the author/funder. All rights reserved. No reuse allowed without permission.

References

1. Bertram, L. and R.E. Tanzi, The genetic epidemiology of neurodegenerative disease. J Clin Invest. **115**, 1449-57 (2005).

2. Soto, C. and S. Pritzkow, Protein misfolding, aggregation, and conformational strains in neurodegenerative diseases. Nat Neurosci. **21**, 1332-1340 (2018).

3. Balch, W.E., et al., Adapting proteostasis for disease intervention. Science. **319**, 916-9 (2008).

4. Kaushik, S. and A.M. Cuervo, Proteostasis and aging. Nat Med. **21**, 1406-15 (2015).

5. Martinez, G., et al., Endoplasmic reticulum proteostasis impairment in aging. Aging Cell. **16**, 615-623 (2017).

6. Scheper, W. and J.J. Hoozemans, The unfolded protein response in neurodegenerative diseases: a neuropathological perspective. Acta Neuropathol. **130**, 315-31 (2015).

7. Smith, H.L. and G.R. Mallucci, The unfolded protein response: mechanisms and therapy of neurodegeneration. Brain. **139**, 2113-21 (2016).

8. Hetz, C. and S. Saxena, ER stress and the unfolded protein response in neurodegeneration. Nat Rev Neurol. **13**, 477-491 (2017).

9. Wang, M. and R.J. Kaufman, Protein misfolding in the endoplasmic reticulum as a conduit to human disease. Nature. **529**, 326-35 (2016).

10. Hetz, C. and F.R. Papa, The Unfolded Protein Response and Cell Fate Control. Mol Cell. **69**, 169-181 (2018).

11. Walter, P. and D. Ron, The unfolded protein response: from stress pathway to homeostatic regulation. Science. **334**, 1081-6 (2011).

12. Hetz, C., The unfolded protein response: controlling cell fate decisions under ER stress and beyond. Nat Rev Mol Cell Biol. **13**, 89-102 (2012).

13. Acosta-Alvear, D., et al., XBP1 controls diverse cell type- and condition-specific transcriptional regulatory networks. Mol Cell. **27**, 53-66 (2007).

14. Lee, A.H., N.N. Iwakoshi, and L.H. Glimcher, XBP-1 regulates a subset of endoplasmic reticulum resident chaperone genes in the unfolded protein response. Mol Cell Biol. **23**, 7448-59 (2003).

15. Shoulders, M.D., et al., Stress-independent activation of XBP1s and/or ATF6 reveals three functionally diverse ER proteostasis environments. Cell Rep. **3**, 1279-92 (2013).

bioRxiv preprint doi: https://doi.org/10.1101/2020.05.28.119164. this version posted June 10, 2020. The copyright holder for this preprint (which was not certified by peer review) is the author/funder. All rights reserved. No reuse allowed without permission.

16. Taylor, R.C. and A. Dillin, XBP-1 is a cell-nonautonomous regulator of stress resistance and longevity. Cell. **153**, 1435-47 (2013).

17. Henis-Korenblit, S., et al., Insulin/IGF-1 signaling mutants reprogram ER stress response regulators to promote longevity. Proc Natl Acad Sci U S A. **107**, 9730-5 (2010).

18. Hetz, C., et al., XBP-1 deficiency in the nervous system protects against amyotrophic lateral sclerosis by increasing autophagy. Genes Dev. **23**, 2294-306 (2009).

19. Valdes, P., et al., Control of dopaminergic neuron survival by the unfolded protein response transcription factor XBP1. Proc Natl Acad Sci U S A. **111**, 6804-9 (2014).

20. Safra, M., et al., The ire-1 ER stress-response pathway is required for normal secretory-protein metabolism in C. elegans. J Cell Sci. **126**, 4136-46 (2013).

21. Duran-Aniotz, C., et al., IRE1 signaling exacerbates Alzheimer's disease pathogenesis. Acta Neuropathol. **134**, 489-506 (2017).

22. Vidal, R.L., et al., Targeting the UPR transcription factor XBP1 protects against Huntington's disease through the regulation of FoxO1 and autophagy. Hum Mol Genet. **21**, 2245-62 (2012).

23. Bates, G.P., et al., Huntington disease. Nat Rev Dis Primers. **1**, 15005 (2015).

24. Di Prospero, N.A. and K.H. Fischbeck, Therapeutics development for triplet repeat expansion diseases. Nat Rev Genet. **6**, 756-65 (2005).

25. Zuccato, C., M. Valenza, and E. Cattaneo, Molecular mechanisms and potential therapeutical targets in Huntington's disease. Physiol Rev. **90**, 905-81 (2010).

26. Vidal, R., et al., Converging pathways in the occurrence of endoplasmic reticulum (ER) stress in Huntington's disease. Curr Mol Med. **11**, 1-12 (2011).

27. Hetz, C., et al., Unfolded protein response transcription factor XBP-1 does not influence prion replication or pathogenesis. Proc Natl Acad Sci U S A. **105**, 757-62 (2008).

28. Mellott, T.J., et al., IGF2 ameliorates amyloidosis, increases cholinergic marker expression and raises BMP9 and neurotrophin levels in the hippocampus of the APPswePS1dE9 Alzheimer's disease model mice. PLoS One. **9**, e94287 (2014).

29. Pascual-Lucas, M., et al., Insulin-like growth factor 2 reverses memory and synaptic deficits in APP transgenic mice. EMBO Mol Med. **6**, 1246-62 (2014).

30. Allodi, I., et al., Differential neuronal vulnerability identifies IGF-2 as a protective factor in ALS. Sci Rep. **6**, 25960 (2016).

31. Chamberlain, S.J., Disease modelling using human iPSCs. Hum Mol Genet. **25**, R173-R181 (2016).

bioRxiv preprint doi: https://doi.org/10.1101/2020.05.28.119164. this version posted June 10, 2020. The copyright holder for this preprint (which was not certified by peer review) is the author/funder. All rights reserved. No reuse allowed without permission.

32. Naphade, S., K.T. Tshilenge, and L.M. Ellerby, Modeling Polyglutamine Expansion Diseases with Induced Pluripotent Stem Cells. Neurotherapeutics. **16**, 979-998 (2019).

33. McLoughlin, H.S., L.R. Moore, and H.L. Paulson, Pathogenesis of SCA3 and implications for other polyglutamine diseases. Neurobiol Dis. **134**, 104635 (2020).

34. Koch, P., et al., Excitation-induced ataxin-3 aggregation in neurons from patients with Machado-Joseph disease. Nature. **480**, 543-6 (2011).

35. Sarkar, S. and D.C. Rubinsztein, Huntington's disease: degradation of mutant huntingtin by autophagy. FEBS J. **275**, 4263-70 (2008).

36. Ortega, Z. and J.J. Lucas, Ubiquitin-proteasome system involvement in Huntington's disease. Front Mol Neurosci. **7**, 77 (2014).

37. Mizushima, N., T. Yoshimori, and B. Levine, Methods in mammalian autophagy research. Cell. **140**, 313-26 (2010).

38. Wild, E.J., et al., Quantification of mutant huntingtin protein in cerebrospinal fluid from Huntington's disease patients. J Clin Invest. **125**, 1979-86 (2015).

39. Cicchetti, F., et al., Neural transplants in patients with Huntington's disease undergo disease-like neuronal degeneration. Proc Natl Acad Sci U S A. **106**, 12483-8 (2009).

40. Trajkovic, K., H. Jeong, and D. Krainc, Mutant Huntingtin Is Secreted via a Late Endosomal/Lysosomal Unconventional Secretory Pathway. J Neurosci. **37**, 9000-9012 (2017).

41. Pecho-Vrieseling, E., et al., Transneuronal propagation of mutant huntingtin contributes to non-cell autonomous pathology in neurons. Nat Neurosci. **17**, 1064-72 (2014).

42. Babcock, D.T. and B. Ganetzky, Transcellular spreading of huntingtin aggregates in the Drosophila brain. Proc Natl Acad Sci U S A. **112**, E5427-33 (2015).

43. Jeon, I., et al., Human-to-mouse prion-like propagation of mutant huntingtin protein. Acta Neuropathol. **132**, 577-92 (2016).

44. Zhang, X., et al., Potential Transfer of Polyglutamine and CAG-Repeat RNA in Extracellular Vesicles in Huntington's Disease: Background and Evaluation in Cell Culture. Cell Mol Neurobiol. **36**, 459-70 (2016).

45. Melentijevic, I., et al., C. elegans neurons jettison protein aggregates and mitochondria under neurotoxic stress. Nature. **542**, 367-371 (2017).

46. Soares Martins, T., et al., Exosome isolation from distinct biofluids using precipitation and column-based approaches. PLoS One. **13**, e0198820 (2018).

bioRxiv preprint doi: https://doi.org/10.1101/2020.05.28.119164. this version posted June 10, 2020. The copyright holder for this preprint (which was not certified by peer review) is the author/funder. All rights reserved. No reuse allowed without permission.

47. Plate, L., et al., Small molecule proteostasis regulators that reprogram the ER to reduce extracellular protein aggregation. Elife. **5**, (2016).

48. Porat-Shliom, N., et al., Multiple roles for the actin cytoskeleton during regulated exocytosis. Cell Mol Life Sci. **70**, 2099-121 (2013).

49. Riedl, J., et al., Lifeact: a versatile marker to visualize F-actin. Nat Methods. **5**, 605-7 (2008).

50. Ridley, A.J., Rho family proteins: coordinating cell responses. Trends Cell Biol. **11**, 471-7 (2001).

51. Etienne-Manneville, S. and A. Hall, Rho GTPases in cell biology. Nature. **420**, 629-35 (2002).

52. Henriquez, D.R., et al., The light chain 1 subunit of the microtubule-associated protein 1B (MAP1B) is responsible for Tiam1 binding and Rac1 activation in neuronal cells. PLoS One. **7**, e53123 (2012).

53. Zuleta, A., et al., AAV-mediated delivery of the transcription factor XBP1s into the striatum reduces mutant Huntingtin aggregation in a mouse model of Huntington's disease. Biochem Biophys Res Commun. **420**, 558-63 (2012).

54. Slow, E.J., et al., Selective striatal neuronal loss in a YAC128 mouse model of Huntington disease. Hum Mol Genet. **12**, 1555-67 (2003).

55. Passini, M.A. and J.H. Wolfe, Widespread gene delivery and structure-specific patterns of expression in the brain after intraventricular injections of neonatal mice with an adeno-associated virus vector. J Virol. **75**, 12382-92 (2001).

56. Van Raamsdonk, J.M., et al., Cognitive dysfunction precedes neuropathology and motor abnormalities in the YAC128 mouse model of Huntington's disease. J Neurosci. **25**, 4169-80 (2005).

57. Van Raamsdonk, J.M., et al., Loss of wild-type huntingtin influences motor dysfunction and survival in the YAC128 mouse model of Huntington disease. Hum Mol Genet. **14**, 1379-92 (2005).

58. Graham, R.K., et al., Levels of mutant huntingtin influence the phenotypic severity of Huntington disease in YAC128 mouse models. Neurobiol Dis. **21**, 444-55 (2006).

59. Proenca, C.C., et al., Atg4b-dependent autophagic flux alleviates Huntington's disease progression. PLoS One. **8**, e68357 (2013).

60. Huang, G.S., et al., Insulin-like growth factor 2 expression modulates Taxol resistance and is a candidate biomarker for reduced disease-free survival in ovarian cancer. Clin Cancer Res. **16**, 2999-3010 (2010).

bioRxiv preprint doi: https://doi.org/10.1101/2020.05.28.119164. this version posted June 10, 2020. The copyright holder for this preprint (which was not certified by peer review) is the author/funder. All rights reserved. No reuse allowed without permission.

61. Zanella, E.R., et al., IGF2 is an actionable target that identifies a distinct subpopulation of colorectal cancer patients with marginal response to anti-EGFR therapies. Sci Transl Med. **7**, 272ra12 (2015).

62. Wong, E. and A.M. Cuervo, Autophagy gone awry in neurodegenerative diseases. Nat Neurosci. **13**, 805-11 (2010).

63. Garcia-Huerta, P., et al., The intersection between growth factors, autophagy and ER stress: A new target to treat neurodegenerative diseases? Brain Res. **1649**, 173-180 (2016).

64. Hawkes, C., et al., Single transmembrane domain insulin-like growth factor-II/mannose-6-phosphate receptor regulates central cholinergic function by activating a G-protein-sensitive, protein kinase C-dependent pathway. J Neurosci. **26**, 585-96 (2006).

65. Li, R., A. Pourpak, and S.W. Morris, Inhibition of the insulin-like growth factor-1 receptor (IGF1R) tyrosine kinase as a novel cancer therapy approach. J Med Chem. **52**, 4981-5004 (2009).

66. Bergman, D., et al., Insulin-like growth factor 2 in development and disease: a mini-review. Gerontology. **59**, 240-9 (2013).

67. Fernandez, A.M. and I. Torres-Aleman, The many faces of insulin-like peptide signalling in the brain. Nat Rev Neurosci. **13**, 225-39 (2012).

68. Hawkes, C. and S. Kar, The insulin-like growth factor-II/mannose-6-phosphate receptor: structure, distribution and function in the central nervous system. Brain Res Brain Res Rev. **44**, 117-40 (2004).

69. Kessler, S.M., J. Haybaeck, and A.K. Kiemer, Insulin-Like Growth Factor 2 - The Oncogene and its Accomplices. Curr Pharm Des. **22**, 5948-5961 (2016).

70. Ferron, S.R., et al., Differential genomic imprinting regulates paracrine and autocrine roles of IGF2 in mouse adult neurogenesis. Nat Commun. **6**, 8265 (2015).

71. DeChiara, T.M., E.J. Robertson, and A. Efstratiadis, Parental imprinting of the mouse insulin-like growth factor II gene. Cell. **64**, 849-59 (1991).

72. Wise, T.L. and D.D. Pravatcheva, Perinatal lethality in H19 enhancers-Igf2 transgenic mice. Mol Reprod Dev. **48**, 194-207 (1997).

73. Pravtcheva, D.D. and T.L. Wise, Igf2r improves the survival and transmission ratio of Igf2 transgenic mice. Mol Reprod Dev. **75**, 1678-87 (2008).

74. Chen, D.Y., et al., A critical role for IGF-II in memory consolidation and enhancement. Nature. **469**, 491-7 (2011).

75. Alberini, C.M. and D.Y. Chen, Memory enhancement: consolidation, reconsolidation and insulin-like growth factor 2. Trends Neurosci. **35**, 274-83 (2012).

bioRxiv preprint doi: https://doi.org/10.1101/2020.05.28.119164. this version posted June 10, 2020. The copyright holder for this preprint (which was not certified by peer review) is the author/funder. All rights reserved. No reuse allowed without permission.

76. Schmeisser, M.J., et al., IkappaB kinase/nuclear factor kappaB-dependent insulin-like growth factor 2 (Igf2) expression regulates synapse formation and spine maturation via Igf2 receptor signaling. J Neurosci. **32**, 5688-703 (2012).

77. Agis-Balboa, R.C., et al., A hippocampal insulin-growth factor 2 pathway regulates the extinction of fear memories. EMBO J. **30**, 4071-83 (2011).

78. Stern, S.A., D.Y. Chen, and C.M. Alberini, The effect of insulin and insulin-like growth factors on hippocampus- and amygdala-dependent long-term memory formation. Learn Mem. **21**, 556-63 (2014).

79. Steinmetz, A.B., et al., Insulin-Like Growth Factor II Targets the mTOR Pathway to Reverse Autism-Like Phenotypes in Mice. J Neurosci. **38**, 1015-1029 (2018).

80. Ziegler, A.N., et al., Insulin-like Growth Factor II: An Essential Adult Stem Cell Niche Constituent in Brain and Intestine. Stem Cell Reports. **12**, 816-830 (2019).

81. Bracko, O., et al., Gene expression profiling of neural stem cells and their neuronal progeny reveals IGF2 as a regulator of adult hippocampal neurogenesis. J Neurosci. **32**, 3376-87 (2012).

82. Engstrom, W., et al., Transcriptional regulation and biological significance of the insulin like growth factor II gene. Cell Prolif. **31**, 173-89 (1998).

83. Feil, R., et al., Developmental control of allelic methylation in the imprinted mouse Igf2 and H19 genes. Development. **120**, 2933-43 (1994).

84. Mikaelsson, M.A., et al., Placental programming of anxiety in adulthood revealed by Igf2-null models. Nat Commun. **4**, 2311 (2013).

85. Walter, H.J., et al., Distinct sites of insulin-like growth factor (IGF)-II expression and localization in lesioned rat brain: possible roles of IGF binding proteins (IGFBPs) in the mediation of IGF-II activity. Endocrinology. **140**, 520-32 (1999).

86. Ouchi, Y., et al., Reduced adult hippocampal neurogenesis and working memory deficits in the Dgcr8-deficient mouse model of 22q11.2 deletion-associated schizophrenia can be rescued by IGF2. J Neurosci. **33**, 9408-19 (2013).

87. Rivera, E.J., et al., Insulin and insulin-like growth factor expression and function deteriorate with progression of Alzheimer's disease: link to brain reductions in acetylcholine. J Alzheimers Dis. **8**, 247-68 (2005).

88. Kitraki, E., et al., Aging-related changes in IGF-II and c-fos gene expression in the rat brain. Int J Dev Neurosci. **11**, 1-9 (1993).

89. Silva, D., et al., Decreased motoneuron survival in Igf2 null mice after sciatic nerve transection. Neuroreport. **20**, 1414-8 (2009).

bioRxiv preprint doi: https://doi.org/10.1101/2020.05.28.119164. this version posted June 10, 2020. The copyright holder for this preprint (which was not certified by peer review) is the author/funder. All rights reserved. No reuse allowed without permission.

90. Caroni, P. and P. Grandes, Nerve sprouting in innervated adult skeletal muscle induced by exposure to elevated levels of insulin-like growth factors. J Cell Biol. **110**, 1307-17 (1990).

91. Near, S.L., et al., Insulin-like growth factor II stimulates motor nerve regeneration. Proc Natl Acad Sci U S A. **89**, 11716-20 (1992).

92. Suh, H.S., et al., Insulin-like growth factor 1 and 2 (IGF1, IGF2) expression in human microglia: differential regulation by inflammatory mediators. J Neuroinflammation. **10**, 37 (2013).

93. Zhao, T., et al., Compartment-Dependent Degradation of Mutant Huntingtin Accounts for Its Preferential Accumulation in Neuronal Processes. J Neurosci. **36**, 8317-28 (2016).

94. Saleh, N., et al., High insulinlike growth factor I is associated with cognitive decline in Huntington disease. Neurology. **75**, 57-63 (2010).

95. Salem, L., et al., Insulin-Like Growth Factor-1 but Not Insulin Predicts Cognitive Decline in Huntington's Disease. PLoS One. **11**, e0162890 (2016).

96. Pouladi, M.A., et al., Full-length huntingtin levels modulate body weight by influencing insulin-like growth factor 1 expression. Hum Mol Genet. **19**, 1528-38 (2010).

97. Wong, B.K.Y., et al., Partial rescue of some features of Huntington Disease in the genetic absence of caspase-6 in YAC128 mice. Neurobiol Dis. **76**, 24-36 (2015).

98. Mangiarini, L., et al., Exon 1 of the HD gene with an expanded CAG repeat is sufficient to cause a progressive neurological phenotype in transgenic mice. Cell. **87**, 493-506 (1996).

99. Eijssen, L.M., et al., A user-friendly workflow for analysis of Illumina gene expression bead array data available at the arrayanalysis.org portal. BMC Genomics. **16**, 482 (2015).

100. Tusher, V.G., R. Tibshirani, and G. Chu, Significance analysis of microarrays applied to the ionizing radiation response. Proc Natl Acad Sci U S A. **98**, 5116-21 (2001).

101. Khomtchouk, B.B., D.J. Van Booven, and C. Wahlestedt, HeatmapGenerator: high performance RNAseq and microarray visualization software suite to examine differential gene expression levels using an R and C++ hybrid computational pipeline. Source Code Biol Med. **9**, 30 (2014).

102. Turner, B.J., et al., Impaired extracellular secretion of mutant superoxide dismutase 1 associates with neurotoxicity in familial amyotrophic lateral sclerosis. J Neurosci. **25**, 108-17 (2005).

103. Ryno, L.M., et al., Characterizing the altered cellular proteome induced by the stress-independent activation of heat shock factor 1. ACS Chem Biol. **9**, 1273-83 (2014).

bioRxiv preprint doi: https://doi.org/10.1101/2020.05.28.119164. this version posted June 10, 2020. The copyright holder for this preprint (which was not certified by peer review) is the author/funder. All rights reserved. No reuse allowed without permission.

104. O'Riordan, C.R., et al., Scaleable chromatographic purification process for recombinant adeno-associated virus (rAAV). J Gene Med. **2**, 444-54 (2000).

105. Vonsattel, J.P., C. Keller, and E.P. Cortes Ramirez, Huntington's disease - neuropathology. Handb Clin Neurol. **100**, 83-100 (2011).

106. Vonsattel, J.P., et al., Neuropathological classification of Huntington's disease. J Neuropathol Exp Neurol. **44**, 559-77 (1985).

107. Dickson, D.W. and R.O. Weller, *Neurodegeneration: The Molecular Pathology of Dementia and Movement Disorders*. 2011.

108. Kemp, P.J., et al., Improving and accelerating the differentiation and functional maturation of human stem cell-derived neurons: role of extracellular calcium and GABA. J Physiol. **594**, 6583-6594 (2016).

109. Thiruvalluvan, A., et al., DNAJB6, a key factor in neuronal sensitivity to amyloidogenesis. Molecular Cell. **in press**, (2020).

bioRxiv preprint doi: https://doi.org/10.1101/2020.05.28.119164. this version posted June 10, 2020. The copyright holder for this preprint (which was not certified by peer review) is the author/funder. All rights reserved. No reuse allowed without permission.

Acknowledgements.

We are grateful to Dr. Oliver Bracko for providing IGF2 overexpression constructs. We thank the Harvard Brain Tissue Resource Center for providing HD post-mortem samples. We also thank Drs Dimitri Krainc and Katarina Trajkovic for feedback on protocols to detect mHtt secretion. We also thank Dr Cristina Alberini for feedback and providing tools to study IGF2 signaling. We thank Marioly Müller and Dr. Josefina Barrera and her team for their kind help taking the blood samples. We thank Dr. Felipe Oyarzun and Rodrigo Sierpe for the kindly help with the use of the Nanosight NS300. We specially acknowledge Carolina Jerez, Claudia Rivera, Valentina Castillo and Constanza Gonzalez for their technical assistance. **Funding:** This work was directly funded by FONDAP program 15150012, Millennium Institute P09-015-F, CONICYT-Brazil 441921/2016-7, FONDEF ID16I10223, FONDEF D11E1007 and FONDECYT 1180186 (CH). In addition, we thank the support from the U.S. Air Force Office of Scientific Research FA9550-16-1-0384, and Muscular Dystrophy Association, US Office of Naval Research-Global (ONR-G) N62909-16-1-2003, (C.H.). We also thank FONDECYT 3150097 (P.G-H.), FONDECYT 1191003 (R.V.), FONDECYT 1150069 (H.G.R.), CONICYT Ph.D. fellowship 21160843 (P.T-E.), CSC and the Postgraduate Student Research and Innovation Project of Jiangsu Province KYLX15_0558 (D.W.), the Hersenstichting and NWO-ALW (S.B.) and NIH NS092829 (R.L.W.).

Authors contribution: P.G-H, P.T-E, C.H and R.L.V designed the study; P.G-H and P.T-E designed, performed and analyzed most of the *in vitro* and *in vivo* experiments; D.W and S.B designed, performed and analyzed the pulse-chase experiments; C.S and F.C analyzed the NTA experiments and assisted with the extracellular vesicle experiments; P.C-C provided the information and blood samples from Chilean HD patients; D.R.H and C.G-B designed and performed the experiments of actin remodeling; P.T, K.A.L and B.J.G performed the microarray analysis using the brains samples from the $XBP1_{cko}$ mice; L.P and L.W performed the quantitative proteomics in Neuro2a cells; C.S and H.G.R performed the Ingenuity pathway analysis; P.S produced the AAV2-IGF2 and AAV2-Mock; G.L.L, N.S and M.S performed the experiments in HEK293 cells using the full-lenght$HttQ_{103}$-myc plasmid; S.N and L.M.E designed, performed and analyzed the experiments using MSNs derived from HD patients.

bioRxiv preprint doi: https://doi.org/10.1101/2020.05.28.119164. this version posted June 10, 2020. The copyright holder for this preprint (which was not certified by peer review) is the author/funder. All rights reserved. No reuse allowed without permission.

Competing interests: The authors declare no conflict of interest in this study. AAV-IGF2 for gene therapy and its use in misfolded protein diseases as Huntington's disease (Chile nº 201603282 and PCT. provisional application no. PCT/CL2017/000040).

Data and materials availability: MTA may be required for access to AAV-IGF2 and some vectors. All data are available upon request from C.H.

bioRxiv preprint doi: https://doi.org/10.1101/2020.05.28.119164. this version posted June 10, 2020. The copyright holder for this preprint (which was not certified by peer review) is the author/funder. All rights reserved. No reuse allowed without permission.

Figures legends

Figure 1. XBP1 deficiency increases *Igf2* expression levels. (A) Gene expression was determined in the brain cortex and striatum of XBP1$_{cKO}$ (n = 17) and litter mate control (n = 12) animals using Illumina BeadChip® platform and analyzed as described in materials and methods. Heatmaps of microarray analysis of cortex or striatum tissue of two experimental groups considering 1.5 or 1.6-fold change as cutoff, respectively. The normalized average signal of each group was displayed in the heatmap. Red color is used to indicate upregulated genes and green color for downregulation. **(B)** Network of significantly enriched in genes differentially expressed in the brain cortex and striatum of XBP1$_{cKO}$. This set of genes was grouped in the Ingenuity Top Network 2 'Cancer, Drug Metabolism, Endocrine System Development and Function'. Red: significantly up-regulated gene; Green: significantly down-regulated gene; Gray: non-significant differential expression; White: biological terms related with the network. **c** *Igf2* mRNA levels were measured by real-time PCR in cDNA generated from cortex, striatum, substantia nigra and hippocampus region of 9-months old XBP$_{WT}$ and XBP1$_{cKO}$ mice. Data represents the average and SEM of the analysis of 3-6 animals per group. Statistically significant differences detected by one-tailed unpaired *t*-test (***: $p < 0.001$; *: $p < 0.05$).

Figure 2. IGF2 expression reduces the levels of polyQ$_{79}$ aggregates. (A) Neuro2a cells were co-transfected with a polyQ$_{79}$-EGFP expression vector and IGF2 plasmid or empty vector (Mock). 24 or 48 h later, the number of polyQ$_{79}$-EGFP inclusions were visualized by fluorescence microscopy (left panel). Quantification of inclusions was normalized by the number of GFP-positive cells (right panel; n = 100 to 350 cells per experiment). Scale bar, 20 µm. **(B)** PolyQ$_{79}$-EGFP expression was analyzed in whole cell extracts by western blot analysis using an anti-GFP antibody. A non-tagged version of IGF2 expression vector was also included. The presence of high molecular weight (HMW) species is indicated. Hsp90 and IGF2 levels were also determined (left panel). PolyQ$_{79}$-EGFP aggregates levels were quantified and normalized to Hsp90 levels (right panel). **(C)** Filter trap assay was performed in the same cells extracts analyzed in (B) (left panel) and quantified at 24 h (right panel). **(D)** Neuro2a cells were transiently co-transfected with polyQ$_{79}$-EGFP together with plasmids to express IGF1, IGF2 or empty vector (Mock). The presence of polyQ$_{79}$-EGFP aggregates was analyzed in whole cell extracts after 24 h

bioRxiv preprint doi: https://doi.org/10.1101/2020.05.28.119164. this version posted June 10, 2020. The copyright holder for this preprint (which was not certified by peer review) is the author/funder. All rights reserved. No reuse allowed without permission.

by western blot analysis. Hsp90 expression was monitored as loading control. **(E)** Neuro2a cells were co-transfected with polyQ$_{79}$-EGFP or SOD1$_{G85R}$-GFP and IGF2 plasmid or empty vector (Mock). After 24 h, polyQ$_{79}$ and SOD1 aggregation were measured in total cell extracts using western blot under non-reducing conditions (without DTT). Hsp90 expression was monitored as loading control. In all quantifications, values represent the mean and SEM of at least three independent experiments. Statistically significant differences detected by two-tailed unpaired *t*-test (***: $p < 0.001$; **: $p < 0.01$; *: $p < 0.05$).

Figure 3. IGF2 treatment reduces the accumulation of polyQ$_{79}$ and mHttQ$_{85}$ aggregates. (A) Neuro2a cells were transfected with polyQ$_{79}$-EGFP expression vectors in the presence of IGF2-enriched cell culture media. 24 h later polyQ$_{79}$-EGFP and mHttQ$_{85}$-GFP inclusions were visualized by microscopy (upper panel) and quantified (bottom panel; n = 100 to 350 cells per experiment). Scale bar, 20 µm. **(B)** Neuro2a cells were transfected with polyQ$_{79}$-EGFP or mHttQ$_{85}$-GFP expression vectors in presence of IGF2-enriched cell culture media. 24 h later the aggregation levels of polyQ$_{79}$-EGFP or mHttQ$_{85}$-GFP were determined by western blot analysis using anti-GFP antibody. Hsp90 expression was monitored as loading control. **(C)** Filter trap assay was performed using the same protein extracts analyzed in (b) to quantify polyQ$_{79}$-EGFP and mHttQ$_{85}$-GFP aggregates. **(D)** Neuro2a cells were transfected with polyQ$_{79}$-EGFP in presence of 1 µM insulin. 24 h later the aggregation of polyQ$_{79}$-EGFP protein was measured in total cell extracts by western blot. Hsp90 expression was monitored as loading control. **(E)** Neuro2a cells were transfected with polyQ$_{79}$-EGFP or mHttQ$_{85}$-GFP expression vectors. After 24 h cells were treated with IGF2-enriched cell culture media and 24 h later aggregation levels determined and quantified by western blot analysis using anti-GFP antibody. Hsp90 levels were monitored as loading control. **(F)** Filter trap assay was performed in the same cell extracts analyzed in (e) and polyQ$_{79}$-EGFP and mHttQ$_{85}$-GFP aggregates were detected using anti-GFP antibody. In all quantifications, average and SEM of at least three independent experiments are shown. Statistically significant differences detected by two-tailed unpaired *t*-test (***: $p < 0.001$; **: $p < 0.01$; *: $p < 0.05$).

Figure 4. IGF2 overexpression reduced the levels of huntingtin in MSNs derived from HD patients. (A) HEK293T cells were co-transfected with full length (FL) HttQ$_{103}$-myc and IGF2 or empty vector (Mock). 24 h later, FL HttQ$_{103}$-myc levels were analyzed

bioRxiv preprint doi: https://doi.org/10.1101/2020.05.28.119164. this version posted June 10, 2020. The copyright holder for this preprint (which was not certified by peer review) is the author/funder. All rights reserved. No reuse allowed without permission.

in whole cell extracts by western blot analysis using an anti-Htt antibody. The arrow indicates the migration of full-length huntingtin. **(B)** HEK293T cells were co-transfected with FL $HttQ_{103}$-myc and IGF2 or empty vector (Mock). After 24 h, FL $HttQ_{103}$-myc was detected in cell lysates by dot blot. Statistically significant differences detected by two-tailed unpaired *t*-test (***: $p < 0.001$). **(C)** Schematic representation of the differentiation process to generate mature medium spiny neurons (MSNs) from induced human pluripotent stem cells (iPSCs), showing cell morphology using contrast phase microscopy. **(D)** Confirmation of the expression of GABAergic (DARPP-32) and neuronal (MAP2) markers in control and HD patients MSNs using immunofluorescence. **(E), (F)** MSNs from control subjects and HD patients were transduced with adeno-associated viral (AAV) vectors expressing IGF2 o empty vector (Mock). 17 days later, huntingtin protein levels were measured in total protein extracts by western blot using anti-Htt antibody. Vinculin expression was monitored as loading control (lower panel). Values represent the mean and SEM of three independent experiments. Statistically significant differences detected by one-way ANOVA (*: $p < 0.05$). **(G)** Schematic representation of the generation of neuronal cultures generated from SCA-derived iPSCs. **(H)** Ataxin 3 levels were monitored in control and SCA3 patient fibroblasts using western blot analysis. * represent the mutant protein. **(I)** Differentiated SCA3 iPSC-derived neurons at 90 days post differentiation were stained for βIII-tubulin neuronal marker. Scale bars: 50 µm. **(J)** Neurons were treated with 0.1 mM L-glutamate for 1 h. Then, detergent insoluble protein extracts were generated in triton X100 (TX-100) and pellets were resuspended in SDS to yield an SDS-soluble fraction (SDS) and SDS-insoluble fraction that was then dissolved in formic acid (FA). Ataxin 3 levels were monitored in all fractions using western blots analysis (*-expanded allele). Two independent experiments were performed. **(K)** SCA3 cells were stimulated with IGF2-conditioned media for indicated time points followed by stimulation with 0.1 mM L-glutamate followed by western blot analysis as described in j. GAPDH levels were determined as loading control and βIII-tubulin as a neuronal marker.

Figure 5. Stimulation of cells with IGF2 reduces the half-life of mHtt aggregates. **(A)** HEK293T cells were co-transfected with GFP-$mHttQ_{43}$ expression vector with IGF2 plasmid (middle panel) or empty vector (Mock) (upper panel), and then pulse labeled with ^{35}S for indicated time points. Autoradiography (AR) indicated the ^{35}S signal for each time point. Data were quantified and normalized to time point 0 h (lower panel). **(B)**

bioRxiv preprint doi: https://doi.org/10.1101/2020.05.28.119164. this version posted June 10, 2020. The copyright holder for this preprint (which was not certified by peer review) is the author/funder. All rights reserved. No reuse allowed without permission.

HEK293T cells were co-transfected with GFP-mHttQ$_{43}$ expression vector with IGF2 plasmid (middle panel) or empty vector (Mock) (upper panel), and then pulse labeled with ^{35}S for indicated time points and the decay of the radioactive signal during chasing was monitored as described in materials and methods. Autoradiography (AR) indicated the ^{35}S signal for each time point. Data were quantified and normalized to the time point 1 h (lower panel). **(C)** HEK293T cells were transfected with GFP-mHttQ$_{43}$ and IGF2 expression vectors. Pulse was performed 24 h after transfection. Cells were treated with 30 μM chloroquine (CQ) or 1 μM bortezomib (Bort) at the beginning of the chasing for additional 21 h (upper panel). Data were quantified and normalized to time point 1 h (lower panel). **(D)** Neuro2a cells were co-transfected with a polyQ$_{79}$-EGFP expression vector and IGF2 plasmid or empty vector (Mock) for 8 h and then treated with 1 μM lactacystin (Lact) for additional 16 h (upper panel). Quantification of aggregates per GFP-positive cell was performed (lower panel; N=100 to 350 cells per experiment). **(E)** Neuro2a cells were co-transfected with a polyQ$_{79}$-EGFP expression vector and IGF2 plasmid or empty vector (Mock) for 8 h, and then treated with 1 μM lactacystin (Lact) or 1 μM MG132 for additional 16 h. PolyQ$_{79}$-EGFP aggregation was analyzed in whole cells extracts by western blot using anti-GFP antibody and quantified (lower panel). Hsp90 expression was analyzed as loading control (upper panel). **(F)** Neuro2a cells where co-transfected with a polyQ$_{79}$-EGFP expression vector and IGF2 plasmid or empty vector (Mock) for 8 h, and then treated with 30 μM chloroquine (CQ) for additional 16 h. Endogenous lipidated LC3-II levels were monitored by western blot using anti-LC3 antibody. Hsp90 expression was monitored as loading control (upper panel). LC3 II levels were quantified and normalized to Hsp90 (lower panel). **(G)** Neuro2a cells were co-transfected with polyQ$_{79}$-EGFP and IGF2 expression vectors or empty vector (Mock) for 8 h, and then treated with 30 μM CQ for additional 16 h (upper panel). Quantification of aggregates per GFP-positive cell was performed (lower panel; N=100 to 350 cells per experiment). **(H)** Neuro2a cells were co-transfected with polyQ$_{79}$-EGFP and IGF2 expression vectors or empty vector (Mock) for 8 h, and then treated with 30 μM CQ for additional 16 h. PolyQ$_{79}$-EGFP aggregation was analyzed in whole cells extracts by western blot using anti-GFP antibody and quantified (lower panel). Hsp90 expression was monitored as loading control (upper panel). **(I)** Filter trap was performed using the same cells extracts analyzed in (H). In all quantifications, average and SEM of at least three independent experiments are shown. Statistically significant differences detected by two-tailed unpaired *t*-test (***: $p < 0.001$; **: $p < 0.01$; *: $p < 0.05$).

bioRxiv preprint doi: https://doi.org/10.1101/2020.05.28.119164. this version posted June 10, 2020. The copyright holder for this preprint (which was not certified by peer review) is the author/funder. All rights reserved. No reuse allowed without permission.

Figure 6. IGF2 enhances the extracellular release of polyQ$_{79}$ and mHttQ$_{85}$ through unconventional secretion. (A) Neuro2a cells were co-transfected with polyQ$_{79}$-EGFP or SOD1$_{G85R}$ plasmid and IGF2 plasmid or empty vector (Mock). After 16 h, cell culture media was replaced for Optimem and then collected after 24 h for dot blot or **(B)** filter trap analysis. **(C)** Neuro2a cells were transfected with siRNAs against InsR or IGF1R mRNAs. After 24 h, cells were co-transfected with polyQ$_{79}$-EGFP and IGF2 expression vector or empty vector (Mock). Then, cell culture media was replaced for Optimem for 24 h. In addition, an anti-IGF2R was added when indicated. The presence of polyQ$_{79}$-EGFP in the cell culture media analyzed by dot blot using an anti-GFP antibody and quantified. The knockdown of indicated proteins was confirmed in cell extracts using semi-quantitative PCR (right panel). **(D)** Neuro2a cells were co-transfected with polyQ$_{79}$-EGFP and IGF2 plasmid or empty vector (Mock). Then, cell culture media was replaced for Optimem for 8 h and treated with 2 μM brefeldin A (Bref A) or vehicle for additional 16 h. Cell culture media was collected and analyzed by dot blot using an anti-GFP antibody (upper panel) and quantified (lower panel). Image was cropped from the same membrane and film exposure. **(E)** Neuro2a cells were co-transfected with polyQ$_{79}$-EGFP plasmid and IGF2 plasmid or empty vector (Mock) for 8 h and then treated with 2 μM brefeldin A (Bref A) or vehicle for additional 16 h. PolyQ$_{79}$-EGFP aggregates were analyzed in cell lysates by western blot using anti-GFP antibody. Hsp90 expression was monitored as loading control. PolyQ$_{79}$-EGFP aggregates were quantified and normalized to Hsp90 (lower panel). **(F)** Extracellular vesicles from Neuro2a were analyzed by NanoSight nanotracking analysis and plotted by size (upper panel) and total concentration (lower panel) in cells expressing or not with IGF2. **(G)** Extracellular vesicles from Neuro2a cells co-transfected with polyQ$_{79}$-EGFP and IGF2 expression vectors or empty vector (Mock) were concentrated followed by western blot analysis. **(H)** Isolated microvesicles (MV) and exosomes, together with total cell extracts from Neuro2a cells co-transfected with polyQ$_{79}$-EGFP and IGF2 expression vectors or empty vector (Mock) were analyzed by western blot. In all quantifications, average and SEM of at least three independent experiments are shown. Statistically significant differences detected by two-tailed unpaired *t*-test (***: $p < 0.001$; **: $p < 0.01$; *: $p < 0.05$).

Figure 7. IGF2 signaling induces the release of polyQ$_{79}$ aggregates through cytoskeleton remodeling. (A) Quantitative proteomics was performed in protein extracts derived from Neuro2a cells transiently transfected with IGF2 or empty vector (Mock) for

bioRxiv preprint doi: https://doi.org/10.1101/2020.05.28.119164. this version posted June 10, 2020. The copyright holder for this preprint (which was not certified by peer review) is the author/funder. All rights reserved. No reuse allowed without permission.

24 h. Data was analyzed and plotted in a volcano graph as fold-change. Vertical dashed lines indicate a log2 > 0.1 of fold change. Proteins related to actin cytoskeleton function are highlighted in green. Dots in blue represent associated proteins to actin cytoskeleton with a log2 < 0.1 fold-change. **(B)** Bioinformatics analysis of quantitative proteomics to uncover molecular processes affected by IGF2 expression after a functional enrichment analysis. Blue scale refers to the number of proteins that are known to be involved in each pathway. Red scale refers to the number of proteins altered in IGF2 overexpressing cells for each pathway. **(C)** Neuro2a cells were transfected with a plasmid encoding Life-Actin to monitor actin cytoskeleton dynamics. Cells were plated onto fibronectin-coated plates and recorded by time-lapse confocal microscopy every 40 s for 5 min. Time-lapse microscopy was performed after treatment with IGF2-enriched media (left panel). Quantification of cortical and internal actin clusters is shown (right panel). **(D)** Phalloidin-rhodamine staining of MEF cells after 5 min of treatment with IGF2-enriched media. Scale bar, 50 µm (right panel). Quantification of actin clusters is presented (left panel). **(E)** Neuro2a cells were treated with IGF2-enriched media or control media derived from Mock transfected cells. After 5 min, cells were lysed and cell extracts prepared to measure Rac1-GTP levels by pull-down assay using GST-CRIB domain. Pull down and total cell lysates were evaluated by western blot using anti-Rac1 antibody. Total Rac1 and tubulin monitored as loading control (upper panel). Rac1-GTP levels were quantified and normalized to total Rac1 and tubulin (lower panel). **(F)** Neuro2a cells were transfected with Rac_{N17} or Rac_{V12} or empty vector (Mock). 24 h later cells were co-transfected with expression vectors for $polyQ_{79}$-EGFP and IGF2 or empty vector (Mock) and then incubated with Optimem. The presence of $polyQ_{79}$-EGFP in the cell culture media was determined using dot blot (upper panel) and quantified (lower panel). **(G)** Neuro2a cells were co-transfected with expression vectors for $polyQ_{79}$-EGFP and IGF2 or empty vector (Mock). Then, cell culture media was replaced for Optimem for 8 h and treated with 100 µM NSC23766 (NSC) for additional 16 h. Cell culture media was collected and analyzed by dot blot using an anti-GFP antibody (upper panel) and quantified (lower panel). Image was cropped from the same membrane and film exposure. **(H)** Neuro2a cells were co-transfected with $polyQ_{79}$-EGFP plasmid and IGF2 plasmid or empty vector (Mock) for 8 h and then treated with 100 µM NSC23766 (NSC) or vehicle for additional 16 h. $PolyQ_{79}$-EGFP aggregates were analyzed in cell lysates by western blot using anti-GFP antibody. Hsp90 expression was monitored as loading control (left panel). $PolyQ_{79}$-EGFP aggregates were quantified and normalized to Hsp90 levels (right

bioRxiv preprint doi: https://doi.org/10.1101/2020.05.28.119164. this version posted June 10, 2020. The copyright holder for this preprint (which was not certified by peer review) is the author/funder. All rights reserved. No reuse allowed without permission.

panel). In all quantifications, average and SEM of at least three independent experiments are shown. Statistically significant differences detected by two-tailed unpaired *t*-test (***: $p < 0.001$; *: $p < 0.05$).

Figure 8. Gene therapy to deliver IGF2 into the striatum reduces mHtt aggregation in HD mouse models. (A) Three-month-old wild type mice were co-injected with adeno-associated viral (AAV) vectors expressing mHtt588Q$_{95}$-RFP and IGF2 or empty vector (Mock). Two weeks later, the striatum was dissected and mHtt aggregation was analyzed in total protein extracts by western blot analysis using anti-polyQ antibody. DARPP32 levels were also determined in the same samples. Hsp90 and tubulin expression were monitored as loading control. The presence of the monomer is indicated with an arrowhead. mHtt588Q$_{95}$-RFP aggregates and monomers or DARPP32 levels were quantified and normalized to Hsp90 levels (lower panel) (AAV-Mock: n = 5; AAV-IGF2: n = 6). **(B)** Three-month-old YAC128 transgenic mice were injected with AAV-IGF2 or AAV-Mock into the striatum using bilateral stereotaxis. Four weeks later, the striatum was dissected and mHtt aggregation monitored by western blot using anti-polyQ antibody. Tubulin expression was monitored as loading control (upper panel). mHtt aggregates levels were quantified and normalized to tubulin levels (lower panel) (AAV-Mock: n = 6; AAV-IGF2: n = 5). **(C)** YAC128 mice were injected at postnatal stage (P1-P2) into the ventricle with AAV-IGF2 or AAV-Mock. Three months later, striatum was dissected and mHtt aggregation levels were analysed by western blot using anti-polyQ antibody. Hsp90 levels were determined as loading control (left panel). mHtt aggregates levels were quantified and normalized to Hsp90 levels (right panel) (AAV-Mock: n = 5; AAV-IGF2: n = 4). **(D)** YAC128 and littermate control mice were injected with AAVs as indicated in (c). Motor performance was monitored once every two weeks from 3 months to 8 months old. The analysis shows the average of the group at each time point (AAV-Mock: n = 11; AAV-IGF2: n = 9). Statistically significant differences detected by two-tailed unpaired *t*-test (**: $p < 0.001$; *: $p < 0.05$). **(E)** R6/2 mice were injected at 4 weeks of age with AAV-IGF2 of AAV-Mock into the striatum using bilateral stereotaxis. Four weeks after the injection, mice were perfused, the brain was extracted and coronal slices from the striatum were obtained. Mutant huntingtin and HA-epitope were detected using the EM48 and anti-HA antibodies, respectively. Nuclei were stained using DAPI. High-resolution images of the slices were obtained using fluorescence microscopy and quantification of mutant huntingtin and DAPI-positive cells was performed using Image

bioRxiv preprint doi: https://doi.org/10.1101/2020.05.28.119164. this version posted June 10, 2020. The copyright holder for this preprint (which was not certified by peer review) is the author/funder. All rights reserved. No reuse allowed without permission.

J software. **(F)** Quantification of the number of mutant huntingtin inclusions was performed by total area (left panel) and number of DAPI-positive cells (right panel). (AAV-Mock: n = 4; AAV-IGF2: n = 4). Statistically significant differences detected by two-tailed unpaired t-test (***: $p<0.001$; **: $p<0.01$; *: $p<0.05$)

Figure 9. IGF2 levels are downregulated in the brain and blood of HD patients. (A) IGF2 protein levels were measured by western blot in human post mortem samples containing the caudate-putamen region from HD patients in stages 3 and 4. GADPH was monitored as loading control (left panel). IGF2 levels were quantified and normalized to GADPH levels (right panel). **(B)** Total protein extracts were generated from freshly isolated peripheral blood mononuclear cells (PBMCs) from HD patients and control subjects. IGF2 expression levels were determined using western blot analysis. GADPH was determined as loading control (left panel). IGF2 levels were quantified and normalized to GADPH levels (right panel). **(C)** *Igf2* mRNA levels were measured by real-time PCR in PBMCs obtained from HD patients and control subjects. **(D)** IGF2 content in plasma from blood obtained from HD patients and control subjects was measured by ELISA. In all quantifications, statistically significant differences detected by two-tailed unpaired *t*-test (***: p <0.001; **: p < 0.01; *: p < 0.05). **(E)** Proposed model: IGF2 reduces mHtt levels through unconventional secretion. In HD patients, the downregulation of IGF2 expression enhances the content of mHtt (left panel). When IGF2 is upregulated using gene therapy, IGF2R signalling enhances the secretion of mHtt into the extracellular space involving actin cytoskeleton remodelling and possibly microvesicles and exosomes (right panel).

Supplementary material

Supplementary Fig. S1 XBP1 deficiency does not alter *Igf1* mRNA levels. (A) *Igf2* mRNA levels were measured by real-time PCR in cDNA generated from striatal tissue of 9-months old XBP1$_{cKO}$-YAC128 mice. Data represents the average and SEM of the analysis of 3 animals per group. **(B)** *Igf1* mRNA levels were measured by real-time PCR in cDNA generated from striatal tissue of 9-months old XBP1$_{cKO}$-YAC128 mice. Data represents the average and SEM of 5 animals. Statistically significant differences detected by one-tailed unpaired *t*-test (**: p < 0.01).

bioRxiv preprint doi: https://doi.org/10.1101/2020.05.28.119164. this version posted June 10, 2020. The copyright holder for this preprint (which was not certified by peer review) is the author/funder. All rights reserved. No reuse allowed without permission.

Supplementary Fig. S2 IGF2 expression reduces polyQ$_{79}$ aggregation. (A) PolyQ$_{79}$-EGFP monomers from Fig. 2B were analyzed in whole cell extracts by western blot analysis using an anti-GFP antibody (left panel). PolyQ$_{79}$-EGFP monomer levels after 24 and 48h of expression were quantified and normalized to Hsp90 levels (middle and right panel, respectively). **(B)** Neuro2a cells were co-transfected with a polyQ$_{79}$-EGFP expression vector and IGF2 plasmid or empty vector (Mock). 24 h later, cells were collected in Trizol and *Gfp* mRNA levels were measured by semi-quantitative PCR. Values represent the mean and SEM of at least three independent experiments. **c** Quantification of filter trap experiment from Fig. 2c (time point 48 h).

Supplementary Fig. S3 IGF2 does not inhibit global protein synthesis or degradation. (A) HEK293T cells were co-transfected with GFP-mHttQ$_{43}$ expression vector with IGF2 plasmid (right, upper panel) or empty vector (left, upper panel), and then pulse labeled with ^{35}S for indicated time points. Autoradiography (AR) represents total proteins that were synthesized in the time of harvesting cells. All data were normalized to time point 0 h (lower panel). **(B)** HEK293T cells were co-transfected with GFP-mHttQ$_{43}$ expression vector with IGF2 plasmid (right, upper panel) or empty vector (Mock) (left, upper panel), and then pulse labeled with ^{35}S for indicated time points to follow the decay of the labeled protein while chasing with unlabeled precursor. Autoradiography (AR) represents total extracts in each time (upper panel). All data were normalized to time point 1 h (lower panel). **(C)** HEK293T cells were transfected with GFP-mHttQ$_{43}$ and IGF2 expression vectors. Pulse was performed 24 h after transfection. Cells were treated with 30 μM chloroquine (CQ) or 1 μM bortezomib (Bort) at the beginning of the chasing for additional 21 h (upper panel). Ubiquitin, p62 and LC3 were measured as control of the autophagy inhibition.

Supplementary Fig. S4 Proteasome, autophagy or conventional secretion are not involved in the reduction of polyQ$_{79}$ levels after IGF2 expression (control experiments). (A) Neuro2a cells were co-transfected with expression vectors for polyQ$_{79}$-EGFP and IGF2 or empty vector (Mock). After 8 h, cells were treated with 1 μM MG132 for additional 16 h. PolyQ$_{79}$-EGFP inclusions were visualized by fluorescence microscopy (upper panel) and polyQ$_{79}$-EGFP aggregation levels measured by filter trap (lower panel). Image cropped from the same membrane and film. **(B)** Filter trap assay was performed to detect polyQ$_{79}$-EGFP aggregates using the same cells extracts of Fig. 4E using an anti-GFP antibody (upper panel) and quantified (lower panel). Image cropped

bioRxiv preprint doi: https://doi.org/10.1101/2020.05.28.119164. this version posted June 10, 2020. The copyright holder for this preprint (which was not certified by peer review) is the author/funder. All rights reserved. No reuse allowed without permission.

from the same membrane and film. **(C)** Neuro2a cells were transfected with IGF2 for 8 h and then treated with 1 μM lactacystin (Lact) or 1 μM MG132 for additional 16 h. Ubiquitin accumulation was measured by western blot to confirm the activity of the inhibitors. Hsp90 expression was measured as loading control. **(D)** Neuro2a cells where co-transfected with IGF2 plasmid or empty vector (Mock) in the presence or absence of polyQ$_{79}$-EGFP expression vector for 8 h, and then treated with 30 μM chloroquine (CQ) for additional 16 h. p62 levels were monitored by western blot using anti-p62 antibody. Hsp90 expression was monitored as loading control (upper panel). p62 levels were quantified and normalized to Hsp90 (lower panel). **(E)** Neuro2a cells were co-transfected with polyQ$_{79}$-EGFP and IGF2 expression vectors or empty vector (Mock) for 8 h, and then treated with 30 μM CQ for additional 16 h. p62 and LC3 levels were measured by western blot as control for autophagy inhibitors in experiment shown in Fig. 4H. Hsp90 levels were determined as loading control. **(F)** HEK293T cells were co-transfected with polyQ$_{79}$-EGFP and IGF2 expression vectors or empty vector (Mock). After 8 h cells were treated with 30 μM chloroquine (CQ) for additional 16 h. PolyQ$_{79}$-EGFP aggregation was analyzed in whole cells extracts by western blot using anti-GFP antibody. Hsp90 expression was monitored as loading control (left panel). PolyQ$_{79}$-EGFP aggregates levels were quantified and normalized to Hsp90 levels (right panel). **(G)** Filter trap assay was performed using the same cells extracts analyzed in (F) and polyQ$_{79}$-EGFP aggregates detected using anti-GFP antibody (upper panel) and quantified (lower panel). **(H)** HEK293T cells were transiently transfected with IGF2 expressing vector (IGF2) or empty plasmid (Mock) for 8 h, and then treated with 30 μM CQ for additional 16 h. p62 and LC3 levels were measured by western blot as control for autophagy inhibitors in experiment shown in Fig. 4F and Fig. 4G. Hsp90 levels were determined as loading control. **(I, J)** Neuro2a cells were co-transfected with polyQ$_{79}$-EGFP and IGF2 or empty vector (Mock) for 8 h and then treated with 200 nM bafilomycin A$_1$ (Baf) or 250 mM 3-methyladenine (3-MA) for additional 16 h. PolyQ$_{79}$-EGFP aggregation was analyzed in cell lysates using western blot with an anti-GFP antibody. Hsp90 or GAPDH expressions were monitored as loading control. In all quantifications, average and SEM of at least three independent experiments are shown. Statistically significant differences detected by two-tailed unpaired *t*-test (**: $p < 0.01$; *: $p < 0.05$). **(K)** HEK293 cells were co-transfected with FL-Htt103Q and IGF2 plasmid or empty vector (Mock). 24 h later, culture media was collected and loaded for dot blot detection of FL-Htt103Q using anti-Htt antibody. **(L)** Neuro2a cells were co-transfected with a polyQ$_{79}$-EGFP expression

bioRxiv preprint doi: https://doi.org/10.1101/2020.05.28.119164. this version posted June 10, 2020. The copyright holder for this preprint (which was not certified by peer review) is the author/funder. All rights reserved. No reuse allowed without permission.

vector and IGF2 plasmid or empty vector (Mock). 48 h later, cell death was measured by FACS after propidium iodide staining. **(M)** NanoSight profile of exosomes purified form IGF2 expressing cells. Isolated exosomes from Neuro2a cells co-transfected with polyQ$_{79}$-EGFP and IGF2 plasmid or empty vector (Mock) were analyzed by NanoSight nanotracking analysis and plotted by size to confirm proper purification method. **(M)** Western blot analysis of enriched fractions of microvesicles (MV) and exosomes using the markers Alix and CD63.

Supplementary Fig. S5 Gene therapy to deliver IGF2 into the brain. (A) Neuro2a cells were co-transfected with expression vectors for mHtt588Q$_{95}$-RFP and IGF2 plasmid or empty vector (Mock) using an AAV back bound. After 24 h, mHttQ$_{95}$-RFP inclusions were visualized by fluorescence microscopy (left panel). Protein aggregation was analyzed in whole cells extracts by western blot (right panel). Hsp90 was measured as loading control. **(B)** *Igf2-HA* expression was confirmed by conventional PCR in cDNA obtained from dissected striatum of animals co-injected with AAV mHtt588Q$_{95}$-RFP and AAV-IGF2 or AAV-Mock showed in Figure 8A. **(C)** *Igf2-HA* expression was confirmed by conventional PCR in cDNA obtained from dissected striatum of YAC128 animals injected with AAV-IGF2 or AAV Mock intra-cerebroventricular at neonatal stage P1-P2 showed in Figure 8C.

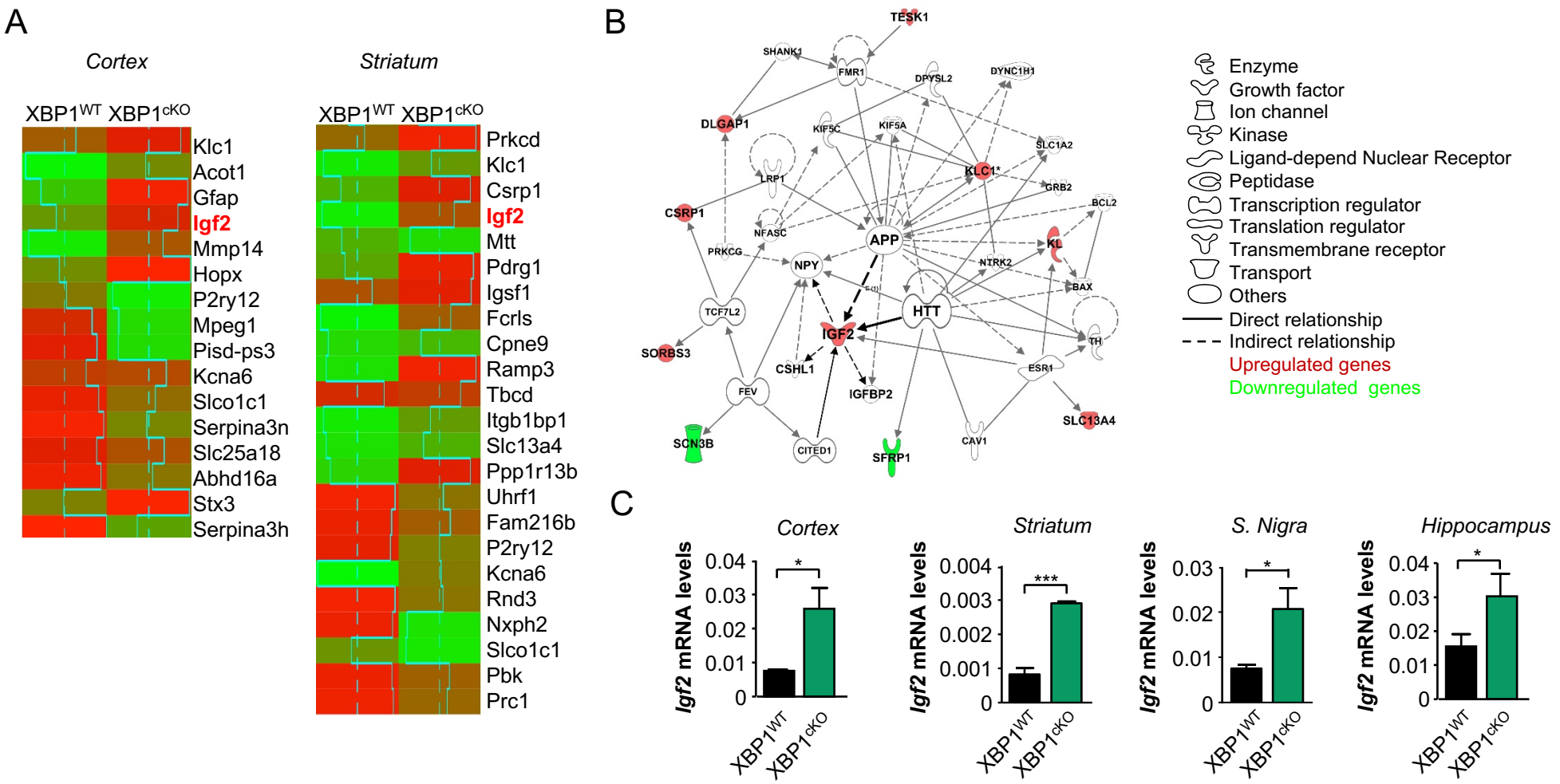
A
Cortex
XBP1WT XBP1cKO
Klc1
Acot1
Gfap
Igf2
Mmp14
Hopx
P2ry12
Mpeg1
Pisd-ps3
Kcna6
Slco1c1
Serpina3n
Slc25a18
Abhd16a
Stx3
Serpina3h
Striatum
XBP1WT XBP1cKO
Prkcd
Klc1
Csrp1
Igf2
Mtt
Pdrg1
Igsf1
Fcrls
Cpne9
Ramp3
Tbcd
Itgb1bp1
Slc13a4
Ppp1r13b
Uhrf1
Fam216b
P2ry12
Kcna6
Rnd3
Nxph2
Slco1c1
Pbk
Prc1
B
TESK1
SHANK1
FMR1
DPYSL2
DYNC1H1
DLGAP1
KIF5C
KIF5A
SLC1A2
LRP1
KLC1*
GRB2
CSRP1
NFASC
APP
BCL2
PRKCG
NPY
NTRK2
KL
BAX
TCF7L2
HTT
SORBS3
IGF2
TH
CSHL1
ESR1
FEV
IGFBP2
SLC13A4
SCN3B
CITED1
CAV1
SFRP1
Enzyme
Growth factor
Ion channel
Kinase
Ligand-depend Nuclear Receptor
Peptidase
Transcription regulator
Translation regulator
Transmembrane receptor
Transport
Others
Direct relationship
Indirect relationship
Upregulated genes
Downregulated genes
C
Cortex
Striatum
S. Nigra
Hippocampus
Igf2 mRNA levels
0.04
0.03
0.02
0.01
0
0.004
0.003
0.002
0.001
*
***
XBP1WT
XBP1cKO

Figure 1

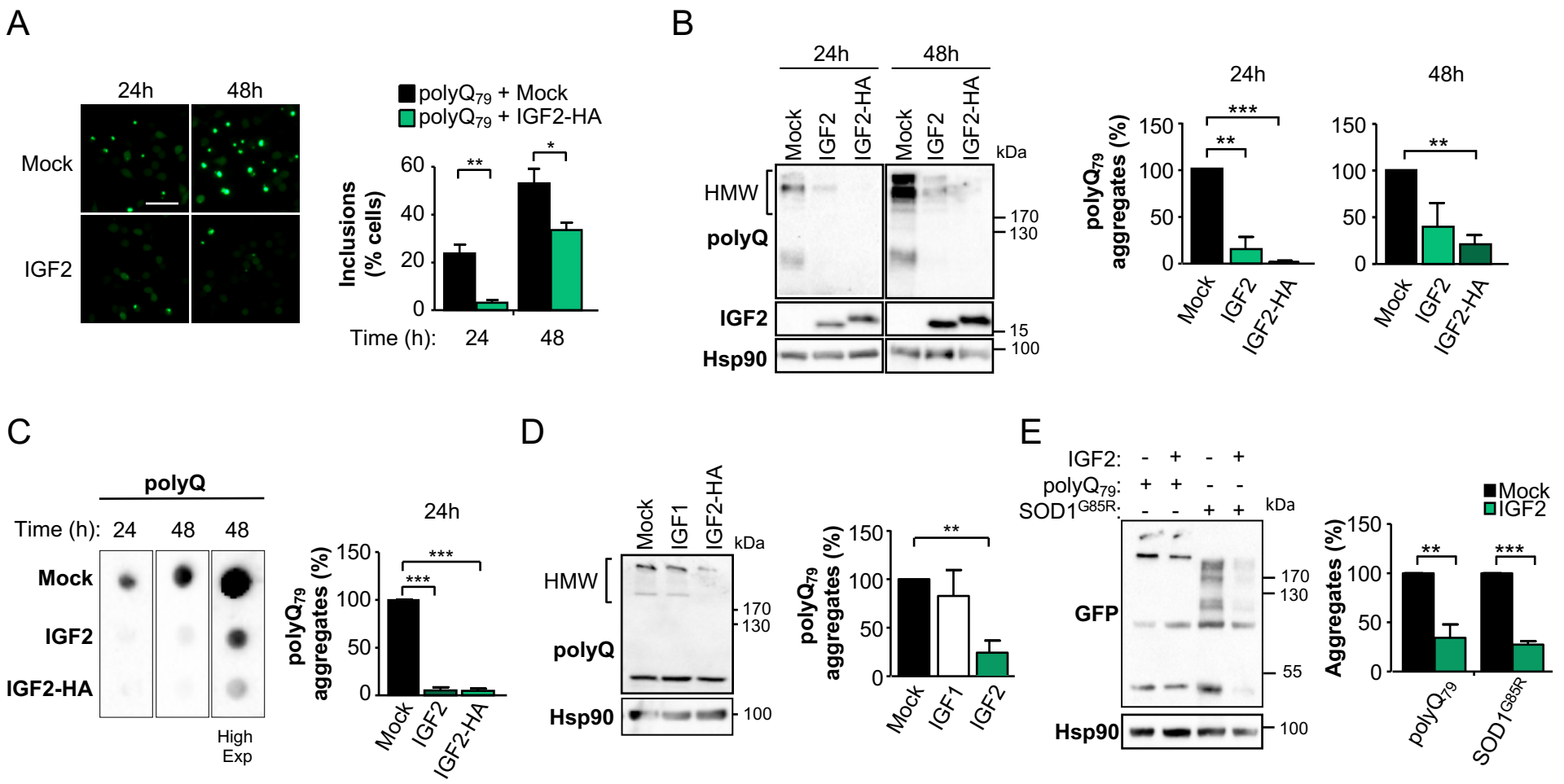
A
24h
48h
Mock
IGF2
polyQ79 + Mock
polyQ79 + IGF2-HA
Inclusions (% cells)
60
40
20
0
**
*
Time (h): 24 48
B
24h
48h
Mock
IGF2
IGF2-HA
kDa
HMW
polyQ
IGF2
Hsp90
170
130
15
100
polyQ79 aggregates (%)
150
100
50
0
***
**
C
polyQ
Time (h): 24 48 48
Mock
IGF2
IGF2-HA
High Exp
D
Mock
IGF1
IGF2-HA
E
IGF2:
polyQ79:
SOD1G85R:
GFP
55
Aggregates (%)
polyQ79
SOD1G85R

Figure 2

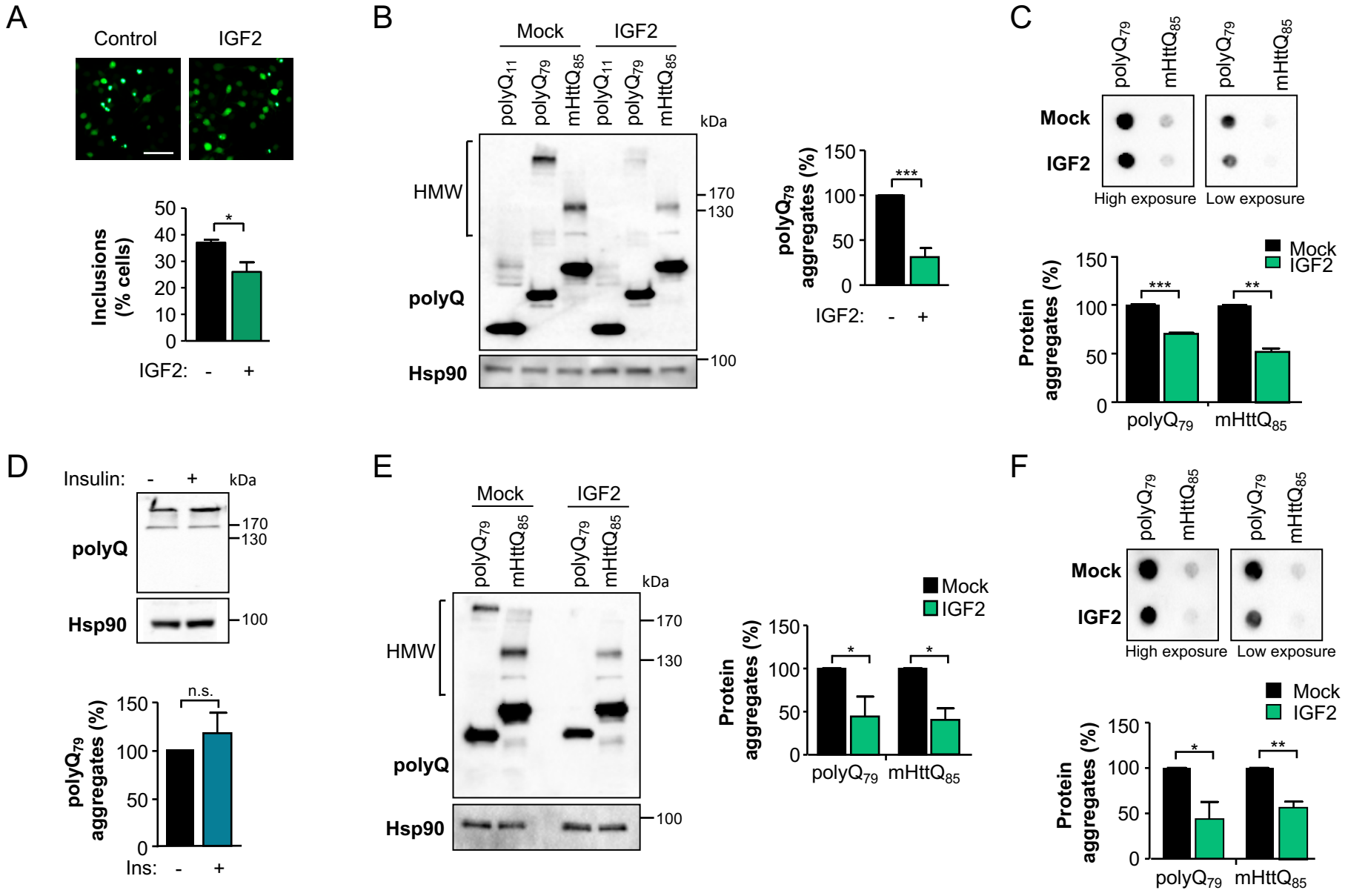
A
Control
IGF2
Inclusions (% cells)
IGF2: - +
B
Mock
IGF2
polyQ11
polyQ79
mHttQ85
kDa
HMW
polyQ
Hsp90
170
130
100
polyQ79 aggregates (%)
IGF2: - +
C
High exposure
Low exposure
Mock
IGF2
Protein aggregates (%)
polyQ79
mHttQ85
D
Insulin: - +
kDa
polyQ
Hsp90
polyQ79 aggregates (%)
n.s.
Ins: - +
E
Mock
IGF2
polyQ79
mHttQ85
kDa
HMW
polyQ
Hsp90
Protein aggregates (%)
F
High exposure
Low exposure
Mock
IGF2
Protein aggregates (%)

Figure 3

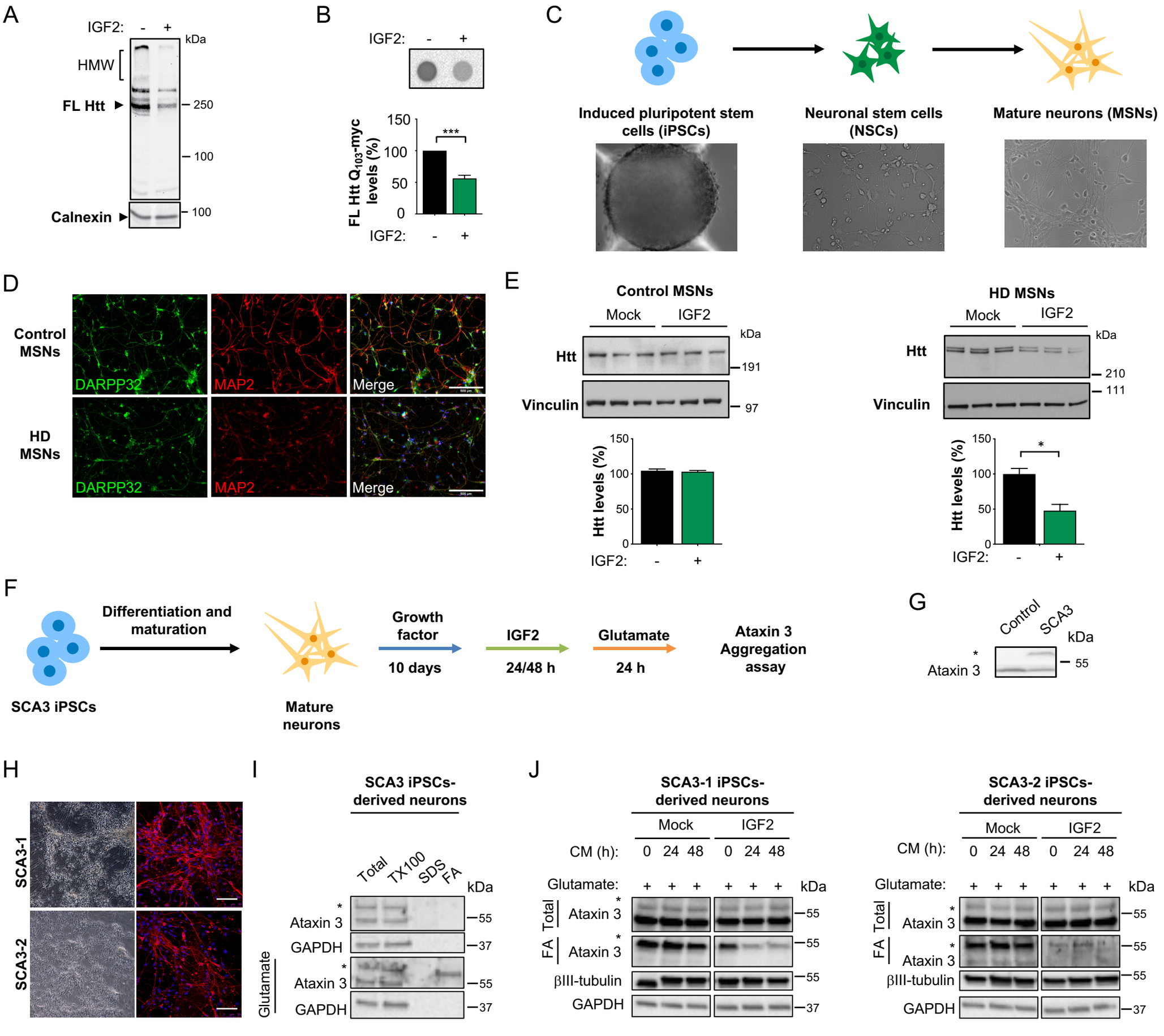
A
IGF2: - +
kDa
HMW
FL Htt
250
100
Calnexin
100
B
IGF2: - +
FL Htt Q103-myc levels (%)
150
100
50
0
***
IGF2: - +
C
Induced pluripotent stem cells (iPSCs)
Neuronal stem cells (NSCs)
Mature neurons (MSNs)
D
Control MSNs
HD MSNs
DARPP32
MAP2
Merge
E
Control MSNs
Mock IGF2
kDa
Htt
191
Vinculin
97
Htt levels (%)
150
100
50
0
IGF2: - +
HD MSNs
Mock IGF2
kDa
Htt
210
111
Vinculin
Htt levels (%)
*
F
Differentiation and maturation
SCA3 iPSCs
Mature neurons
Growth factor
10 days
IGF2
24/48 h
Glutamate
24 h
Ataxin 3 Aggregation assay
G
Control SCA3
kDa
Ataxin 3
55
H
SCA3-1
SCA3-2
I
SCA3 iPSCs-derived neurons
Total TX100 SDS FA
kDa
Glutamate
Ataxin 3
GAPDH
55
37
J
SCA3-1 iPSCs-derived neurons
Mock IGF2
CM (h): 0 24 48 0 24 48
Glutamate: + + + + + +
kDa
Total
FA
Ataxin 3
βIII-tubulin
GAPDH
55
37
SCA3-2 iPSCs-derived neurons
Mock IGF2
CM (h): 0 24 48 0 24 48
Glutamate: + + + + + +
kDa
Total
FA
Ataxin 3
βIII-tubulin
GAPDH
55
37

Figure 4

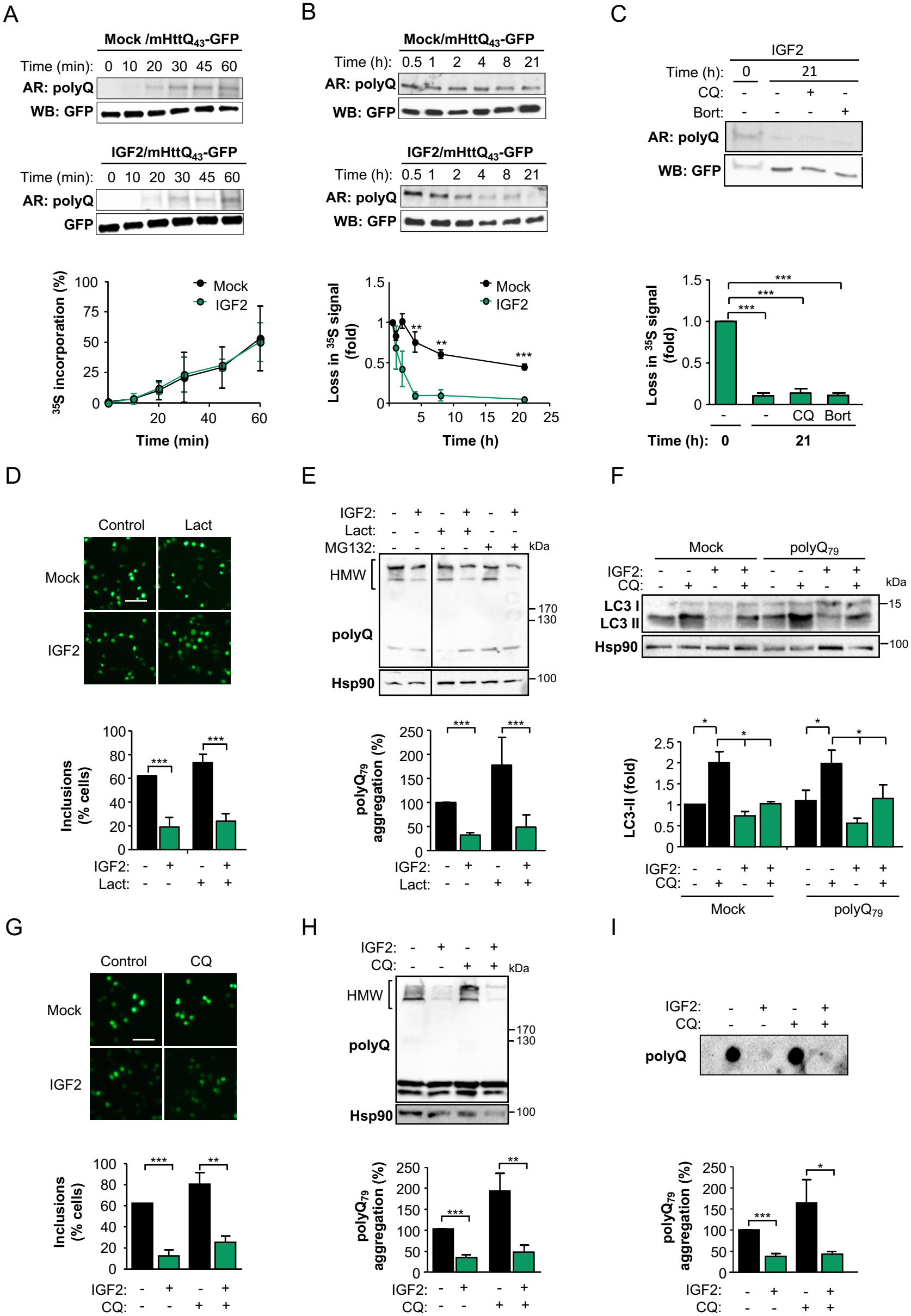
A
Mock /mHttQ43-GFP
Time (min): 0 10 20 30 45 60
AR: polyQ
WB: GFP
IGF2/mHttQ43-GFP
Time (min): 0 10 20 30 45 60
AR: polyQ
GFP
35S incorporation (%)
Mock
IGF2
Time (min)
B
Mock/mHttQ43-GFP
Time (h): 0.5 1 2 4 8 21
AR: polyQ
WB: GFP
IGF2/mHttQ43-GFP
Time (h): 0.5 1 2 4 8 21
AR: polyQ
WB: GFP
Loss in 35S signal (fold)
Mock
IGF2
Time (h)
C
IGF2
Time (h): 0 21
CQ:
Bort:
AR: polyQ
WB: GFP
Loss in 35S signal (fold)
CQ
Bort
Time (h): 0 21
D
Control
Lact
Mock
IGF2
E
IGF2:
Lact:
MG132:
kDa
HMW
polyQ
Hsp90
170
130
100
F
Mock
polyQ79
IGF2:
CQ:
kDa
LC3 I
LC3 II
Hsp90
15
100
Inclusions (% cells)
IGF2:
Lact:
polyQ79 aggregation (%)
IGF2:
Lact:
LC3-II (fold)
IGF2:
CQ:
Mock
polyQ79
G
Control
CQ
Mock
IGF2
Inclusions (% cells)
IGF2:
CQ:
H
IGF2:
CQ:
kDa
HMW
polyQ
Hsp90
170
130
100
polyQ79 aggregation (%)
IGF2:
CQ:
I
IGF2:
CQ:
polyQ
polyQ79 aggregation (%)
IGF2:
CQ:

Figure 5

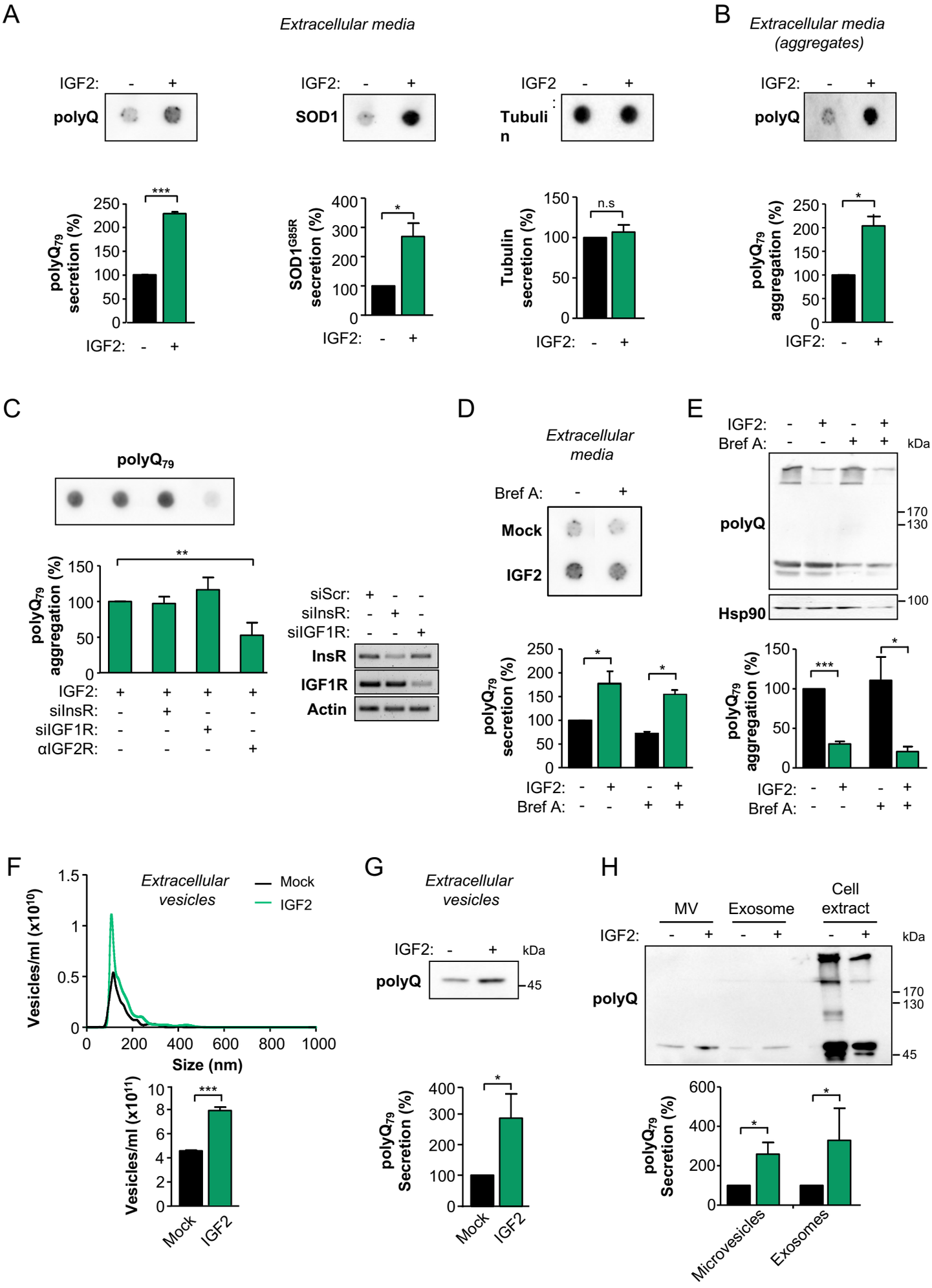
A
Extracellular media
IGF2: - +
polyQ
SOD1
Tubulin
polyQ79 secretion (%)
SOD1G85R secretion (%)
Tubulin secretion (%)
n.s
B
Extracellular media (aggregates)
polyQ79 aggregation (%)
C
polyQ79
polyQ79 aggregation (%)
siScr:
siInsR:
siIGF1R:
αIGF2R:
InsR
IGF1R
Actin
D
Extracellular media
Bref A:
Mock
IGF2
polyQ79 secretion (%)
E
kDa
polyQ
Hsp90
170
130
100
F
Extracellular vesicles
Mock
IGF2
Vesicles/ml (x10^10)
Size (nm)
Vesicles/ml (x10^11)
G
Extracellular vesicles
45
H
MV
Exosome
Cell extract
Microvesicles
Exosomes

Figure 6

A

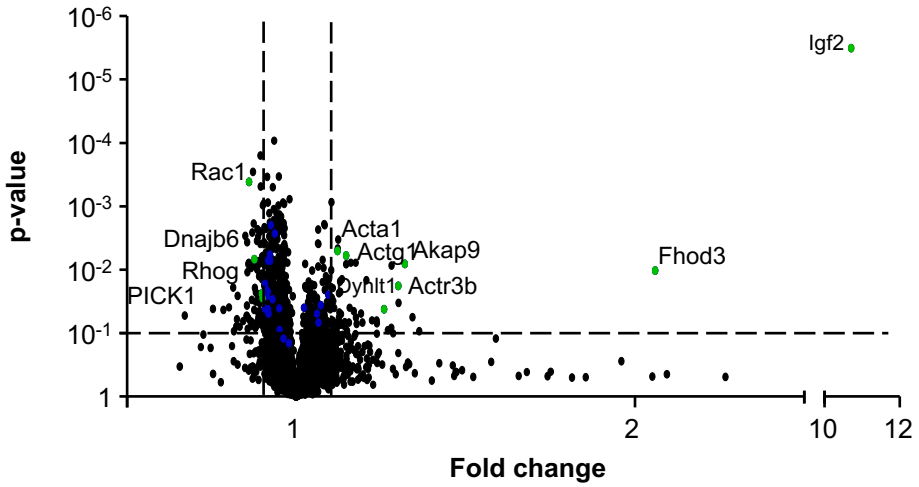

B

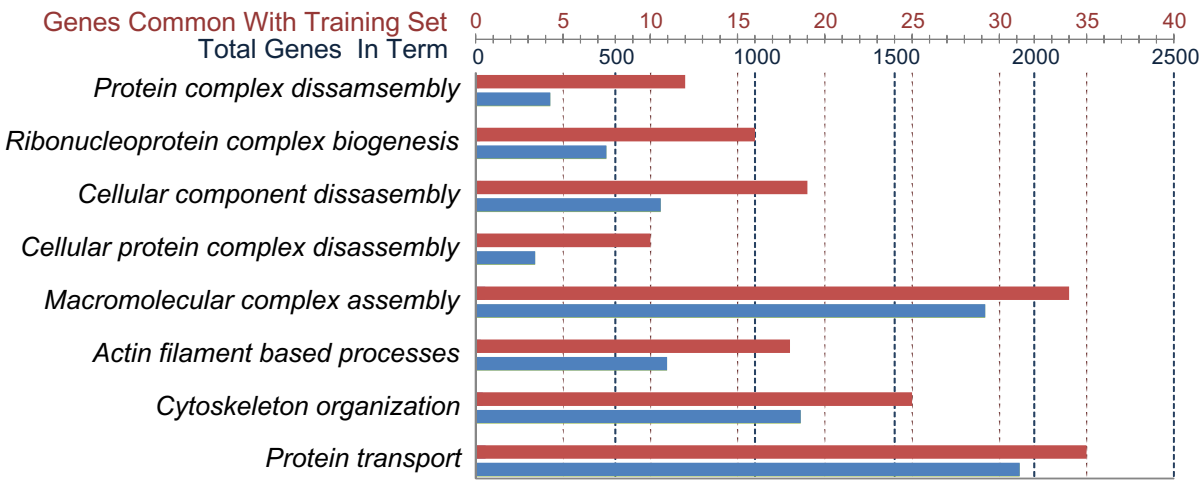

C

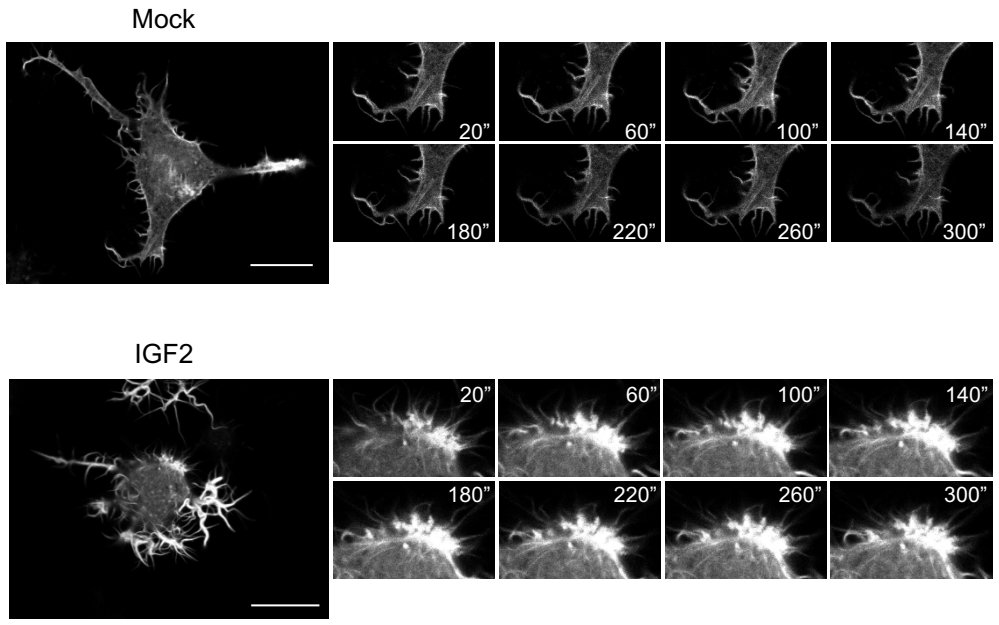

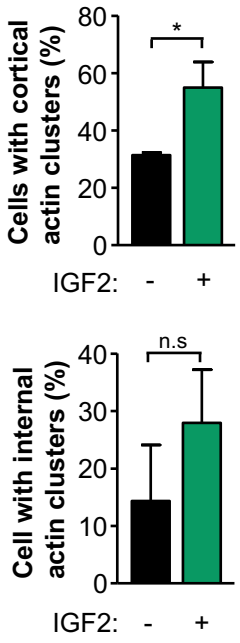

D

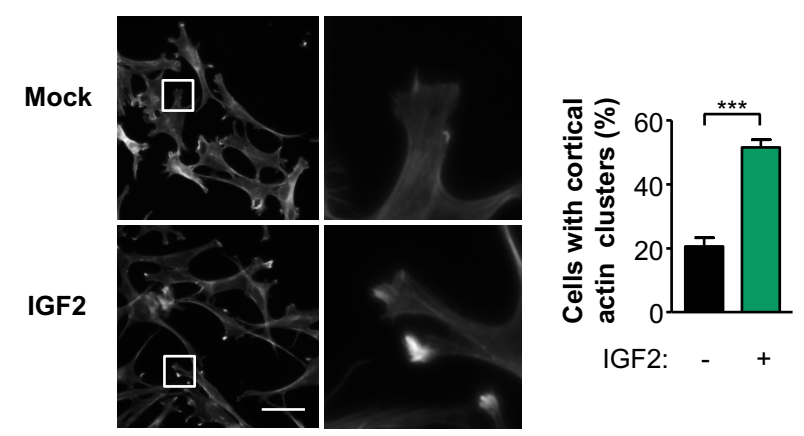

E

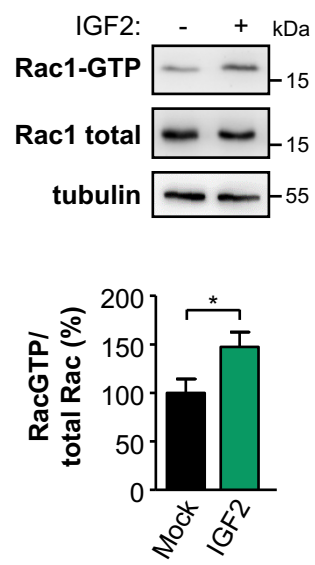

F

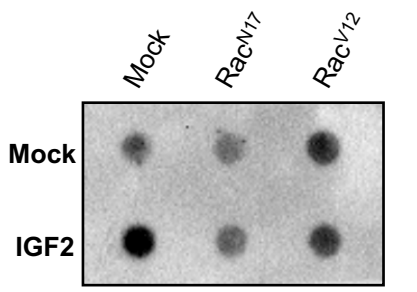

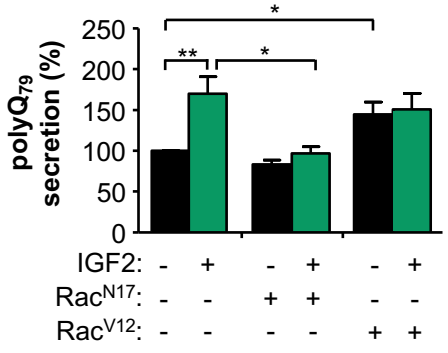

G

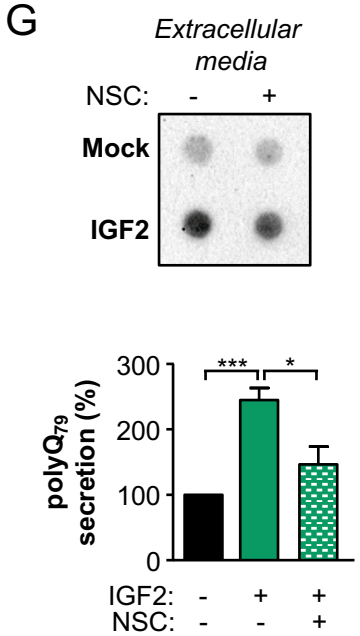

H

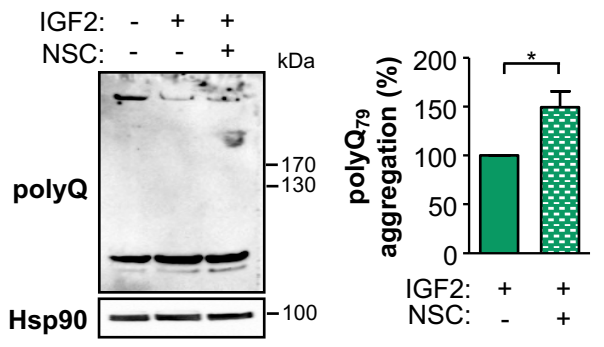

Figure 7

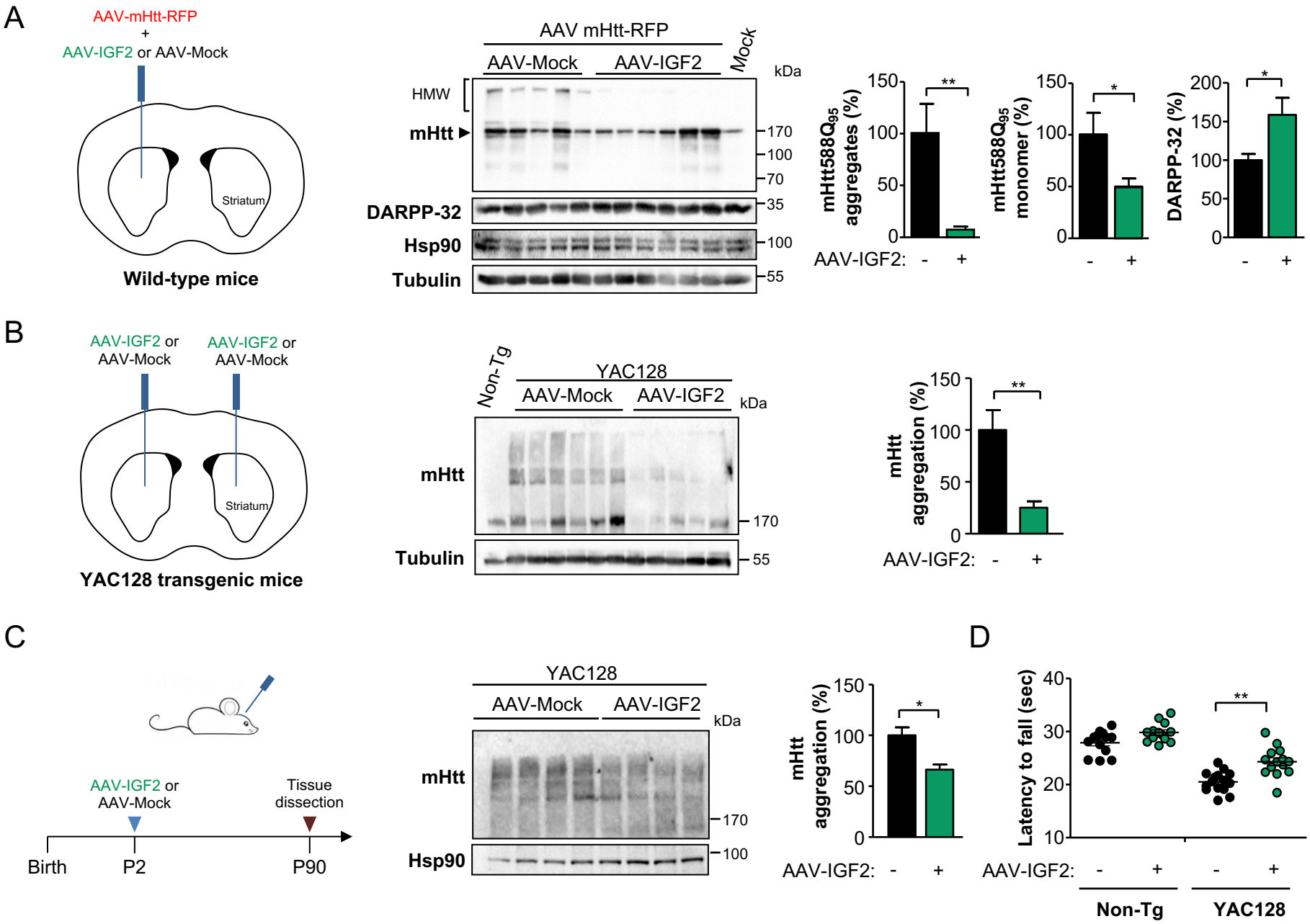
A
AAV-mHtt-RFP
+
AAV-IGF2 or AAV-Mock
Striatum
Wild-type mice
AAV mHtt-RFP
AAV-Mock
AAV-IGF2
Mock
kDa
HMW
mHtt
DARPP-32
Hsp90
Tubulin
170
100
70
35
100
55
mHtt588Q95 aggregates (%)
mHtt588Q95 monomer (%)
DARPP-32 (%)
AAV-IGF2: - +
B
AAV-IGF2 or AAV-Mock
AAV-IGF2 or AAV-Mock
Striatum
YAC128 transgenic mice
Non-Tg
YAC128
AAV-Mock
AAV-IGF2
kDa
mHtt
Tubulin
170
55
mHtt aggregation (%)
AAV-IGF2: - +
C
AAV-IGF2 or AAV-Mock
Tissue dissection
Birth
P2
P90
YAC128
AAV-Mock
AAV-IGF2
kDa
mHtt
Hsp90
170
100
mHtt aggregation (%)
AAV-IGF2: - +
D
Latency to fall (sec)
AAV-IGF2: - + - +
Non-Tg
YAC128
E
AAV-IGF2 or AAV-Mock
AAV-IGF2 or AAV-Mock
Striatum
R6/2 transgenic mice
R6/2 Mock
R6/2 IGF2
EM48
HA
Merge
F
mHtt inclusion/area
mHtt inclusion/DAPI
AAV-IGF2: - +
AAV-IGF2. - +

Figure 8

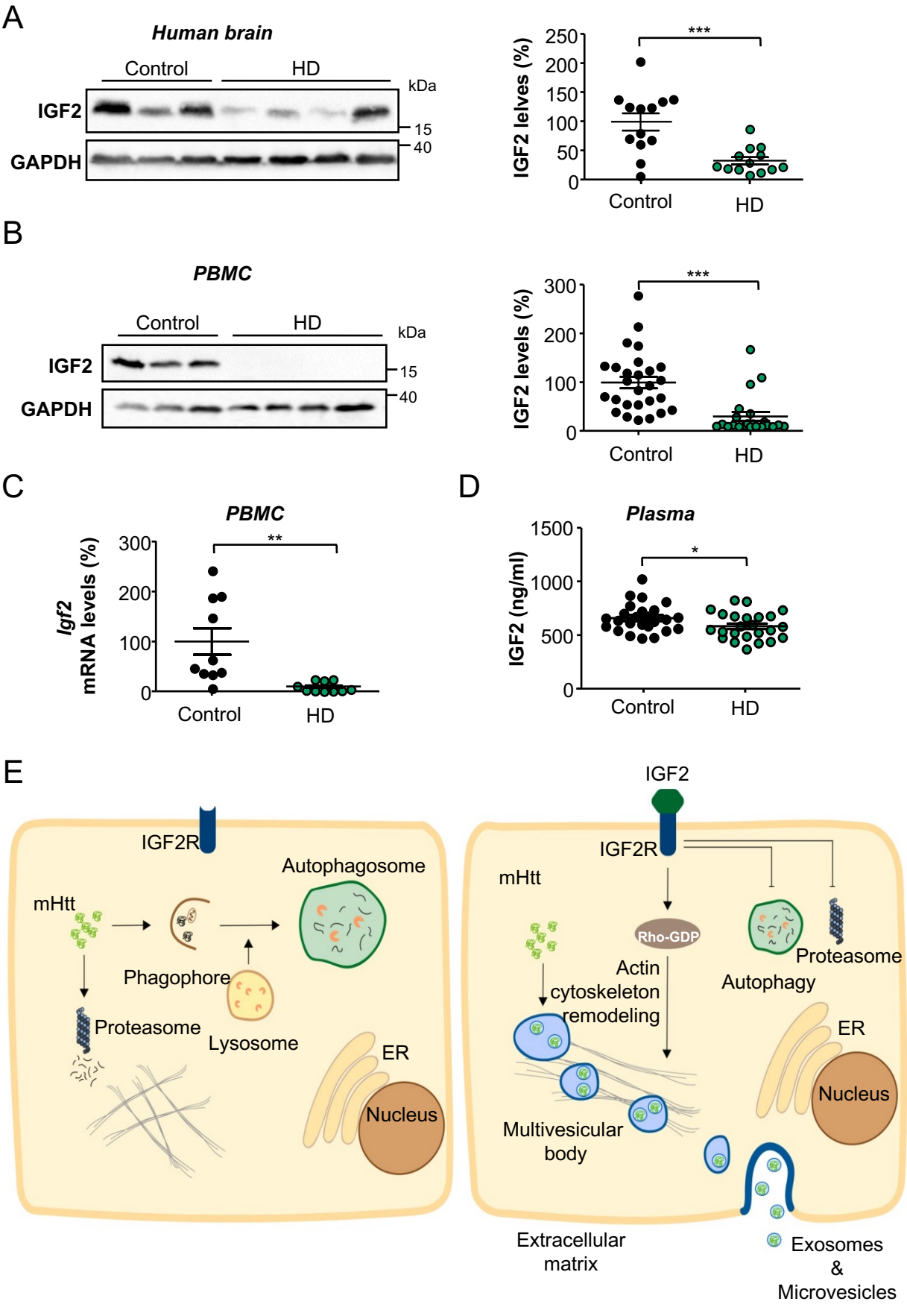
A
Human brain
Control
HD
kDa
IGF2
GAPDH
15
40
IGF2 lelves (%)
250
200
150
100
50
0
***
Control
HD
B
PBMC
Control
HD
kDa
IGF2
GAPDH
15
40
IGF2 levels (%)
300
200
100
0
***
Control
HD
C
PBMC
Igf2 mRNA levels (%)
300
200
100
0
**
Control
HD
D
Plasma
IGF2 (ng/ml)
1500
1000
500
0
*
Control
HD
E
IGF2R
Autophagosome
mHtt
Phagophore
Lysosome
Proteasome
ER
Nucleus
IGF2
IGF2R
mHtt
Rho-GDP
Actin cytoskeleton remodeling
Autophagy
Proteasome
ER
Nucleus
Multivesicular body
Extracellular matrix
Exosomes & Microvesicles

Figure 9

A

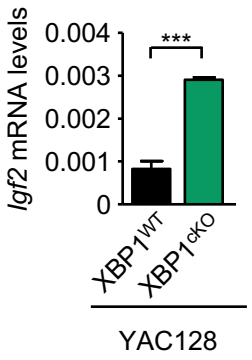

B

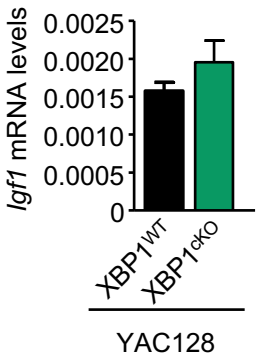

Suplementary figure 1

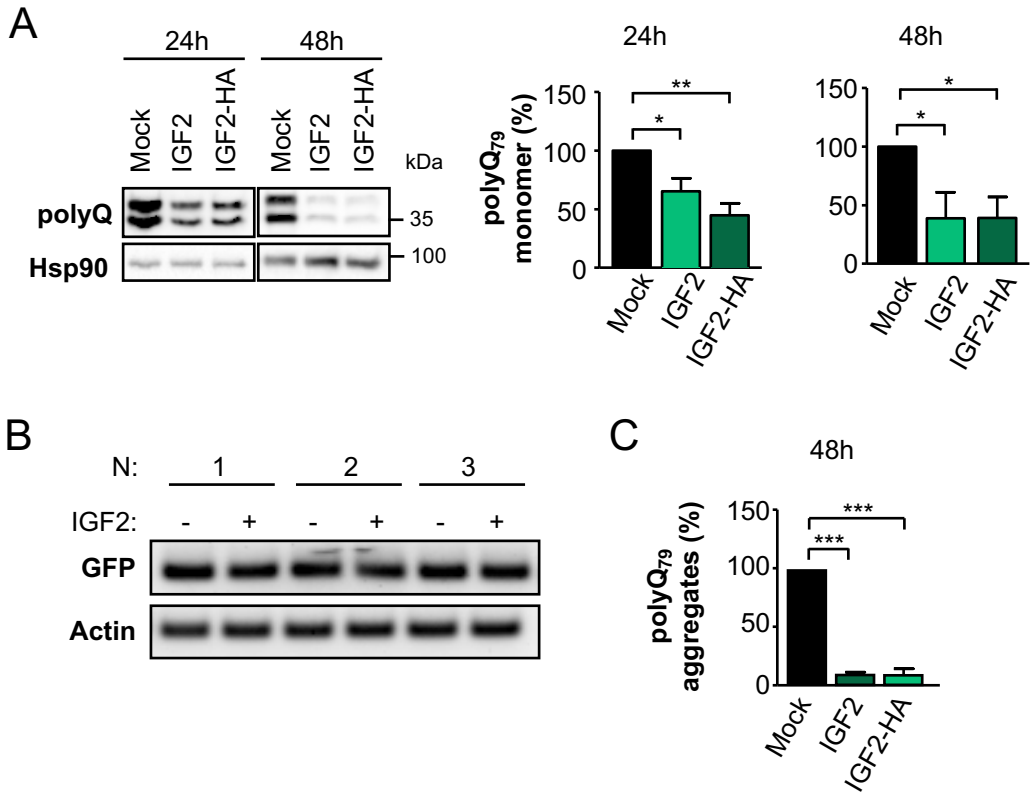

Suplementary figure 2

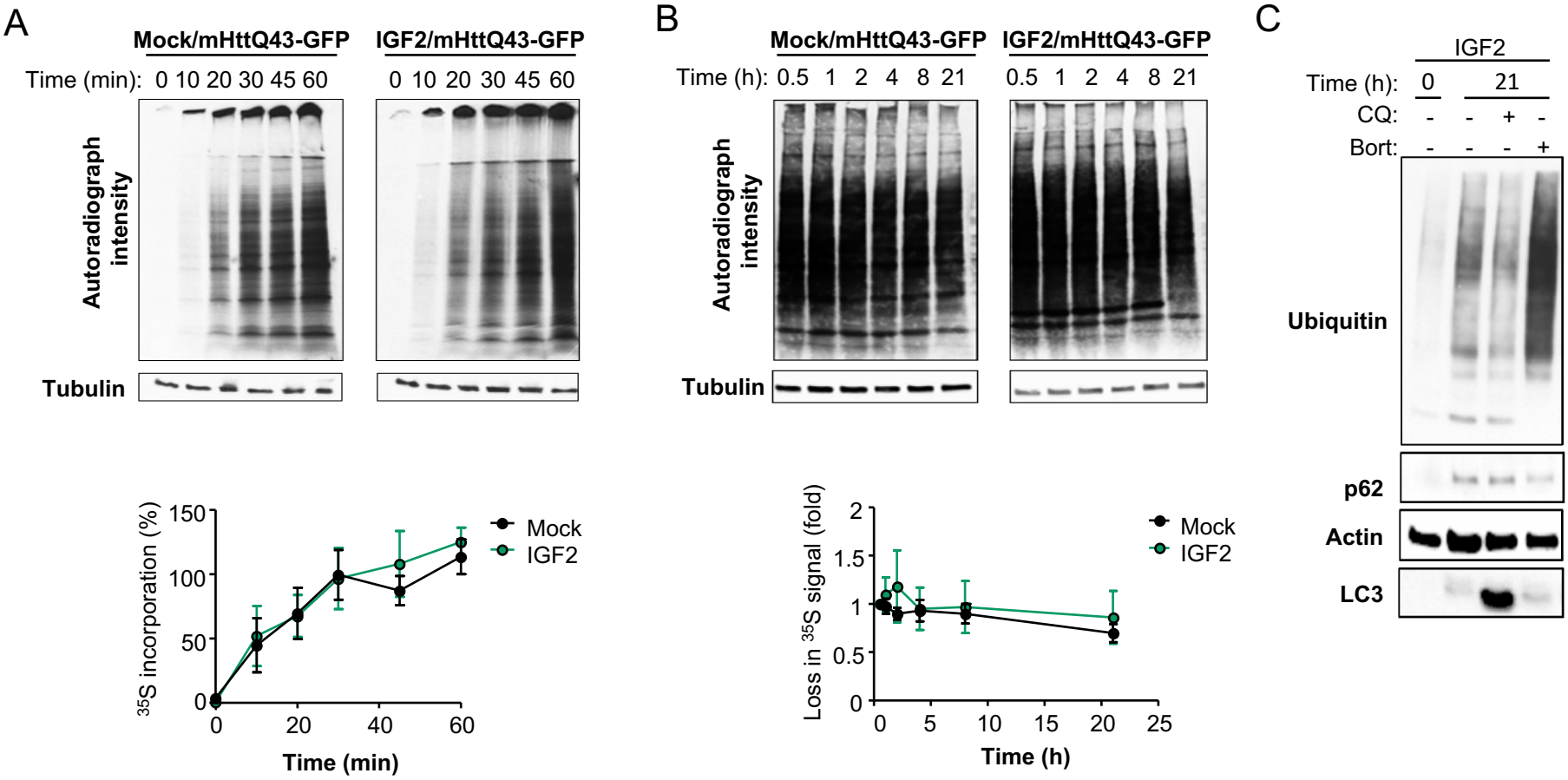

Suplementary figure 3

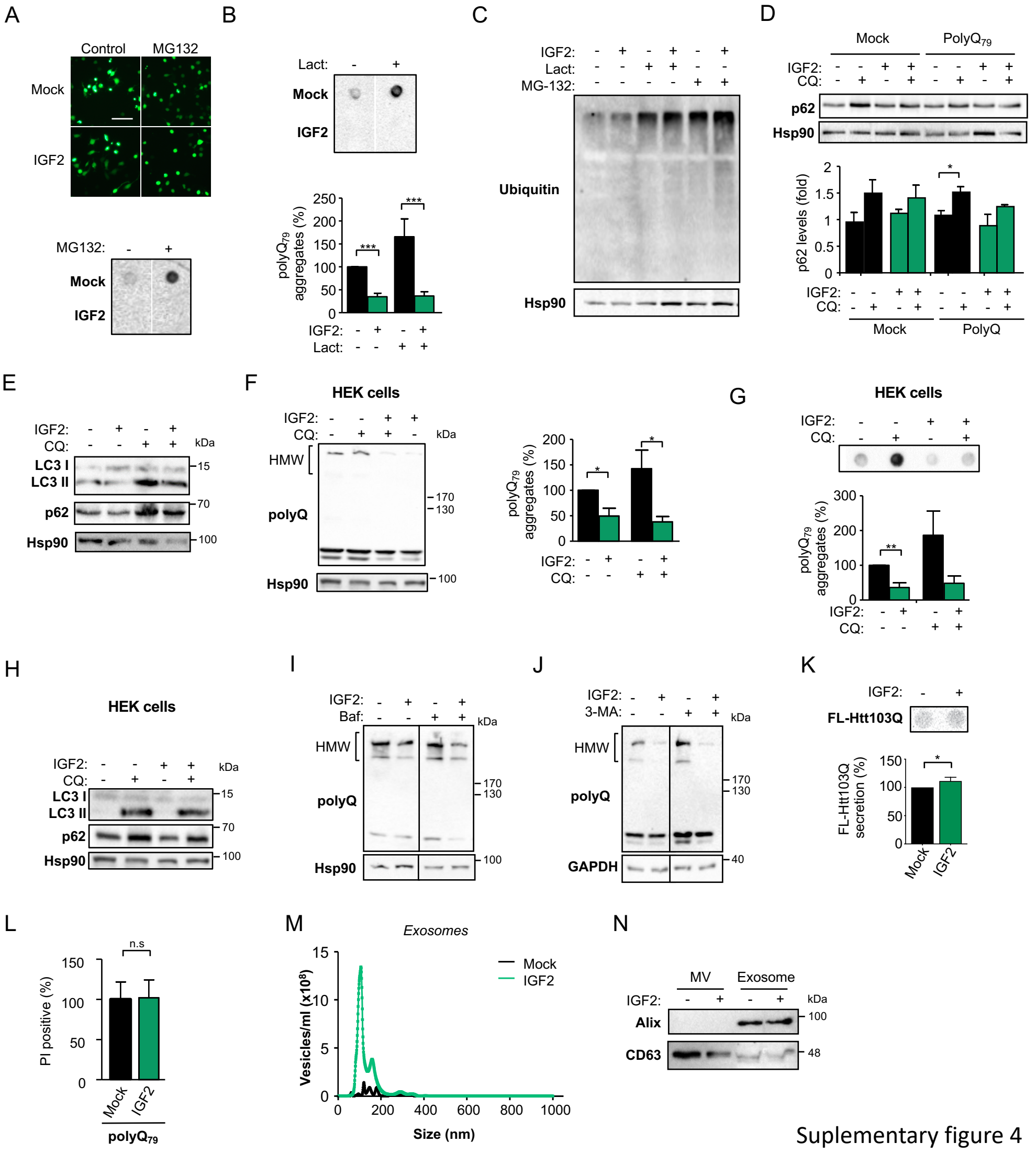

Suplementary figure 4

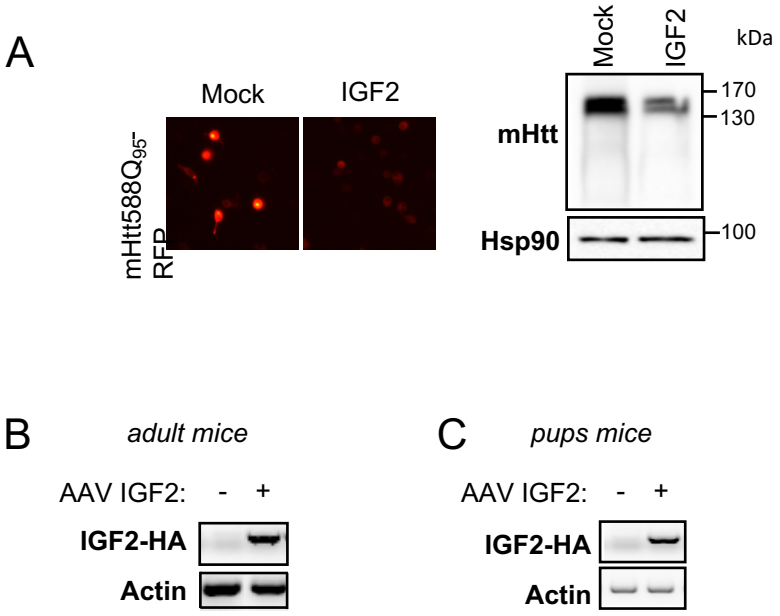

Supplementary figure 5

Table S1A. Top regulated genes in brain cortex of XBP1cKO

Gene	Fold change	q-value (%)
Klc1	1,9	10,7
Acot1	**1,6**	**0**
Gfap	**1,6**	**0**
Igf2	**1,5**	**0**
Mmp14	**1,5**	**0**
Hopx	**1,5**	**0**
P2ry12	-1,8	84,1
Mpeg1	-1,6	89,2
Pisd-ps3	-1,6	89,2
Kcna6	-1,6	89,2
Slco1c1	-1,6	84,1
Serpina3n	-1,6	89,2
Slc25a18	-1,5	89,2
Abhd16a	-1,5	106,4
Stx3	-1,5	89,2
Serpina3h	-1,5	89,2

Table S1B. Top regulated genes in brain striatum of XBP1cKO

Gene	Fold change	q-value (%)
Prkcd	1,9	103,4
Klc1	1,9	103,4
Csrp1	1,8	103,4
Igf2	**1,8**	**0**
Mff	1,8	103,4
Pdrg1	1,7	103,4
Igsf1	1,6	103,4
Fcrls	1,6	103,4
Cpne9	1,6	103,4
Ramp3	1,6	103,4
Tbcd	1,6	103,4
Itgb1bp1	1,6	103,4
Slc13a4	1,6	103,4
Ppp1r13b	1,6	103,4
Uhrf1	**-1,9**	**0**
Fam216b	-1,7	44,6
P2ry12	-1,7	58,3
Kcna6	-1,6	64,1
Rnd3	-1,6	44,6
Nxph2	-1,6	44,6
Slco1c1	-1,6	64,1
Pbk	-1,6	44,6
Prc1	-1,6	44,6

Table S2. Set of proteins modified by IGF2 expression

UniProt ID	Gene	Fold change	St. Dev.	p-value
P09535	Igf2	3,42	0,37	3,2197E-06
Q70FJ1	Akap9	0,40	0,23	0,00814542
Q8BTU1	Gtl3	0,36	0,12	0,00861902
Q8BY02	Nkrf	0,23	0,07	0,00782644
Q8BUV3	Gphn	0,22	0,00	0,00779753
Q9CXV1	Sdhd	0,20	0,00	0,00830573
P63260	Actg1	0,20	0,11	0,00599788
P04441	Cd74	0,17	0,04	0,00337567
P62075	Timm13	0,17	0,08	0,00466175
P68134	Acta1	0,17	0,00	0,00509022
Q99N84	Mrps18b	0,14	0,02	0,00086847
Q6AXC6	Ddx11	0,12	0,00	0,00201253
Q8K2H1	Pphln1	0,11	0,00	0,00191645
Q9CWT6	Ddx28	0,11	0,00	0,0093989
Q78WZ7	Twistnb	0,11	0,03	0,00706014
A2AIV2	Kiaa1429	-0,10	0,06	0,00710668
Q5FWI3	Tmem2	-0,10	0,05	0,00275463
Q9CQS8	Sec61b	-0,10	0,02	0,00291827
P42669	Pura	-0,10	0,05	0,00423537
P17918	Pcna	-0,10	0,03	0,00050641
Q3TIX9	Usp39	-0,11	0,06	0,00724438
Q3TKY6	Cwc27	-0,11	0,03	0,00409785
Q9D1Q6	Erp44	-0,11	0,06	0,00481933
Q05186	Rcn1	-0,11	0,05	0,00371755
Q922P9	Glyr1	-0,11	0,06	0,00671462
Q9DBC7	Prkar1a	-0,11	0,05	0,00201344
Q9JHP7	Kdelc1	-0,11	0,00	0,00486525
P15331	Prph	-0,12	0,06	0,00721058
Q9D0K2	Oxct1	-0,12	0,06	0,00642713
Q99LB2	Dhrs4	-0,12	0,05	0,00219168
P55821	Stmn2	-0,12	0,06	0,00577458
Q61081	Cdc37	-0,12	0,05	0,0018031
Q8VBZ3	Clptm1	-0,12	0,05	0,002963
Q6PHZ2	Camk2d	-0,12	0,07	0,00927241
Q5SUF2	Luc7l3	-0,12	0,05	0,00301674
P46638	Rab11b	-0,12	0,05	0,00128965
Q9D172	D10Jhu81e	-0,12	0,06	0,00455223
Q8JZM7	Cdc73	-0,13	0,07	0,00535922
Q9QYB1	Clic4	-0,13	0,07	0,00718055
O88967	Yme1l1	-0,13	0,04	0,00087173
Q9EQU5	Set	-0,13	0,08	0,00901552
Q9Z277	Baz1b	-0,13	0,04	0,00034304
Q9CQL1	Magohb	-0,13	0,07	0,00571278
Q9WV70	Noc2l	-0,13	0,07	0,00668888
Q99KP6	Prpf19	-0,13	0,07	0,00768284
P23198	Cbx3	-0,13	0,06	0,00228108
Q9EQI8	Mrpl46	-0,14	0,07	0,00542227
Q9R0Q7	Ptges3	-0,14	0,07	0,00391555
P07742	Rrm1	-0,14	0,06	0,00216069

Q61207	Psap	-0,14	0,08	0,00838784
O35638	Stag2	-0,14	0,03	0,00370622
Q8BXZ1	Tmx3	-0,14	0,08	0,00739821
Q8VDF2	Uhrf1	-0,15	0,05	0,00090211
P97379	G3bp2	-0,15	0,08	0,00757702
Q4QQM4	Trp53i11	-0,15	0,08	0,00605888
P51912	Slc1a5	-0,15	0,08	0,00770938
Q8CFE6	Slc38a2	-0,15	0,02	0,00096789
Q91XV3	Basp1	-0,15	0,08	0,00617845
Q921F2	Tardbp	-0,16	0,05	0,00049407
P06837	Gap43	-0,16	0,04	0,00015915
O08807	Prdx4	-0,16	0,08	0,00394998
P10404	1	-0,16	0,07	0,0025349
Q9ET30	Tm9sf3	-0,17	0,10	0,00806924
P11370	Fv4	-0,17	0,08	0,0030267
Q9CPT4	D17Wsu104e	-0,17	0,10	0,00737196
Q9D1M4	Eef1e1	-0,18	0,08	0,00230051
Q61334	Bcap29	-0,18	0,04	0,00352452
O54946	Dnajb6	-0,19	0,11	0,00689517
P18608	Hmgn1	-0,19	0,11	0,00849088
O08688	Capn5	-0,19	0,08	0,00188022
O35887	Calu	-0,20	0,05	0,00028739
P35564	Canx	-0,20	0,09	0,00262034
P47867	Scg3	-0,21	0,07	0,00937008
P63001	Rac1	-0,22	0,06	0,00041265
P35546	Ret	-0,22	0,12	0,00784446
P26350	Ptma	-0,22	0,13	0,00826147
Q9D6J6	Ndufv2	-0,22	0,11	0,00369809
P30051	Tead1	-0,24	0,00	0,00294122
Q76LL6	Fhod3	1,04	0,02	0,01037508
Q3V009	Tmed1	0,38	0,03	0,03376769
Q641P0	Actr3b	0,38	0,02	0,01808386
P51807	Dynlt1	0,33	0,03	0,04246115
Q9CYN9	Atp6ap2	0,27	0,01	0,01464056
O35454	Clcn6	0,25	0,03	0,04914482
P33609	Pola1	0,23	0,02	0,04551773
Q9DCM0	Ethe1	0,21	0,19	0,03981076
Q64337	Sqstm1	0,18	0,12	0,0141381
Q8BVI5	Stx16	0,18	0,08	0,02258133
Q00724	Rbp4	0,18	0,07	0,0153195
Q8JZK9	Hmgcs1	0,17	0,11	0,04771886
P35922	Fmr1	0,17	0,08	0,02367627
Q9ESP1	Sdf2l1	0,15	0,14	0,04046959
Q80Y14	Glrx5	0,15	0,12	0,03160352
Q61586	Gpam	0,15	0,01	0,01952259
Q9CQF9	Pcyox1	0,14	0,07	0,02806429
P19182	Ifrd1	0,14	0,05	0,0103493
Q9CR00	Psmd9	0,14	0,06	0,01864067
Q6PFD9	Nup98	0,14	0,13	0,04219202
Q8BLJ3	Plcxd3	0,13	0,05	0,01412407
O09005	Degs1	0,13	0,07	0,03602864
O08808	Diaph1	0,13	0,01	0,02499661

Q3U2P1	Sec24a	0,13	0,05	0,01728928
Q80ZI6	Lrsam1	0,13	0,01	0,03934567
Q8K183	Pdxk	0,12	0,07	0,03247405
Q9JKK1	Stx6	0,12	0,07	0,03879596
Q9D0R8	Lsm12	0,12	0,08	0,01266606
Q9CQS5	Riok2	0,12	0,00	0,01526551
Q8VBT9	Aspscr1	0,12	0,05	0,02094789
Q9WTS5	Tenm2	0,12	0,01	0,02113111
P84099	Rpl19	0,12	0,11	0,04487326
Q8BIA4	Fbxw8	0,11	0,07	0,04355164
Q8VCN5	Cth	0,11	0,01	0,04045547
Q3ULD5	Mccc2	0,11	0,07	0,01571615
Q8K1K4	Cenpi	0,11	0,01	0,04801915
P97298	Serpinf1	0,10	0,01	0,04238307
Q62523	Zyx	0,10	0,09	0,03639347
Q60900	Elavl3	-0,10	0,08	0,02389572
P26443	Glud1	-0,10	0,07	0,01460191
Q9CPX7	Mrps16	-0,10	0,00	0,01914623
Q6PIX9	D11Wsu47e	-0,10	0,01	0,02726181
P61750	Arf4	-0,10	0,07	0,01474062
Q9D706	Rpap3	-0,10	0,07	0,01544031
Q03141	Mark3	-0,10	0,05	0,02564228
Q80UZ2	Sdad1	-0,11	0,09	0,02918585
P58064	Mrps6	-0,11	0,06	0,03234395
Q80X41	Vrk1	-0,11	0,08	0,02766198
Q61701	Elavl4	-0,11	0,08	0,02623708
Q9D1D6	Cthrc1	-0,11	0,09	0,02933413
Q99JI4	Psmd6	-0,11	0,07	0,01089438
Q6ZWU9	Rps27	-0,11	0,10	0,04063182
Q60899	Elavl2	-0,11	0,09	0,03047369
O89017	Lgmn	-0,11	0,09	0,03538061
Q99020	Hnrnpab	-0,11	0,09	0,02635546
Q62425	Ndufa4	-0,11	0,10	0,03944117
Q8VDM6	Hnrnpul1	-0,11	0,06	0,03214363
P62702	Rps4x	-0,11	0,08	0,01801366
P03975	Iap	-0,11	0,09	0,02371692
Q9ER38	Tor3a	-0,11	0,09	0,0287123
Q8CDM1	Atad2	-0,11	0,04	0,01186825
Q9DC50	Crot	-0,11	0,06	0,03905885
P97868	Rbbp6	-0,12	0,07	0,0122537
Q8BP92	Rcn2	-0,12	0,08	0,01302874
Q8K2P7	Slc38a1	-0,12	0,11	0,04989337
P56382	Atp5e	-0,12	0,09	0,02368528
P58137	Acot8	-0,12	0,06	0,02590074
Q9JI19	Fibp	-0,12	0,00	0,01329023
Q9ERF3	Wdr61	-0,12	0,08	0,01079275
P46660	Ina	-0,12	0,12	0,04957188
Q91YT7	Ythdf2	-0,12	0,10	0,0290305
Q9Z1K6	Arih2	-0,12	0,01	0,03897271
Q9DBJ3	Baiap2l1	-0,13	0,07	0,04229498
Q9CQF0	Mrpl11	-0,13	0,06	0,02358654
Q3UQ28	Pxdn	-0,13	0,10	0,0237694

P62827	Ran	-0,13	0,10	0,02221639
Q9CYI4	Luc7l	-0,13	0,07	0,0408074
Q61735	Cd47	-0,13	0,12	0,04410784
Q8BHD7	Ptbp3	-0,13	0,01	0,0385284
P18760	Cfl1	-0,13	0,10	0,02618272
P70696	Hist1h2ba	-0,13	0,01	0,03883967
Q8BK72	Mrps27	-0,13	0,09	0,01573936
Q8K1S3	Unc5b	-0,13	0,07	0,03135463
P53986	Slc16a1	-0,13	0,10	0,02413132
P20152	Vim	-0,13	0,10	0,02028974
Q7TMF2	Eri1	-0,14	0,07	0,03085698
O88653	Lamtor3	-0,14	0,07	0,03044699
Q3UQ44	Iqgap2	-0,14	0,06	0,01683552
Q8JZS9	Mrpl48	-0,14	0,06	0,01822439
O88522	Ikbkg	-0,14	0,01	0,02643784
Q6Y685	Tacc1	-0,14	0,01	0,04130194
Q03172	Hivep1	-0,14	0,10	0,02140373
P18242	Ctsd	-0,14	0,09	0,01423513
Q99N92	Mrpl27	-0,14	0,09	0,04661129
Q8R5K4	Nol6	-0,14	0,09	0,01206534
O70252	Hmox2	-0,14	0,10	0,01798772
Q62083	Pick1	-0,15	0,08	0,02841296
Q8K1J5	Sde2	-0,15	0,00	0,01174233
Q8K201	Kct2	-0,15	0,10	0,01420705
Q9CQ45	Nenf	-0,15	0,01	0,02779116
P84096	Rhog	-0,15	0,12	0,02393586
O54962	Banf1	-0,16	0,10	0,01172035
P09602	Hmgn2	-0,16	0,13	0,02449267
Q8VEH3	Arl8a	-0,16	0,15	0,04530024
O88708	Orc4	-0,16	0,01	0,0342017
Q3V3R4	Itga1	-0,17	0,11	0,01282694
Q8C570	Rae1	-0,17	0,11	0,04669334
O35683	Ndufa1	-0,17	0,01	0,02516811
Q9D024	Ccdc47	-0,18	0,11	0,01005164
Q8R1V4	Tmed4	-0,18	0,10	0,03200719
Q9WTX5	Skp1	-0,18	0,14	0,02287986
Q923T9	Camk2g	-0,19	0,08	0,01929234
Q8BLB8	Ankrd34c	-0,19	0,11	0,04349633
Q9Z0S9	Rabac1	-0,20	0,10	0,0300988
E9QAM5	Helz2	-0,22	0,08	0,01106673
Q9CQW2	Arl8b	-0,23	0,20	0,03694855
Q9CQK7	Rwdd1	-0,27	0,13	0,02626167
P13011	Scd2	-0,30	0,13	0,01912501
A2AJN7	Slc4a11	-0,32	0,18	0,03964411
Q9CPT5	Nop16	-0,35	0,03	0,04323205
Q91WS0	Cisd1	-0,41	0,24	0,04198445

Table S3. Set of proteins modified by IGF2 expression related to actin cytoskeleton dynamics.

Gene	Fold change	p-value
Dbnl	0,98	0,145
Actg1	1,15	0,006
Acta1	1,12	0,005
Actr3b	1,30	0,018
Fhod3	2,06	0,010
Arpc1b	0,95	0,041
Dctn4	1,06	0,050
Ablim1	1,07	0,069
Arpc2	0,95	0,089
Actl6a	0,96	0,123
Rac1	0,86	0,000
Cdc42	0,94	0,003
Rhog	0,90	0,024
Arhgap26	1,02	0,040
Cfl1	0,91	0,026
Iqgap2	0,91	0,017
Zyx	1,07	0,036
BAIAP2L1	0,92	0,042
DIAPH1	1,09	0,025
TACC1	0,91	0,041
PICK1	0,90	0,028
Vim	0,91	0,020
Ran	0,92	0,022
Akap9	1,32	0,008
Dnajb6	0,88	0,007
STMN2	0,92	0,006
CLIC4	0,92	0,007
Dynlt1	1,26	0,042
Sdad1	0,93	0,029
Ina	0,92	0,050
Slc16a1	0,91	0,024
Prkar1a	0,93	0,002
PRPH	0,92	0,007

Table S4. Human post-mortem brain samples.

Group	Sex	Age	PMI	Region	Familiar antecedents
Control	m	53	15,98	caudate	0
Control	m	63	17,92	caudate	0
Control	m	64	18,85	putamen	0
Control	m	55	19,18	caudate	0
Control	f	58	19,38	putamen	0
Control	m	54	19,9	putamen	0
Control	m	63	19,91	caudate	0
Control	m	63	20,58	caudate	0
Control	m	65	21	caudate	0
Control	f	60	28,15	caudate	0
Control	m	53	23,57	caudate	0
Control	m	58	26,3	caudate	0
Control	m	52	19,55	caudate	0
HD, Grade 3	f	51	14,8	caudate	1
HD, Grade 3	m	60	14,9	putamen	N/a
HD, Grade 3	f	58	15,33	putamen	1
HD, Grade 3	m	39	16,08	putamen	1
HD, Grade 3	m	52	16,33	caudate	1
HD, Grade 3	m	65	19,9	caudate	N/a
HD, Grade 3	m	38	25,92	caudate	N/a
HD, Grade 3	m	62	19,4	caudate/putamen	N/a
HD, Grade 3	f	64	19,65	caudate	1
HD, Grade 4	f	59	12,91	putamen	1
HD, Grade 4	m	48	19,68	caudate	1
HD, Grade 4	m	48	27,15	caudate	1
HD, Grade 4	m	58	27,32	putamen	1

Table S5. Blood samples from HD chilean patients and healthy controls.

Age	Familiar history	Participant category	Allele 1	Allele 2	Onset year	UHDRS Total Funtional Capacity
53	1	pre-manifest HD				13
67	1	pre-manifest HD				13
23	1	pre-manifest HD	18	50		13
77	1	pre-manifest HD				13
25	1	pre-manifest HD				13
48	1	pre-manifest HD				13
35	1	pre-manifest HD				13
-	-	pre-manifest HD				13
40	1	HD	26	47	2011	12
53	1	HD	21	43	2014	7
33	1	HD			2012	8
63	1	HD	17	40	2011	13
60	1	HD			2015	6
39	0	HD			2011	11
37	1	HD	15	48	2014	10
61	1	HD			2015	10
55	1	HD			2008	2
43	1	HD			2008	6
45	0	HD			2006	4
63	1	HD			2010	10
49	1	HD	17	42	2006	10
50	1	HD			2006	6